Sierpinski Gasket: Multiband Fractal Antenna for 4G Systems

A thesis submitted in partial fulfillment of the requirements for the award of the Degree of

MASTER of ENGINEERING

in

ELECTRONICS AND COMMUNICATION ENGINEERING

Submitted by:

JASPREET KAUR
Roll No. 800861006

Under the guidance of:

ANKUSH KANSAL
Assistant Professor, ECED

DEPARTMENT OF ELECTRONICS AND COMMUNICATION ENGINEERING

THAPAR UNIVERSITY

PATIALA-147004, Punjab, INDIA.

June 2010

CERTIFICATE

I, Jaspreet Kaur hereby certify that the work which is being presented in this thesis entitled **"Sierpinski Gasket: Multiband Fractal Antenna for 4G Systems"** by me in partial fulfillment of the requirements for the award of degree of Master of Engineering in Electronics and Communication from Thapar University, Patiala is an authentic record of my own work carried under the supervision of Mr. Ankush Kansal.

The matter presented in this thesis has not been submitted in any University/Institute for the award of Master of Engineering.

jaspreet

(Jaspreet Kaur)
Signature of student

Date: 06-07-2010

This is certified that the above statement made by the candidate is correct to the best of my knowledge.

Ankush Kansal

(Mr. Ankush Kansal)
(Supervisor)
Date: 6/07/10

(Dr. A K Chatterjee)
Head of Department
ECED, Thapar University, Patiala

Date: 9.7.10

(Dr. R.K. Sharma)
Dean of Academic Affairs
Thapar University, Patiala

Date:_____

ACKNOWLEDGMENT

This report is completed with prayers of many and love of my family and friends. However, there are a few people that I would like to specially acknowledge and extend my heartfelt gratitude who have made the completion of this report possible .With the biggest contribution to this report; I would like to thank my guide **Ankush Kansal** had given me his full support in guiding me with stimulating suggestions and encouragement to go ahead in all the time of thesis work.

I am also thankful to **Dr. A. K. Chatterjee**, Head, Electronics and Communication Engineering department, for the providing us with adequate infrastructure in carrying the work.

I am very thankful to my friend Surjeet Singh for his encouragement, valuable suggestions and support throughout my work.

With deep sense of gratitude I would express my sincere thanks to my parents. I would also like to thank God for not letting me down at the time of crisis and showing me the silver lining in the dark clouds.

(Jaspreet Kaur)

ABSTRACT

The evolution of the current systems to the 4G is based more and more on a key idea: interoperability. In the futures systems, a single terminal should be capable to work in anywhere, at any moment and in any interface, resulting in a convergence of services. Like this, the futures systems should be so much interoperable with the futures systems as with the legacy, in way to allow a soft migration among the several air interfaces.

With the crescent growth of standards based on access techniques CDMA, the obtaining of the DOA becomes more and more necessary in way to implement SDMA systems. Following this, with the new techniques based on intelligent antennas capable to select the CDMA user wanted (UOA) and to discover the frequency and the delay profile of arrival (FOA and τOA), the use of antennas arrays is configured as indispensable technique in the modern systems.

Multimode, multiband operation presents a formidable challenge to mobile phone designers, particularly for the RF parts. Of these, the antennas occupy the largest volume and, hence, have the biggest impact on the (commercially crucial) styling of the device. It is well-known that antenna bandwidth is proportional to volume. However, the space allocated to the antenna(s) has not increased: on the contrary, it is tending to decrease due to the demand for thinner, more highly stylized devices. If this were not enough, there is also increasing pressure on mobile phone manufacturers to improve performance, particularly in countries with areas of low population density, where, due to the large distances involved, cellular coverage is often “patchy.”

The multiband antenna must be capable of providing a good gain and bandwidth compatible with the future and current systems. Such antenna should still offer good characteristics regarding its size and weight, so that it could be used in mobile, portable or fixed stations terminals. A natural way for these antennas has been the application of the fractal theory, which allows the project of multiband antennas with reduced sizes.

This thesis discus the bowtie antenna geometry which is straightforwardly expanded to one of the simplest fractal antennas: the so-called Sierpinski fractal antenna or Sierpinski gasket. Very basically, the Sierpinski fractal is none other than a bowtie with a specially arranged hole structure. Fractal antennas are not broadband in the conventional sense but rather “multiband”. Detailed analysis of Sierpinski fractal antenna is done with its comparison with bow-tie antenna, the simulation is one based on method of moments (MoM) and is done

using MATLAB®. Numerical results of the antenna radiation characteristics, including input impedance, input reflection coefficient, gain, radiated power and radiation pattern, are presented for mode-2 Sierpinski fractal and compared with that of a bowtie antenna.

Discussion is also done on the use of fractal arrangements for the design of planar antenna arrays. Iterated Function System (IFS) is used to generate the fractal array (Sierpinski gasket). The antenna arrays are generated using MATLAB®, the resulting radiated field is calculated and comparison of two-dimensional periodic, random and fractal arrays is done in detail.

CONTENTS

LIST OF FIGURES

LIST OF TABLES

Chapter 1: Introduction

Antennas are a very important component of communication systems. By definition, an antenna is a device used to transform an RF signal, traveling on a conductor, into an electromagnetic wave in free space. Antennas demonstrate a property known as reciprocity, which means that an antenna will maintain the same characteristics regardless if it is transmitting or receiving. Most antennas are resonant devices, which operate efficiently over a relatively narrow frequency band. An antenna must be tuned to the same frequency band of the radio system to which it is connected; otherwise the reception and the transmission will be impaired. When a signal is fed into an antenna, the antenna will emit radiation distributed in space in a certain way. A graphical representation of the relative distribution of the radiated power in space is called a radiation pattern [1].

1.1 Modern Antennas

There has been an ever growing demand, in both the military as well as the commercial sectors, for antenna design that possesses the following highly desirable attributes:

- Compact size
- Low profile
- Conformal
- Multi- band or broadband

There are a variety of approaches that have been developed over that year, which can be utilized to achieve one or more of these design objectives. The term fractal, which means broken or irregular fragments, was originally coined by Mandelbrot to describe a family of complex shapes that possess an inherent self similarity in their geometrical structure. The original inspiration for the development of fractal geometry came largely from in depth study of the patterns of nature. For instance, fractals have been successfully used to model such complex natural objects as galaxies; cloud boundaries, mountain ranges, coastlines, snowflakes, trees. Leaves, fern, and much more a wide variety of applications for fractals continue to be found in many branches of science and engineering. This geometry, which has been used to model complex objects found in nature such as clouds and coastlines, has space filling properties that can be utilized to miniaturize antennas [2].One such area is fractal electromagnetic theory for the purpose of investigating a new class of radiation, propagation,

and scattering problems. One of the most promising areas of fractal electrodynamics research is in its application to antenna theory and design. Modern telecommunication systems require antennas with wider bandwidths and Smaller Dimensions than conventionally possible. This has initiated antenna research in various directions, one of which is by using fractal shaped antenna elements. In recent years several fractal geometries have been introduced for antenna applications with varying degrees of success in improving antenna characteristics. Some of these geometries have been particularly useful in reducing the size of the antenna, while other designs aim at incorporating multi-band characteristics. These are low profile antennas with moderate gain and can be made operative at multiple frequency bands and hence are multi-functional.

1.2 Antenna Engineering

1.2.1 Input Impedance

For an efficient transfer of energy, the impedance of the radio, of the antenna and of the transmission cable connecting them must be the same. Transceivers and their transmission lines are typically designed for 50 impedance. If the antenna has an impedance different from 50 then there is a mismatch and an impedance matching circuit is required. [1]An antenna's impedance relates the voltage to the current at the input to the antenna.An antenna with a real input impedance (zero imaginary part) is said to be resonant. An antenna's impedance will vary with frequency.

1.2.2 Return loss

The return loss is another way of expressing mismatch. It is a logarithmic ratio measured in dB that compares the power reflected by the antenna to the power that is fed into the antenna from the transmission line. The relationship between SWR and return loss is the following:

$$Return\ Loss\ (in\ dB) = 20\ log_{10}\frac{SWR}{SWR-1} \tag{1.1}$$

1.2.3 Bandwidth

The bandwidth of an antenna refers to the range of frequencies over which the antenna can operate correctly. The antenna's bandwidth is the number of Hz for which the antenna will

exhibit an SWR less than 2:1. The bandwidth can also be described in terms of percentage of the center frequency of the band.

$$BW = 100\frac{F_{H-}F_L}{F_C} \tag{1.2}$$

where F_H is the highest frequency in the band, F_L is the lowest frequency in the band, and $F_C$is the center frequency in the band. In this way, bandwidth is constant relative to frequency. If bandwidth was expressed in absolute units of frequency, it would be different depending upon the center frequency. Different types of antennas have different bandwidth limitations.

1.2.4 Directivity and Gain

Directivity is the ability of an antenna to focus energy in a particular direction when transmitting, or to receive energy better from a particular direction when receiving. In a static situation, it is possible to use the antenna directivity to concentrate the radiation beam in the wanted direction. However in a dynamic system where the transceiver is not fixed, the antenna should radiate equally in all directions, and this is known as an omni-directional antenna.

$$D = \frac{U}{U_0} = \frac{4\pi U}{P_{rad}} \tag{1.3}$$

Where U is radiation intensity and P_{rad} is power radiated.Gain is not a quantity which can be defined in terms of a physical quantity such as the Watt or the Ohm, but it is a dimensionless ratio.

$$G = \frac{4\pi U(\theta, \emptyset)}{P_{in\ (lossless\ isotropic\ source)}} \qquad (dimensionless) \tag{1.4}$$

Gain is given in reference to a standard antenna. The two most common reference antennas are the isotropic antenna and the resonant half-wave dipole antenna. The isotropic antenna radiates equally well in all directions. Real isotropic antennas do not exist, but they provide useful and simple theoretical antenna patterns with which to compare real antennas. Any real antenna will radiate more energy in some directions than in others. Since it cannot create energy, the total power radiated is the same as an isotropic antenna, so in other directions it must radiate less energy. The gain of an antenna in a given direction is the amount of energy

radiated in that direction compared to the energy an isotropic antenna would radiate in the same direction when driven with the same input power. Usually we are only interested in the maximum gain, which is the gain in the direction in which the antenna is radiating most of the power. An antenna gain of $3\,dB$ compared to an isotropic antenna would be written as $3\,dBi$. The resonant half-wave dipole can be a useful standard for comparing to other antennas at one frequency or over a very narrow band of frequencies. To compare the dipole to an antenna over a range of frequencies requires a number of dipoles of different lengths. An antenna gain of $3\,dB$ compared to a dipole antenna would be written as $3\,dBd$. The method of measuring gain by comparing the antenna under test against a known standard antenna, which has a calibrated gain, is technically known as a gain transfer technique. Another method for measuring gain is the 3 antennas method, where the transmitted and received power at the antenna terminals is measured between three arbitrary antennas at a known fixed distance.

1.2.5 Beamwidth

An antenna's beamwidth is usually understood to mean the half-power beamwidth. The peak radiation intensity is found and then the points on either side of the peak which represent half the power of the peak intensity are located. The angular distance between the half power points is defined as the beamwidth. Half the power expressed in decibels is $-3dB$, so the half power beamwidth is sometimes referred to as the $3dB$ beamwidth. Both horizontal and vertical beamwidths are usually considered. Assuming that most of the radiated power is not divided into sidelobes, then the directive gain is inversely proportional to the beamwidth: as the beamwidth decreases, the directive gain increases.

1.2.6 Radiation Pattern

The radiation or antenna pattern describes the relative strength of the radiated field in various directions from the antenna, at a constant distance. The radiation pattern is a reception pattern as well, since it also describes the receiving properties of the antenna. The radiation pattern is three-dimensional, but usually the measured radiation patterns are a two dimensional slice of the three-dimensional pattern, in the horizontal or vertical planes. These pattern measurements are presented in either a rectangular or a polar format. Figure 1.1 and figure 1.2 shows a rectangular plot presentation of a typical 10 element Yagi. The detail is good but it is difficult to visualize the antenna behavior at different directions.

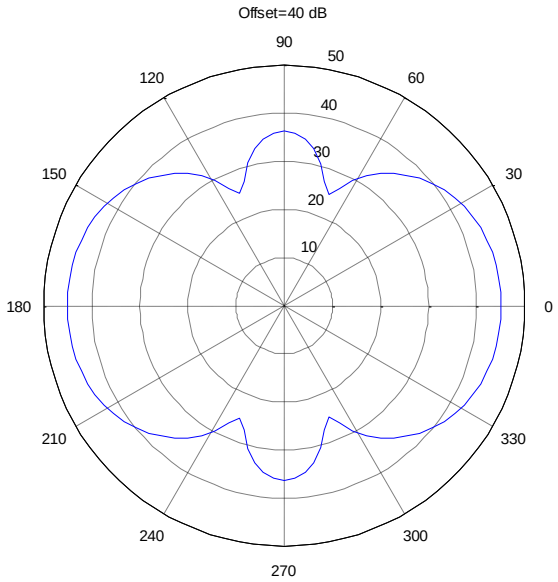

Figure 1.1: Radiation pattern of bowtie antenna at 3 GHz

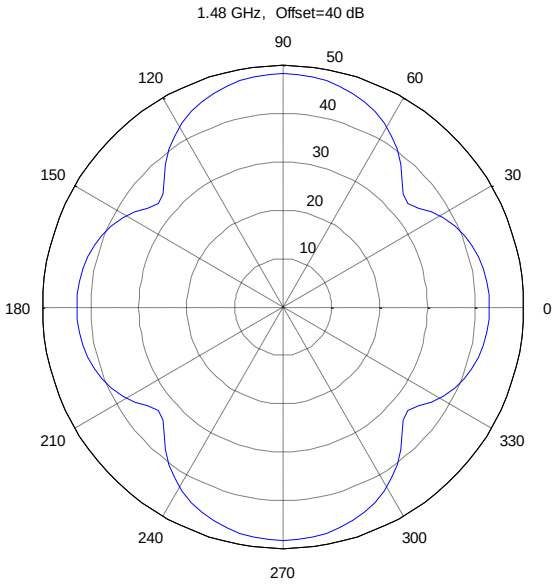

Figure 1.2: Radiation pattern of fractal antenna at 3.36 GHz

1.2.7 Sidelobes

No antenna is able to radiate all the energy in one preferred direction. Some is inevitably radiated in other directions. The peaks are referred to as sidelobes, commonly specified in dB down from the main lobe.

1.2.8 Nulls

In an antenna radiation pattern, a null is a zone in which the effective radiated power is at a minimum. A null often has a narrow directivity angle compared to that of the main beam. Thus, the null is useful for several purposes, such as suppression of interfering signals in a given direction.

1.2.9 Polarization

Polarization is defined as the orientation of the electric field of an electromagnetic wave. Polarization is in general described by an ellipse. Two special cases of elliptical polarization are linear polarization and circular polarization. The initial polarization of a radio wave is determined by the antenna. With linear polarization the electric field vector stays in the same plane all the time. Vertically polarized radiation is somewhat less affected by reflections over the transmission path. Omnidirectional antennas always have vertical polarization. With horizontal polarization, such reflections cause variations in received signal strength. Horizontal antennas are less likely to pick up man-made interference, which ordinarily is vertically polarized. In circular polarization the electric field vector appears to be rotating with circular motion about the direction of propagation, making one full turn for each RF cycle. This rotation may be right hand or left hand. Choice of polarization is one of the design choices available to the RF system designer.

1.2.10 Polarization Mismatch

In order to transfer maximum power between a transmit and a receive antenna, both antennas must have the same spatial orientation, the same polarization sense and the same axial ratio. When the antennas are not aligned or do not have the same polarization, there will be a reduction in power transfer between the two antennas. This reduction in power transfer will reduce the overall system efficiency and performance.When the transmit and receive antennas are both linearly polarized, physical antenna misalignment will result in a polarization mismatch loss which can be determined using the following formula:

$$Polarization\ Mismatch\ Loss\ (dB) = 20\ log\ (cos\theta) \tag{1.5}$$

where θ is the misalignment angle between the two antennas. For $15°$ we have a loss of $0.3\ dB$, for $30°$ we have $1.25\ dB$, for $45°$ we have $3\ dB$ and for $90°$ we have an infinite loss. The actual mismatch loss between a circularly polarized antenna and a linearly polarized

antenna will vary depending upon the axial ratio of the circularly polarized antenna. If polarizations are coincident no attenuation occurs due to coupling mismatch between field and antenna, while if they are not, then the communication can't even take place.

1.3 Brief Background on Fractal Geometry

Recent efforts by several researchers [3] around the world to combine fractal geometry with electromagnetic theory have led to a plethora of new and innovative antenna designs. In this chapter, we provide a comprehensive overview of recent developments in the rapidly growing field of fractal antenna engineering, which has been primarily focused in two areas: the analysis and design of fractal antenna elements, and the application of fractal concepts to the design of antenna arrays.

It has been an intriguing question among the electromagnetic community [4] as to what property of fractals, if any, is really useful, especially when it comes to designing fractal shaped antenna elements. Several fractal geometries have been explored for antennas with special characteristics, in the context of both antenna elements and spatial distribution functions for elements in antenna arrays. Yet there have been no concerted efforts to design antennas using fractal shaped elements. In many fractal antennas, the self-similarity and plane-filling nature of fractal geometries are often qualitatively linked to its frequency characteristics. The fractal geometry has been behind an enormous change in the way scientists and engineers perceive, and subsequently model, the world in which we live [5]. Chemists, biologists, physicists, physiologists, geologists, economists, and engineers (mechanical, electrical, chemical, civil, aeronautical) have all used methods developed in fractal geometry to explain a multitude of diverse physical phenomena: from trees to turbulence, cities to cracks, music to moon craters, measles epidemics, and much more. Many of the ideas within fractal geometry have been in existence for a long time; however, it took the arrival of the computer, with its capacity to accurately and quickly carry out large repetitive calculations, to provide the tool necessary for the in-depth exploration of these subject areas. In recent years, the explosion of interest in fractals has essentially ridden on the back of advances in computer development.

1.3.1 Basics of Fractals

In recent years, the science of fractal geometry has grown into a vast area of knowledge, with almost all branches of science and engineering gaining from the new insights it has provided.

Fractal geometry is concerned with the properties of fractal objects, usually simply known as fractals (see Figure 1.3).

Fractals may be found in nature or generated using a mathematical recipe. The word "fractal" was coined by Benoit Mandelbrot, sometimes referred to as the father of fractal geometry, who said, "I coined fractal from the Latin adjective fractus . The corresponding Latin verb frangere means 'to break' to create irregular fragments. It is therefore sensible—and how appropriate for our need!—that, in addition to 'fragmented' (as in fraction or refraction), fractus should also mean 'irregular', both meanings being preserved in fragment" [6]. Moreover he asked:"Why geometry is often described as 'cold' or 'dry'? One reason lies in its inability to describe the shape of a cloud, a mountain, a coastline, or a tree. Clouds are not spheres, mountains are not cones, coastlines are not circles, and bark is not smooth, nor does lightning travel in a straight line."

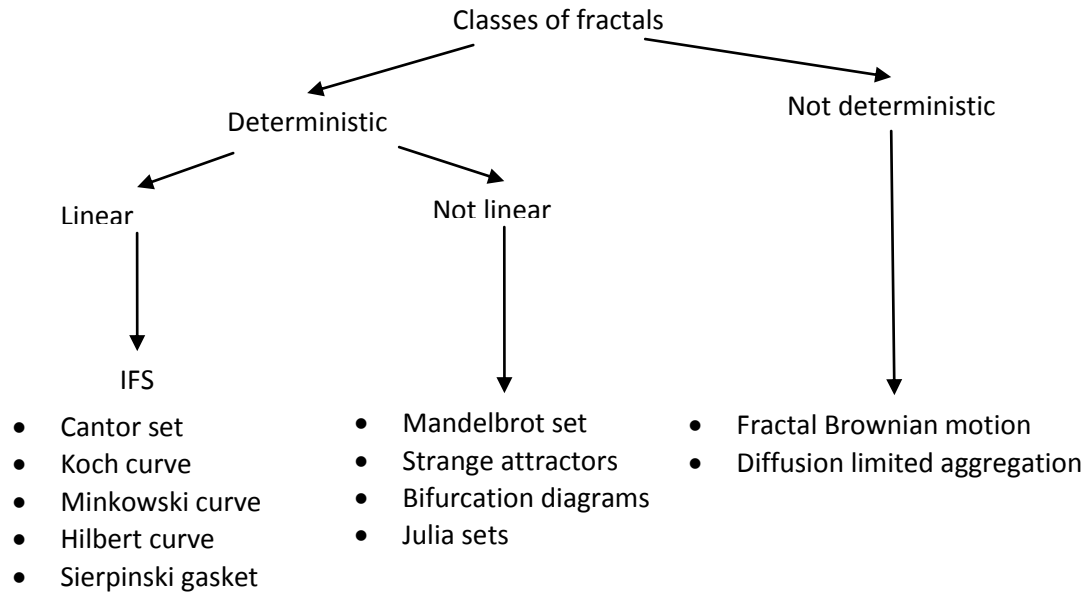

Figure 1.3: Classes of Fractals.

To date, there exists no watertight definition of a fractal object. Mandelbrot offered the following definition: "A fractal is by definition a set for which the Hausdorff dimension strictly exceeds the topological dimension," which he later retracted and replaced with: "A fractal is a shape made of parts similar to the whole in some way." So, possibly the simplest way to define a fractal is as an object that appears self-similar under varying degrees of magnification, and in effect, possessing symmetry across scale, with each small part of the

object replicating the structure of the whole. This is perhaps the loosest of definitions; however, it captures the essential, defining characteristic, that of self-similarity.

But here are five properties that most fractals have:

- Fractals have details on arbitrarily small scales.
- Fractals are usually defined by simple recursive processes.
- Fractals are too irregular to be described in traditional geometric language.
- Fractals have some sort of self-similarity.
- Fractals have fractal dimension.

1.3.2 Random Fractals

The exact structure of regular fractals is repeated within each small fraction of the whole (i.e., they are exactly self-similar). There is, however, another group of fractals, known as random fractals, which contain a random or statistical elements. These fractals are not exactly self-similar, but rather statistically self-similar. Each small part of a random fractal has the same statistical properties as the whole. Random fractals are particularly useful in describing the properties of many natural objects and processes.

Table 1.1 : General comparison of Euclidean and Fractal geometry.

Euclidean geometry	Fractal Geometry
>2,000 years old	10-20 years old
Applicable for artificial objects	Applicable for natural objects
Change shapes with scaling	Invariant under scaling ,self similar
Locally smooth ,differentiable	Locally rough, not differentiable
Objects defined by analytical equations	Objects defined by recursive algorithms
Elements: vertices, edges, surfaces	Elements: iteration of functions

A simple way to generate a fractal with an element of randomness is to add some probabilistic element to the construction process of a regular fractal. While such random fractals do not have the self-similarity of their nonrandom counterparts, their nonuniform appearance is often rather closer to natural phenomena such as coastlines, topographical surfaces, or cloud boundaries. Indeed, random fractal constructions are the basis of many impressive computer- drawn landscapes or skyscapes. A random fractal worthy of the name should display randomness at all scales, so it is appropriate to introduce a random element at

each stage of the construction. By relating the size of the random variations to the scale, we can arrange for the fractal to be statistically self-similar in the sense that enlargements of small parts have the same statistical distribution as the whole set. This compares with (nonrandom) self-similar sets where enlargements of small parts are identical to the whole.

1.3.3 Significance of Fractals in Nature

The original inspiration for the development of fractal geometry came largely from an in-depth study of the patterns of nature. For instance, fractals have been successfully used to model such complex natural objects as galaxies, cloud boundaries, mountain ranges, coastlines, snowflakes, trees, leaves, ferns, and much more.

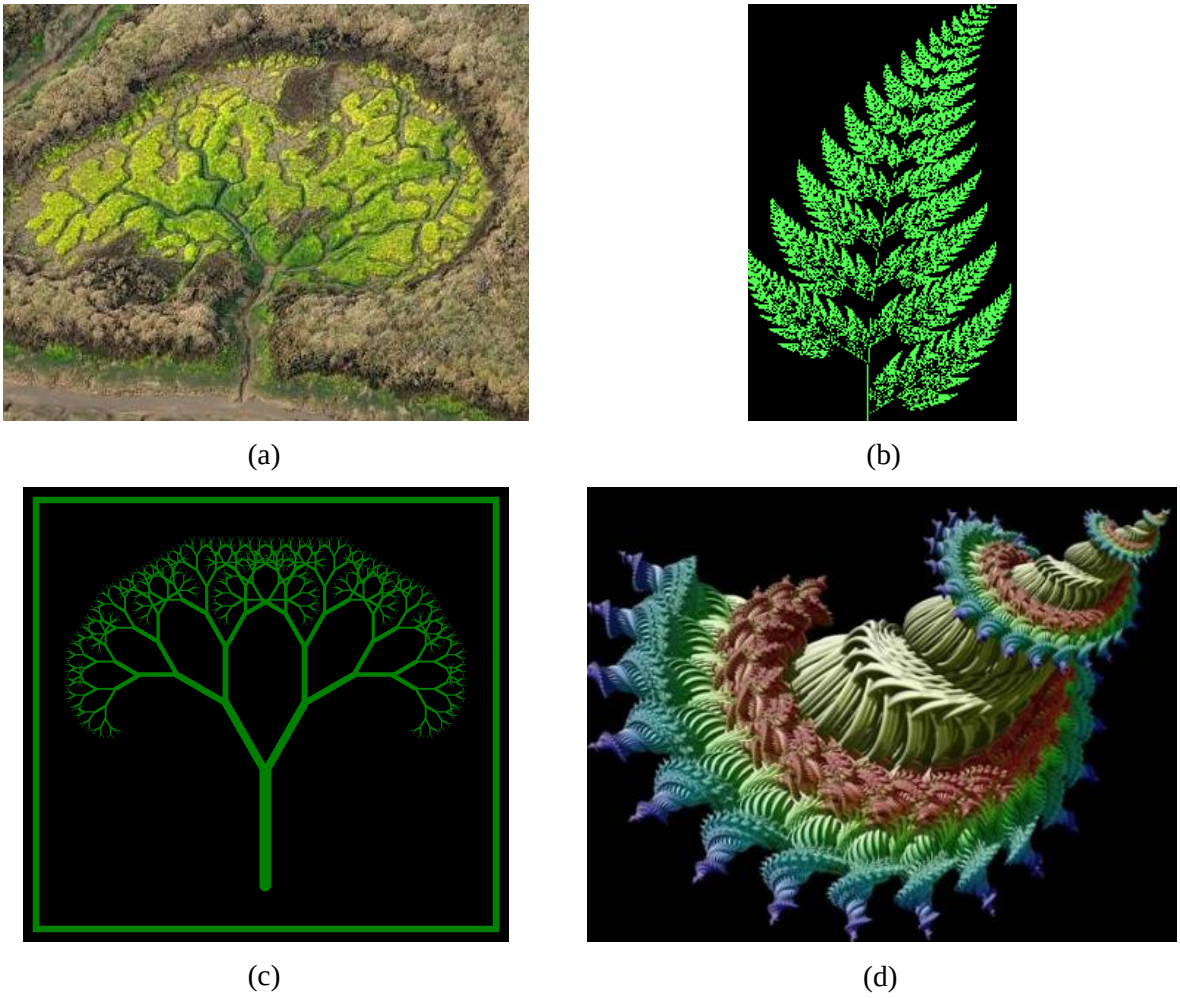

(a) (b)

(c) (d)

Figure 1.4: Natural fractal natural fractal photographs by Hector Garrido (a),a fern leaf looks almost identical to the entire fern (b), a tree branch looks similar to the entire tree (c), and the fractal art(d)[7].

Mandelbrot realized that it is very often impossible to describe nature using only Euclidean geometry that is in terms of straight lines, circles, cubes, and so forth. He proposed that fractals and fractal geometry could be used to describe real objects, such as trees, lightning,

river meanders, and coastlines, to name but a few. Figure 1.4 contains some natural fractals [7].

Fractal geometries have found an intricate place in science as a representation of some of unique geometrical features occurring in nature. Fractals are used to describe the branching of tree leaves and plants, the space filling of water vapor that forms clouds, the random erosion that carves mountain faces, the jaggedness of coastlines and bark, and many more examples in nature. The structure of our universe—superclusters, clusters, galaxies, star systems (solar system), planets, moons—every detail of the universe shows the same clustering patterns. It can be modeled by random Cantor fractal square.

Originally, it was believed that Saturn had only a single ring. After some time, a break in the middle was discovered, and scientists concluded that there were two rings. However, when Voyager I approached Saturn, it was discovered that the two rings were also broken in the middle, and these four smaller rings were broken as well. Eventually, Voyager I identified a very large number of breaks, which continuously broke even small rings into smaller pieces. The overall structure is amazingly similar to the Cantor fractal set.

Weather behaves very unpredictably; sometimes it changes very smoothly, and other times it changes very rapidly. Edward Lorenz came up with three formulas that could model the changes of the weather. These formulas are used to create a 3-D strange attractor; they form the famous Lorenz Attractor, which is a fractal pattern. In the human body the lungs, formed by splitting lines, are fractal canopies; similarly, the surface of the brain contains a large number of folds that are well modeled by fractal shapes.

During electronic transmissions, electronic noise would sometimes interfere with the transmitted data. Although making the signal more powerful would drown out some of this harmful noise, some of it persisted, creating errors during transmissions. Errors occurred in clusters: a period of no errors would be followed by a period with many errors. On any scale of magnification (month, day, hour, 20 minutes), the proportion of error-free transmission to error-ridden transmission stays constant. Mandelbrot studied the mathematical process that enables us to create random Cantor dust, describing perfectly well the fractal structure of the batches of errors on computer lines.

Many more examples could be introduced to prove the fractal nature of universe.therefore, there is a need for a geometry that handles these complex situations better than Euclidean geometry.

Figure 1.5: A uniform cantor Fractal set

1.3.4 Prefractals: Truncating a Fractal to Useable Complexity

There is some terminology that should be established to understand fractals and how they can be applied to practical applications [8]. Even though a fractal is mathematically defined to be infinite in intricacy, this is obviously not the case in nature, and is not desirable if some objects in nature are to be modeled using these geometries. For example, the complexity and repetition of a cloud does not extend to infinitely small or large scales, but can be approximated as doing so for a certain band of scales. From the scale of human perception, a cloud does seem to be infinitely complex in larger and smaller scales. The resulting geometry after truncating the complexity is called a prefractal [9]. A prefractal drops the intricacies that are not distinguishable in the particular applications. In Figure 1.5, the fifth iteration is indistinguishable from the Cantor set obtained at higher iterations.

This problem occurs due to the limit of the finite detail our eyes (or the printer we use to plot the image) can resolve. Thus, to illustrate the set, it is sufficient to repeat the generation process only by the number of steps necessary to fool the eye, and not an infinite number of times. This is true for all illustrations of fractal objects. However, make no mistake, only after an infinite number of iterations do we obtain the Cantor set. For a finite number of iterations the object produced is merely a collection of line segments with finite measurable length. These objects formed en route to the fractal object are termed prefractals.

1.3.5 Fractals as Antennas and Space- Filling Geometries

While Euclidean geometries are limited to points, lines, sheets, and volumes, fractals include the geometries that fall between these distinctions. Therefore, a fractal can be a line that approaches a sheet. The line can meander in such a way as to effectively almost fill the entire sheet. These space-filling properties lead to curves that are electrically very long, but fit into a compact physical space. This property can lead to the miniaturization of antenna elements. In the previous section, it was mentioned that prefractals drop the complexity in the geometry of a fractal that is not distinguishable for a particular application. For antennas, this can mean that the intricacies that are much, much smaller than a wavelength in the band of useable frequencies can be dropped out [10]. This now makes this infinitely complex structure, which could only be analyzed mathematically, but may not be possible to be manufactured. It will be shown that the band of generating iterations required to reap the benefits of miniaturization is only a few before the additional complexities become indistinguishable. There have been many interesting works that have looked at this emerging field of fractal electrodynamics.

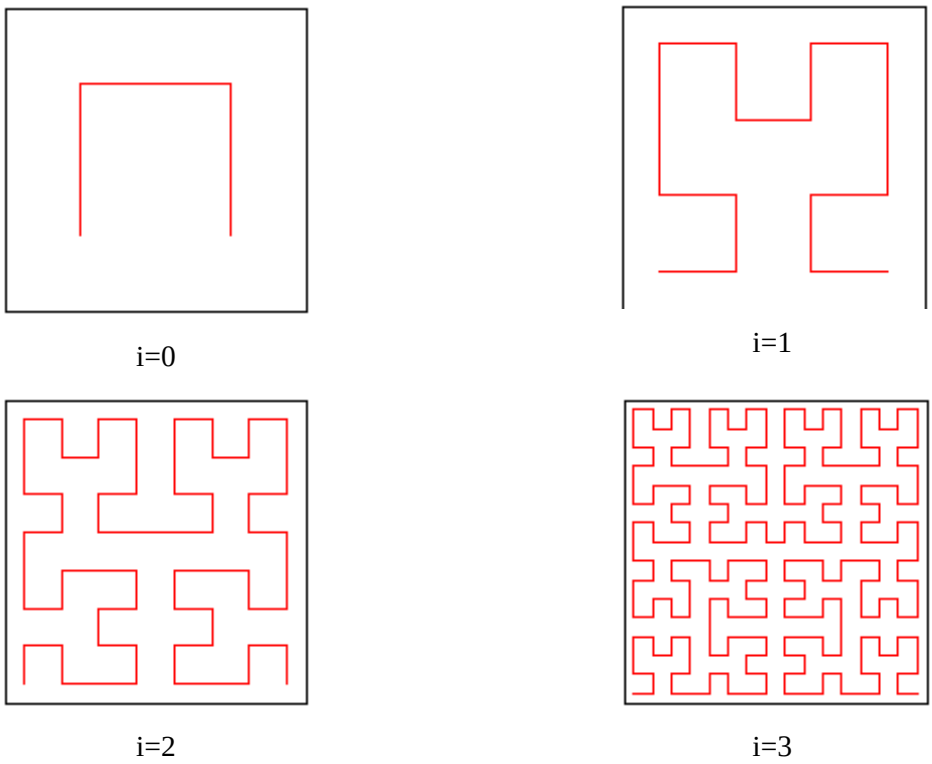

Figure 1.6: Generation of four iterations of Hilbert curves. The segments used to connect the geometry of the previous iteration are shown in dashed lines.

Much of the pioneering work in this area has been documented in [11, 12]. These works include fundamentals about the mathematics as well as studies in fractal antennas and reflections from fractal surfaces. The space-filling properties of the Hilbert curve and related curves (e.g., Peano fractal) make them attractive candidates for use in the design of fractal antennas. The space-filling properties of the Hilbert curve were investigated in [13, 14] as an effective method for designing compact resonant antennas. The first four steps in the construction of the Hilbert curve are shown in Figure 1.6.

The Hilbert curve is an example of a space-filling fractal curve that is selfvoiding (i.e., has no intersection points). In the antenna engineering it can be used as dipole (fed in the center), monopole (fed on one side) antenna, as well as meandered structure of microstrip patch antenna.

1.4 Fractals Defined by Transformations—Self-Similar and Self-Affine Sets

1.4.1 Iterated Function Schemes: The Language of Fractals

Iterated function systems (IFS) represent an extremely versatile method for conveniently generating a wide variety of useful fractal structures [3, 5, 9, 15]. These iterated function systems are based on the application of a series of affine transformations, w, defined by [3]

$$w\begin{pmatrix}x\\y\end{pmatrix}=\begin{pmatrix}a & b\\c & d\end{pmatrix}\begin{pmatrix}x\\y\end{pmatrix}+\begin{pmatrix}e\\f\end{pmatrix} \tag{1.6}$$

or, equivalently, by

$$w(x,y)=(ax+by+e,cx+dy+f) \tag{1.7}$$

where $a,b,c,d,e,and\ f$ are real numbers. Hence, the affine transformation, w, is represented by six parameters

$$\left(\begin{matrix}a & b\\c & d\end{matrix}\middle|\begin{matrix}e\\f\end{matrix}\right) \tag{1.8}$$

whereby $a,b,c,and\ d$ control rotation and scaling, while $e\ and\ f$ control linear translation (see Figure 1.7).

Now suppose we consider $w_1,w_2,\ldots,w_N$ as a set of affine linear transformations, and let A be the initial geometry. Then a new geometry, produced by applying the set of

transformations to the original geometry, A, and collecting the results from $w_1(A), w_2(A), \ldots\ldots\ldots w_N(A)$ can be represented as

$$W(A) = \bigcup_{n=1}^{N} w_n(A) \tag{1.9}$$

where W is known as the Hutchinson operator [3, 13].

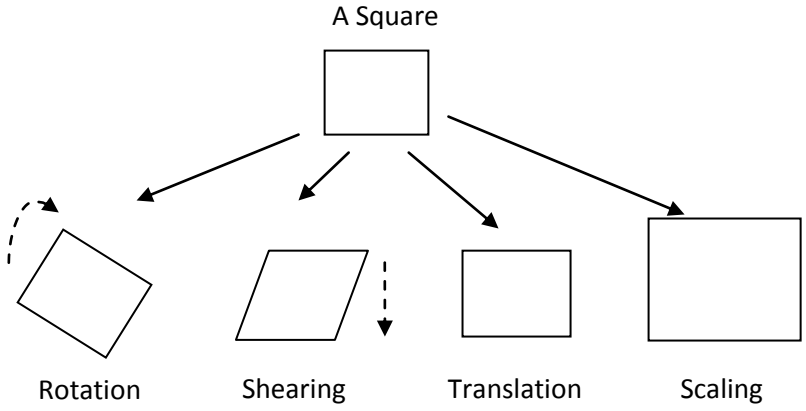

Figure 1.7: The Affine Transforms

Fractal geometry can be obtained by repeatedly applying W to the previous geometry. For example, if the set A_0 represents the initial geometry, then we will have

$$A_1 = W(A_0); \quad A_2 = W(A_1); \ldots\ldots\ldots; \quad A_{k+1} = W(A_k) \tag{1.10}$$

An iterated function system generates a sequence that converges to a final image,A_∞, in such a way that

$$W(A_\infty) = A_\infty \tag{1.11}$$

This image is called the attractor of the iterated function system, and represents a "fixed point" of W. For the Koch fractal curve the matrix of affine transformation has following form:

$$w_q \begin{pmatrix} x \\ y \end{pmatrix} = \begin{pmatrix} \delta_{q1} \cos\theta_{q1} & -\delta_{q2} \sin\theta_{q2} \\ \delta_{q1} \sin\theta_{q1} & \delta_{q2} \cos\theta_{q2} \end{pmatrix} \begin{pmatrix} x \\ y \end{pmatrix} + \begin{pmatrix} t_{q1} \\ t_{q2} \end{pmatrix} \tag{1.12}$$

and scaling factor is expressed as

$$\delta_q = \frac{1}{2 + 2\cos\theta_q} \tag{1.13}$$

where θ_{qi} is the inclination angle of the second subsection with respect to the first, and t_{qi} is an element displacement on the plane. Figure 1.8 illustrates the iterated function system procedure for generating the well-known Koch fractal curve. In this case, the initial set, $A_0$is the line interval of unit length (i.e., A_0= $\{x: x \in [0,1]\}, \theta_q = 60°$, and). Four affine linear transformations are then applied to A_0, as indicated in Figure 1.8. Next, the results of these four linear transformations are combined together to form the first iteration of the Koch curve, denoted byA_1. The second iteration of the Koch curve, A_2 may then be obtained by applying the same four affine transformations to A_1. Higher-order versions of the Koch curve are generated by simply repeating the iterative process until the desired resolution is achieved.

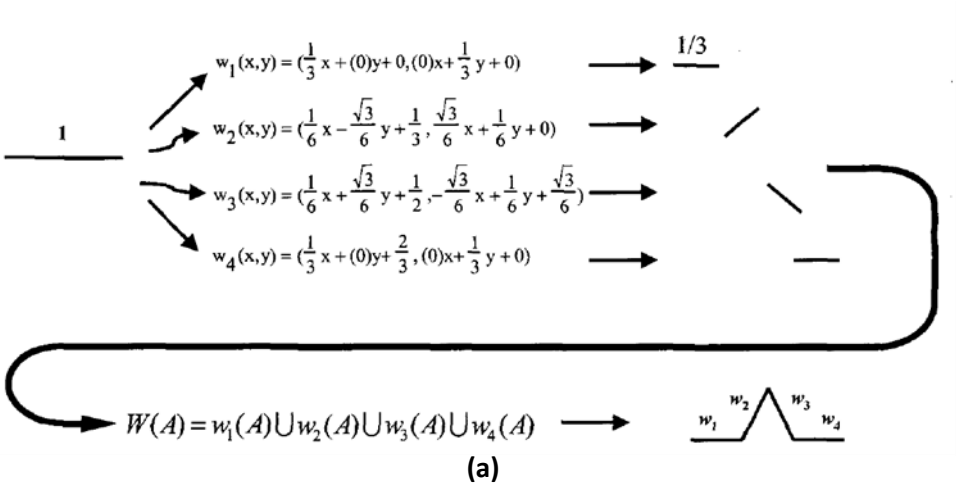

(a)

a	b	c	d	e	f
0.195	-0.488	0.344	0.443	0.4431	0.2452
0.462	0.414	-0.252	0.361	0.2511	0.5692
-0.058	–0.07	0.453	-0.111	0.5976	0.0969
-0.035	0.07	-0.469	-0.022	0.4884	0.5069
-0.637	0.0	0.0	0.501	0.8562	0.2513

(b)

a	b	c	d	e	f
0.500	0.000	0.000	0.500	0.000	0.000
0.500	0.000	0.000	0.500	0.500	0.000
0.500	0.000	0.000	0.500	0.000	0.500

(c)

Figure 1.8: The standard Koch curve as an iterated function system (IFS) (a). The iterated function system code for a fractal tree (b). The iterated function system code for a Sierpinski gasket (c).

In order to further illustrate this important point, the affine transformation matrices for a Sierpinski gasket, and a fractal tree, have been provided in Figure 1.8(b), and (c), respectively

[3, 15]. The first four iterations of the Koch curve are shown in Figure 1.9(a). We note that these curves would converge to the actual Koch fractal, represented by A_∞, as the number of iterations approaches infinity.

Iterated function systems have proven to be a very powerful design tool for fractal antenna engineers. This is primarily because they provide a general framework or the description, classification, and manipulation of fractals.

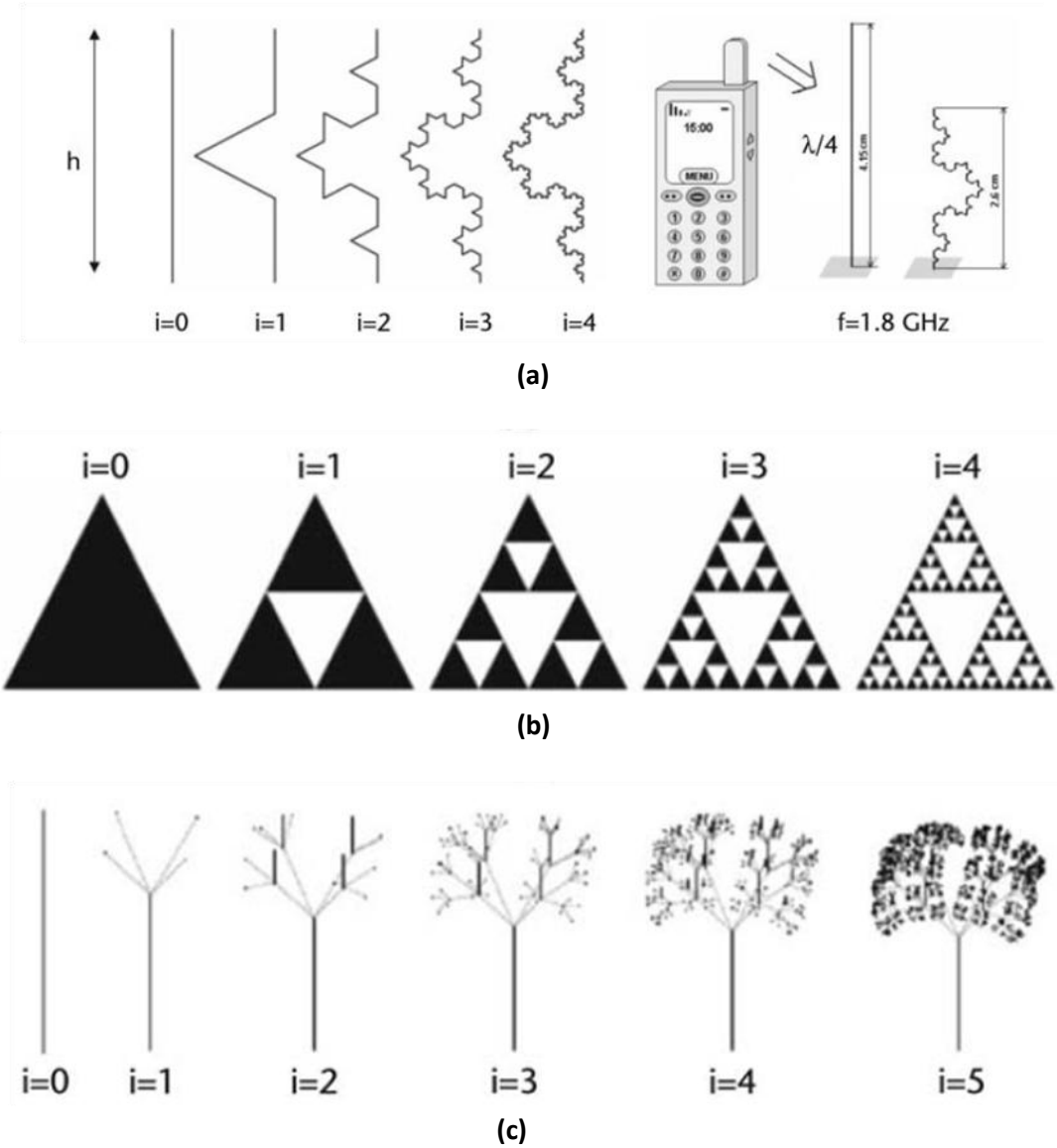

Figure 1.9: (a) The first stages in the construction of the standard Koch curve, (b) the Sierpinski gasket, and (c) the fractal tree via an iterated function system (IFS) approach.

Fractal geometries are generated in an iterative fashion, leading to self-similar structures. This iterative generating technique can best be conveyed pictorially, as in Figure 1.9. The starting geometry of the fractal, called the initiator, depends of final fractal shape: each of the straight segments of the starting structure is replaced with the generator, which is shown on the left of Figure 1.9.

The first few stages in the construction of the Sierpinski gasket are shown in Figure 1.9 (b.) The procedure for geometrically constructing this fractal begins with an equilateral triangle contained in the plane, as illustrated in stage i=0 of Figure 1.9(b). The next step in the construction process (see stage i=1) is to remove the central triangle with vertices that are located at the midpoints of the sides of the original triangle, shown in stage i=0. This process is then repeated for the three remaining triangles, as illustrated in stage i=2 of Figure 1.9 (b). The next two stages (i.e., i=3 and 4) in the construction of the Sierpinski gasket are also shown in Figure 1.9(b). The Sierpinski-gasket fractal is generated by carrying out this iterative process an infinite number of times. It is easy to see from this definition that the Sierpinski gasket is an example of a self-similar fractal.

The fractal tree, shown in Figure 1.9 (c), is similar to a real tree, in that the top of every branch splits into more branches. The planar version of the tree has the top third of every branch split into two sections. The three-dimensional version (this use of the term is only meant to imply that the structure cannot be contained in a plane) has the top third of each branch split into four segments that are each one-third in length. All the branches split with 60° between them. The length of each path remains the same, in that a path walked from the base of the tree to the tip of a branch would be the same length as the initiator. Finding the fractal dimension of these structures is not as easy as it is to find the dimension of the self-similar fractals that were previously observed. This is because the tree fractal is not necessarily self-similar. Mandelbrot suggests that depending on the constructing geometry, the shape may not truly be fractal in the entire structure.

This iterative generating procedure continues for an infinite number of times. The final result is a curve or area with an infinitely intricate underlying structure that is not differentiable at any point. The iterative generation process creates a geometry that has intricate details on an ever-shrinking scale. In a fractal, no matter how closely the structure is studied, there never comes a point where the fundamental building blocks can be observed. The reason for this intricacy is that the fundamental building blocks of fractals are scaled versions of the fractal

shape. This can be compared to it not being possible to see the ending reflection when standing between two mirrors. Closer inspection only reveals another mirror with an infinite number of mirrors reflected inside.

1.4.2 Self-Affine Sets

Self-affine sets form an important class of sets, which include self-similar sets as a particular case. An affine transformation $S: \Re^n \rightarrow \Re^n$ is a transformation of the form [9]

$$w(x, y) = T(x, y) + t \tag{1.14}$$

where t is a linear transformation on $\Re^n$ (which may be represented by an $n \times n$ matrix) and t is a vector in $\Re^n$. Thus an affine transformation w is a combination of a translation, rotation, dilation, and perhaps reflection (see Figure 1.7). In particular, w maps spheres to ellipsoids, squares to parallelograms, and so forth. Unlike similarities, affine transformations contract with differing ratios in different directions.

If $w_1, \ldots, w_m$ are self-affine contractions on $\Re$n, the unique compact invariant set F for the w_i is termed a self-affine set. An example is given in Figure 1.7: w_1, w_2, and w_3 are defined as the transformations that map the square onto the three rectangles in the obvious way.

It is natural to look for a formula for the dimension of self-affine sets that generalizes formula for self-similar sets. We would hope that the dimension depends on the affine transformations in a reasonably simple way, easily expressible in terms of the matrices, and vectors that represent the affine transformation. Unfortunately, the situation is much more complicated than this. If the affine transformations are varied in a continuous way, the dimension of the self-affine set need not change continuously. With such discontinuous behavior, which becomes worse for more involved sets of affine transformations, it is likely to be difficult to obtain a general expression for the dimension of self-affine sets.

1.5 Deterministic Fractals as Antennas

Having seen the geometric properties of fractal geometry, it is interesting to explain what benefits are derived when such geometry is applied to the antenna field [16]. Fractals are abstract objects that cannot be physically implemented. Nevertheless, some related geometries can be used to approach an ideal fractal that are useful in constructing antennas. Usually, these geometries are called prefractals or truncated fractals. In other cases, other

geometries such as multitriangular or multilevel configurations can be used to build antennas that might approach fractal shapes and extract some of the advantages that can theoretically be obtained from the mathematical abstractions. In general, the term fractal antenna technology is used to describe those antenna engineering techniques that are based on such mathematical concepts that enable one to obtain a new generation of antennas with some features that were often thought impossible in the mid-1980s.

After all the work carried out thus far, one can summarize the benefits of fractal technology in the following way:

- Self-similarity is useful in designing multifrequency antennas, as, for instance, in the examples based on the Sierpinski gasket, and has been applied in designing of multiband arrays.
- Fractal dimension is useful to design electrically small antennas, such as the Hilbert, Minkowski, and Koch monopoles or loops, and fractalshaped microstrip patch antennas.
- Mass fractals and boundary fractals are useful in obtaining high-directivity elements, undersampled arrays, and low-sidelobes arrays.

1.6 Fractal Arrays

The term fractal antenna array was originally coined by Kim and Jaggard in 1986 [17] to denote a geometrical arrangement of antenna elements that is fractal. They used properties of random fractals to develop a design methodology for quasirandom arrays. In other words, random fractals were used to generate array configurations that were somewhere between completely ordered (i.e., periodic) and completely disordered (i.e., random). The main advantage of this technique is that it yields sparse arrays that possess relatively low sidelobes. While this is a feature typically associated with periodic arrays, it is not so for random arrays. Another advantage of the technique is that it is also robust, which in turn is a feature typically associated with random arrays, but not with periodic arrays. The time-harmonic and time-dependent radiation produced by deterministic fractal arrays in the form of Paskal-Sierpinski gaskets was first studied by Lakhtakia et al. [18]. In particular, the radiation characteristics were examined for Paskal-Sierpinsi arrays, comprised of Hertzian dipole sources located at each of the gasket nodes. A family of nonuniform arrays, known as Weierstrass arrays, was

first introduced in [19]. These arrays have the property that their element spacings and current distributions are self-scalable and can be generated in a recursive fashion.

Chapter II: Literature Survey

2.1 Frequencies and Systems

Prior to the 1990s, first generation (1G) analog mobile phones operated in a single frequency band. In Europe, for example, the Total Access Communication System (TACS) operated in a band from 880 to 960 MHz, whereas in North America the Advanced Mobile Phone System (AMPS) operated in a band from 824 to 894 MHz. Hence, early antenna designs were single-band and relatively narrowband. We define the fractional bandwidth of a system as

$$B_F = \frac{f_2 - f_1}{\sqrt{f_1 f_2}} \times 100 \tag{2.1}$$

Where f_1 and f_2 are the lower and upper frequencies of the band, respectively. Using this definition, the fractional bandwidths of AMPS and TACS are approximately 9%. Both use a frequency division duplex (FDD): for TACS 880 to 915 MHz is used for transmission and 925 to 960 MHz is used for reception, whereas for AMPS, 824 to 849 MHz and 869 to 894 MHz are used for transmission and reception, respectively.

First generation systems were largely incompatible: a phone bought in one country could not be used in another. This changed with the introduction of digital second generation (2G) systems in the 1990s. The Global System for Mobile Communications (GSM) was introduced in Europe and subsequently much of the world and a digital version of AMPS—the Interim Standard 54 (IS-54)—was introduced in America. The latter evolved into IS-136 and is often referred to as D-AMPS (digital AMPS) or TDMA (since it employs a time division multiple access scheme). GSM allowed global operation in the original TACS band from 880 to 960 MHz, and then later in a band from 1,710 to 1,880 MHz, leading to a requirement for dual-band operation. However, these frequency bands were not available worldwide: in particular, a different band (1,850–1,980 MHz) was utilized in the United States for IS-54, IS-136, a third system, IS-95, and eventually GSM. This led to the introduction and widespread adoption of tri-band GSM phones. Indeed, quad-band GSM phones eventually emerged, as the frequency bands associated with AMPS in the United States (824–894 MHz) were reallocated to GSM (among other systems).

With the aim of increased mobility and functionality compared to their 2G predecessors, third generation (3G) systems were introduced, first in Japan in 2001, then in Europe in 2003, and

subsequently in many other countries worldwide. When second generation systems were introduced, they largely replaced first generation systems. However, 3G systems were introduced to sit alongside existing 2G systems. New spectrum was allocated for 3G services in Europe, Japan, and many other countries, offering the prospect of increased total capacity.

However, once again common new spectrum was not available worldwide, which led to a number of frequencies being allocated for 3G, many of which coincide with the frequencies that are used for 2G. Where this happens, it is expected that the 2G systems will eventually be phased out. The International Telecommunication Union (ITU)—the international body that regulates radio and telecommunications worldwide (and an agency of the United Nations)—allowed several different types of systems to be called 3G under the umbrella of International Mobile Telecommunications-2000 (IMT-2000). Two worldwide variants of 3G emerged, one based on code division multiple access (CDMA) and another based on wideband code division multiple access (WCDMA). The latter is based on work that began in the early 1990s towards a successor of GSM named the Universal Mobile Telecommunications System (UMTS). This later became known as UTRA (UMTS Terrestrial Radio Access)—a term used to describe the UMTS radio access solution. Shared 2G/3G bands are indicated. Common combinations of bands are as follows:

- Tri-band GSM: In bands VIII, III, and II
- Quad-band GSM: In bands V, VIII, III, and II
- Triband GSM, single-band UMTS: GSM in bands VIII, III, and II. UMTS in band I
- Quad-band GSM, triband UMTS: GSM in bands VIII, III, II, and I. UMTS in band V, II, and I.

The bands involved are shown in Figure 2.1. At around the same time that 3G was launched on the market, Bluetooth radios were introduced into phones to allow short-range communications with other devices in an industrial, scientific and medical (ISM) band centered at 2.4 GHz. In effect, this meant that some phones became tri-mode. Since the different modes may also operate in different frequency bands, phones also became increasingly multi-band.

This trend towards the inclusion of more systems operating in more bands continued with the introduction of the Global Positioning System (GPS), Wi-Fi and new systems such as mobile

television (with several standards and bands proposed) and WiMAX (again with several bands). Importantly, many of these systems may be required to operate simultaneously.

The evolution of the current systems to the 4G is based more and more on a key idea: interoperability. In the futures systems, a single terminal should be capable to work in anywhere, at any moment and in any interface, resulting in a convergence of services. Like this, the futures systems should be so much interoperable with the futures systems as with the legacy, in way to allow a soft migration among the several air interfaces.

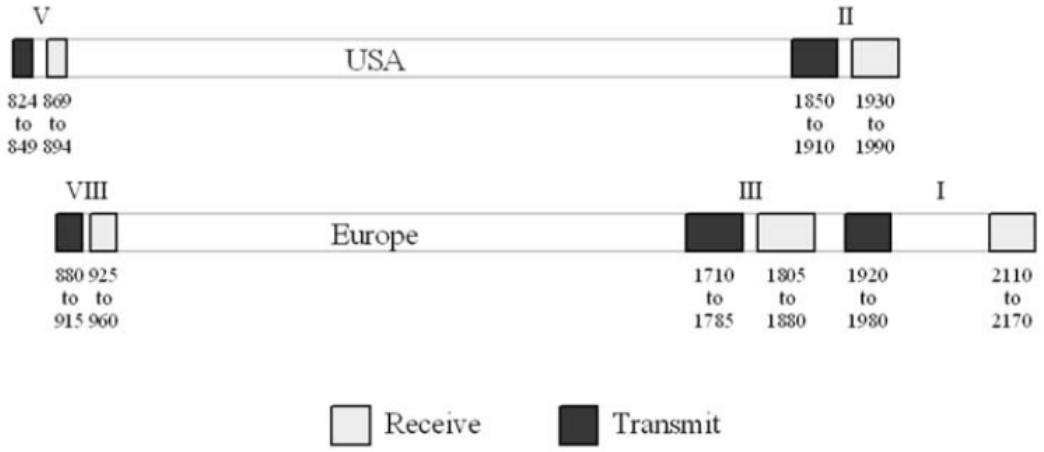

Figure 2.1: Common cellular frequency bands (MHz) used in Europe and the United States, with their UTRA band designations.

With the crescent growth of standards based on access techniques CDMA, the obtaining of the DOA becomes more and more necessary in way to implement SDMA systems. Following this, with the new techniques based on intelligent antennas capable to select the CDMA user wanted (UOA) and to discover the frequency and the delay profile of arrival (FOA and τOA), the use of antennas arrays is configured as indispensable technique in the modern systems.

Multimode, multiband operation presents a formidable challenge to mobile phone designers, particularly for the RF parts. Of these, the antennas occupy the largest volume and, hence, have the biggest impact on the (commercially crucial) styling of the device. It is well-known that antenna bandwidth is proportional to volume. However, the space allocated to the antenna(s) has not increased: on the contrary, it is tending to decrease due to the demand for thinner, more highly stylized devices. If this were not enough, there is also increasing pressure on mobile phone manufacturers to improve performance, particularly in countries

with areas of low population density, where, due to the large distances involved, cellular coverage is often “patchy.”

The multiband antenna must be capable of providing a good gain and bandwidth compatible with the future and current systems. Such antenna should still offer good characteristics regarding its size and weight, so that it could be used in mobile, portable or fixed stations terminals. A natural way for these antennas has been the application of the fractal theory, which allows the project of multiband antennas with reduced sizes.

Fractals make possible the use of a single small antenna operating in several frequency bands. The self-similar properties of certain fractals result in a multiband behaviour of the antennas while, the highly convoluted shape of these fractals makes possible the reduction in size, and consequently in mass and volume of certain antennas [20]. Fractal shapes radiate signals at multiple frequency bands, occupy space more efficiently and offer design solutions meeting the requirements for antennas in future wireless devices. These reductions can make possible to combine multimedia, communication and teledetection functionalities in a reduced space like a handy phone, a wristwatch or a credit card e.g. a fractal antenna can provide GPS (Global Positioning System) services within a conventional mobile cellular phone.

2.2 Limitations on Small Antennas

With fast growing development of wireless communication systems there has been an increasing need for more compact and portable communications systems. Just as the size of circuitry has evolved to transceivers on a single chip, there is also a need to evolve small sized, high-performance and low cost antenna designs which are capable of adjusting frequency of operation for integration of multiple wireless technologies and decrease in overall size. However when the size of the classical antenna (designed using Euclidean geometry) is made much smaller than the operating wavelength it becomes highly inefficient because radiation efficiency and impedance bandwidth decrease with the size of the antennas because these effects are accompanied by high currents in the conductors, high ohmic losses and large values of energy stored in the antenna near field. Limits of an electrically small antenna can be analyzed by assuming the antenna to be enclosed with a radian sphere of radius a [21]. The limit for the smallest possible quality factor, Q for any antenna within the radian sphere regardless of its shape can be described as:

$$Q = \frac{1 + 2(ka)^2}{(ka)^3(1 + (ka)^2)} \tag{2.2}$$

An antenna is said to be small when it can be enclosed into a radian sphere, i.e. a sphere with radius a, where $a = \lambda / 2\pi$. Due to the variations of the current inside, the radian sphere the field outside the radian sphere can be described as a set of orthogonal spherical vector waves. For such antennas a fundamental limitation on the Q is established by Chu as:

$$Q = \frac{1}{k^3 a^3} + \frac{1}{ka} \tag{2.3}$$

This forms the lower fundamental limit of the Q factor that can be achieved by a linearly polarized antenna and is established regardless of the antenna current distribution inside the sphere. The current distribution inside the sphere is not uniquely determined by the field distribution outside the sphere so several current distributions can lead to the same Q factor. Here Q is described according to the stored electric energy W_e , magnetic energy W_m , frequency ω and average radiated power P_r as:

$$Q = \omega \frac{2W_e}{P_r}, \qquad W_e \gg W_m \tag{2.4}$$

$$Q = \omega \frac{2W_m}{P_r}, \qquad W_e \gg W_m \tag{2.5}$$

An infinitesimally small antenna radiates only a TE_{01} or TM_{01} spherical mode that depends on the electric size of the antenna given byka, where k is the wave number at resonance and a is the radius of the smallest sphere that encloses the antenna [22]. The real power is radiated because of propagating modes, while the reactive power is due to all modes. However when the radian sphere becomes very small there are no propagating modes and only less real power. Further the radiation resistance decreases while proportionally the reactive energy stored in the antenna neighbourhood increases rapidly which contributes to large Q values. In general the Q of an antenna is inversely proportional to its bandwidth thus implying narrow bandwidth for antennas with high values of Q. Narrow bandwidth antennas are not usually preferred because of the difficulty of matching. Achieving a low Q antenna basically depends on how efficiently it uses the available volume inside the radian sphere. Thus the high currents in the conductors, high ohmic losses, large values of the stored energy

is the antenna near field and high Q values make the performance of small antennas inefficient.

2.3 Fractals as Antenna Elements

Small antennas are of prime importance because of the available space limitation on devices and the oncoming deployment of diversity and multi-input multi-output (MIMO) systems. The basic antenna miniaturization techniques can be summarized into lumped-element loading, material loading, and use of ground planes, short circuits, the antenna environment and finally the antenna geometry. Among these techniques the antenna geometry optimization and use of ground planes can achieve miniaturization or compactness of the antenna while maintaining the good antenna performance in terms of bandwidth and efficiency. However the classical small antennas suffer from inefficient performance. Fractal geometry provides the solution by designing compact and multiband antennas in a most efficient and sophisticated way. The general concepts of fractals can be applied to develop various antenna elements [23]. The properties of these fractal designed antennas allows for smaller, resonant antennas that are multiband and may be optimized for gain. When antenna elements or arrays are designed with the concept of self-similarity for most fractals, they can achieve multiple frequency bands because different parts of the antenna are similar to each other at different scales. Application of the fractional dimension of fractal structure leads to the gain optimization of wire antenna and the self-similarity makes it possible to design antennas with very wideband performance.

2.3.1 Fractals as Miniaturized Antennas

Wire antennas miniaturization is usually based in packing a long wire inside a small volume with the aim to achieve the smallest antenna having a given resonant frequency or, equivalently, achieving the lowest resonant frequency of an antenna having a fixed size. In the miniaturization of wire antennas it has been found that the electromagnetic coupling between wire angles limits the reduction of the resonant frequency with increasing wire length. In principle, it is expected that the longer the wire length, the lower is the resonant frequency. Fractal geometry can be employed to design self resonant small antennas in which effective reduction in the resonant frequency can be obtained. It should be noted though applying fractal geometry to reduce the size of the wire antenna a reduction in resonant frequency is obtained. The effect can be explained with the help of Koch fractal curve to

understand the behaviour of the resonant frequency of fractal antennas as a function of the antenna geometry and wire length. It has been found that with increase in number of iterations, n, the effective length increases by a factor of $(4 / 3)^{n}$. Thus with an increase of the wire length of a Koch fractal there is a decrease in the resonant frequency. The observed behaviour can be further explained due to the coupling fact between the sharp angles at curve segment junctions as shown in Figures 2.2 and 2.3. These angles radiate a spherical wave with phase center at the vertex. Each angle not only radiates, but also receives the signal radiated by other angles. As a consequence, part of the signal does not follow the wire path, but takes shortcuts that start at a radiating angle. The length of the path travelled by the signal is, therefore, shorter than the total wire length. The degree of coupling between parallel wire segments with opposite current vectors causes a significant reduction in the effective length of the total wire, and therefore an increase in the resonant frequency. When used as wire antenna the fractal antennas leads to more effective coupling of energy from feeding transmission lines to free space in less volume. Similarly when used as loop antennas, the fractal antennas with increased length it raises the input resistance of a loop antenna.

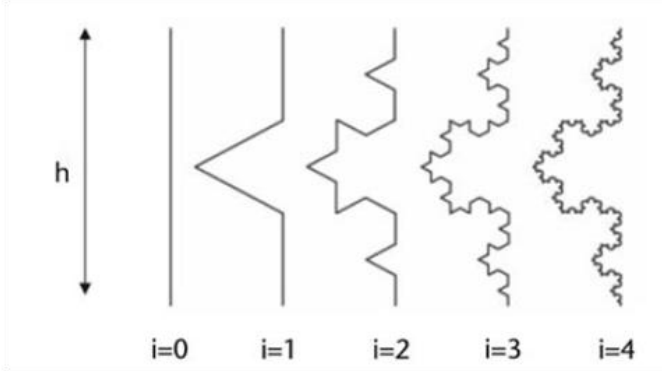

Figure 2.2: Different iterations of the Koch monopole.

2.3.2 Fractals as Multiband Antennas

It has been found that for an antenna, to work well for all frequencies i.e. show a wideband/multiband behaviour, it should be:

- **Symmetrical:** This means that the figure looks the same as its mirror image.
- **Self-similar:** This means that parts of the figure are small copies of the whole figure.

These two properties are very common for fractals and thus make fractals ideal candidates for design of wideband /multiband antennas [24].

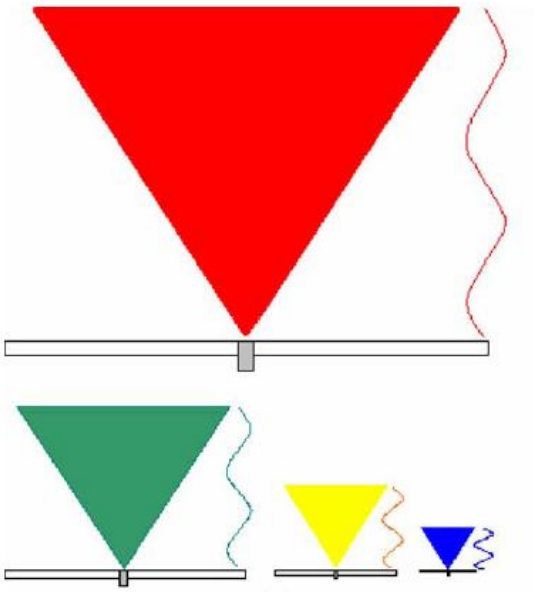

Figure 2.3: Four antennas (with a wave cartoon) intended to be used for four discrete frequency bands.

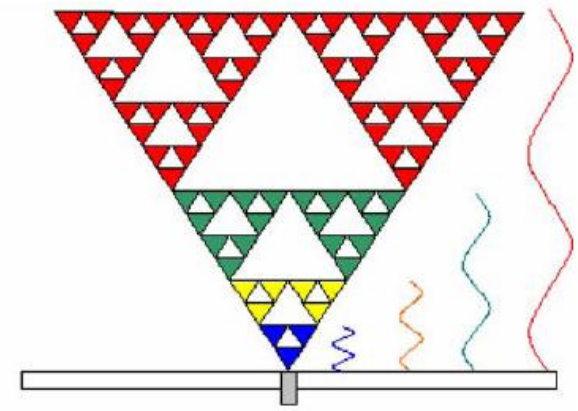

Figure 2.4: One antenna intended to be used as a four-band antenna using the fractal geometry of Sierpinski gasket.

Traditionally a wideband/multiband antenna in the low frequency wireless band can only be achieved with heavily loaded wire antennas which usually imply that different antennas are needed for different frequency bands [25]. Recent progresses in the fractal antennas suggest solution for using a single small antenna operating in several frequency bands. The self similarity properties of the fractal structures are translated into the electromagnetic behavior when used as antenna. This multiband behavior can be explained with the help of a Sierpinski triangle (gasket) antenna employing Sierpinski fractal geometry with a self similar structure. Figure 2.3 show a typical antenna system in which a single antenna is used for each application that is intended for each different frequency band (four bands in this figure).

However, use of Sierpinski triangle (Gasket) allows a structure in which only single antenna is intended to be used for all of the four frequency bands as illustrated in Figure 2.4.

2.3.3 Cost Effectiveness of Fractal Antennas

One practical benefit of fractal antenna is that it is resonant antenna in a small space thereby excluding the need of attaching discrete components to achieve resonance. Usually at UHF and microwave antenna the cost for such parts for the transceivers can become more expensive than the antenna [26]. Further the addition of parts produces reliability issues and breakage/return problems. In most of applications fractal antennas are small bendable etched circuit boards or fractal etchings on mother boards and contain no discrete components. This makes design of fractal antennas a cost effective technique [27].

2.4 Different Fractal Antennas

As discussed earlier the general concepts of fractals can be applied to develop various antenna elements. Several frequency independent antennas can be generalized as fractal antennas. Small antennas have several limitations in tradeoffs of directivity, bandwidth and radiation efficiency. Recent work on fractal elements suggests that apparently complex structures like fractals perform fairly well when their sizes are electrically small (i.e. far less than a wavelength in size, but not in the limit of zero size). Fractal antennas can take on various shapes and forms depending on the different fractal geometries. Antennas using some of these geometries for various telecommunications applications are already available commercially. Cohen was the first to develop an antenna element using the concept of fractals [19]. He demonstrated that the concept of fractal could be used to significantly reduce the antenna size without degrading the performance. The first application of fractals to antenna design was thinned fractal linear and planar arrays as wideband arrays and multiband performance was obtained by arranging elements in a fractal pattern to reduce number of elements in an array. The multiband capability of fractals by studying the behavior of the Sierpinski monopole and dipole was demonstrated by Puente et al [25]. The Sierpinski monopole displayed a similar behavior at several bands for both the input return loss and radiation pattern. Multiband or ultra wideband antennas can also be obtained by using other structures of fractals [28]. In some designs, fractal structures are used to achieve a single very wideband response, such as in printed circuit fractal loop. Some of the different types of fractal antennas which have been found in use are:

2.4.1 Sierpinski Gasket

Carlos Puente has published four works of interest on this antenna .Although description and experimentation is documented in [25] and [29].The authors present variations on the sierpinski geometry and present the effects of these variations on the characteristics of the antenna in [30] and [31].These two papers describe the effects of modifyingthe geometry of the sierpinski gasket.The desired changes are improved matching and control of the multiple bands.The sierpinski antenna is fabricated and measured verifying previous results in [32].

The simulated predictions of the current distribution over the Sirpinski gasket antenna showing the multiband nature of the antenna were verified using infrared thermograms in[33].The authors fabricated the antenna and measured the current distribution with a near field thermogram technique.

In[34] an efficient numerical model is presented for predicting the input performance of a sierpinski gasket antenna .The numerical models are compared with measured input matches of fabricated sirpinski gasket antennas.

Similar experimentation showing how the multiband characteristics of the sierpinki gasket antenna is unique to this geometry and not all fractals is shown in [35].In this work,the sierpinski gasket is compared to a sierpinski carpet,a similar geometry with a square starting shape rather than a triangle ,as is the case for a sierpinski gasket .The results donot show a multiband characteristics like that found with the sierpinski gasket.

The sierpinski gasket antenna was also analyzed using the time domain electric-field integral equation using a marching-on-in-time procedure in[36].

This type of antenna has been explored in other configurations ,as well.In [37],the author shows how sandwiching the antenna between scaled copies of itself increases the bandwidth of the antenna .While a single Sierpinski gasket has distinct bands,this technique can be used to improve the match between bands .Improved bandwidth using this technique and variations of the Sierpinski carpet fractal were shown in[38].

Another use of the sierpinski gasket was explored in [39]. Here, the fractal geometry was utilized to develop a multiband frequency selective surface(FSS).

A design methodology of planar fractal antennas using RCGA in conjunction with electromagnetic simulations has been presented in [40]. One of the major advantages of this

novel scheme for designing fractal microstrip antenna is that it works without the prior knowledge of any design equations.

A planar, dual-wideband monopole antenna using a modified half-Sierpinski fractal concept is proposed in [41]. An improved closed-form formula for the resonant frequencies of a Sierpinski gasket antenna has been proposed in [42]. It includes the number of firactal iterations, the side length of the generating triangle, and substrate parameters.

Sierpinski gasket antenna with an iterative model in detail has been discussed in [43]. Equilateral triangle is the simplest one and the result is compact. But the sample iterative model can be used to other structure Sierpinski gasket antenna and the log-periodic parameter can be obtained.

Sierpinski fractal monopole antenna and its scale factor variations are presented in [44]. In [45] new multiband antenna based on a triangular monopole over a modified ground plane has been presented. The ground plane is based on a Sierpinski gasket. It has been shown as the use of the fractal-based ground plane introduces new matched bands and can improve the existing ones. The behavior of the conformal Sierpinski fractal microstrip antenna has been demonstrated through numerical simulation in [46]. In this conformal antenna, classic Sierpinski gasket is mounted on a cylinder.

2.4.2 Koch Dipole

The Koch dipole has been researched as a means of miniaturizing dipole antennas. There have been several works which have looked into this topic .A descriptive source of information on this antenna can be found in[47].They describe the miniaturization effects as they relate to the iteration of the fractal. The Koch dipole is also used in [48] in an investigation of the necessary requirements for frequency independent antennas. The Koch monopole is fabricated and measured verifying previous results in [32].

2.4.3 Fractal Trees

Electrochemical deposits that grow into tree like patterns have been studied in[49].This particular type of fractal is not deterministic like the other fractals that have been observed. This type of fractal is grown randomly resulting in various scaled branches .The idea of this line of research was to observe the multiband results of this fractal from the variations of scale in the geometry.

A deterministic fractal tree was studied in [50]. Here, the authors studied the correlation between the fractal dimension and the resulting input match. The tree fractal that was used is variational enough to easily control the fractal dimension. In [35], the authors explore the multiband characteristics of a deterministic tree fractal. A correlation is made between the number of resonant bands and the fractal iteration of the geometry. In [51], the authors study a two dimensional ternary tree antenna as a monopole over a ground plane. The antenna shows distinct resonances corresponding to the self similar scales in the geometry .Between the bands, however the input resistance is very low ,leading the authors to suggest that the structure could be well suited as a multiband filter or absorber.

2.4.4 Fractal Arrays

The idea of using fractal spacing for arrays has been investigated by several researches. In references [52, 53, 54], the spacing of the array was shaped using fractal geometrise, while the elements were standard Euclidean shapes. Article [54] is a very thorough study on this topic.

Arrays with the distribution of a cantor set has been the topic of these papers, [55,56]. A cantor set distribution is also implemented in [57, 58] for the spacing of an array .Similar features of the patterns of the arrays compare to similarities in the spacing geometry. Also, Cantor Sets of the different fractal dimension are simulated, showing a correlation between the maximum side lobe level and the fractal dimension. A derivation of the radiation patterns for cantor sets distributed currents is presented in [59]. In paper [60], the authors present an analysis of array elements in a Sierpinski carpet configuration to create sum and difference patterns.

Simple procedure for evaluating the impedance matrix of the Peano-Gosper fractal array has been presented in [61]. Phased array antennas can be focused by deploying proper phase excitations on the array elements. Fractal geometry has been applied to focused arrays. The binary tree fractal geometry was applied to element positions [62]. The performances of the arrays investigated show that fractal antennas can be similarly focused, while giving their favorable properties. The fractal technique was proved efficient for the design of a DRA of 960 elements which produce nineteen pencil beams for a satellite communication network. Sierpinski gasket fractal array antenna has been discussed in detail in [63].

Chapter III: Gaps and Methodology

In the previous chapter detail discussion on the fractal antennas has been done. It is found that the main focus of the previous work done has been mainly on the monopole Sierpinski gasket antenna. No work so far has discussed all the parameters related to Sierpinski gasket dipole antenna design. Taking into consideration the field of fractal array arrays with the distribution of a cantor set, has been the topic of many papers, very little work has been done in implementing different fractal geometries as fractal arrays.

Next chapter discus the bowtie antenna geometry which is straightforwardly expanded to one of the simplest fractal antennas: the so-called Sierpinski fractal antenna or Sierpinski gasket. Very basically, the Sierpinski fractal is none other than a bowtie with a specially arranged hole structure. Fractal antennas are not broadband in the conventional sense but rather "multiband". Detailed analysis of Sierpinski fractal antenna is done with its comparison with bow-tie antenna, the simulation is one based on Method of Moments (MoM) and is done using MATLAB®. Numerical results of the antenna radiation characteristics, including input impedance, input reflection coefficient, gain, radiated power and radiation pattern, are presented for mode-2 Sierpinski fractal and compared with that of a bowtie antenna.

The application of fractal geometries to generate an optimized antenna array is discussed using Sierpinski gasket, the radiation pattern of planar two-dimensional periodic, random and fractal arrays are discussed the simulation is done using MATLAB®

3.1 Impedance Matrix

The square impedance matrix determines electromagnetic interaction between different edge elements .If edge elements m, n are treated as small but finite electric dipoles, the matrix element $Z_{m,n}$ describes the contribution of dipole *n* (through the radiated field)to the electric current of dipole *m* and vice versa. The size of the impedance .matrix is equal to the number of edge elements. The impedance matrix does not depend upon the

The vast majority of computational work is connected to impedance matrix calculations of an antenna structure. The impedance matrix does not depend on the problem statement (radiation or scattering); instead it depends on frequency . The impedance matrix of the electric field integral equation has a typical diagonal dominance.

Below we reproduce the derivation of the impedance matrix for the RWG elements. Quantitatively the impedance matrix of the electric field integral equation is given by

$$Z_{m,n} = l_m[j\omega(\mathrm{A}^{-}_{\mathrm{mn}} \cdot \rho^{\mathrm{c}-}_{\mathrm{m}}/2 + \mathrm{A}^{-}_{\mathrm{mn}} \cdot \rho^{c-}_{\mathrm{m}}/2) + \phi^{-}_{\mathrm{mn}} - \phi^{+}_{\mathrm{mn}}] \tag{3.1}$$

Where indexes m and n correspond to two edge elements; (.) denotes the dot product, l_m is the edge length of elements m; $\rho^{\mathrm{c}-}_{\mathrm{m}}$ are vectors between the free vertex point ,v_m=and the centroid point ,$r_m^{c\pm}$of the two triangles $T_m^{\pm}$ of the edge element m,respectively .ρ_m^{c-} is directed toward the vertex of triangle T_m^{-}.The vectors $\rho_m^{c\pm}$are easily expressed through the known quantities using two simple formulaes

$$\rho_m^{c+} = r_m^{c+} - v_m^{+} \quad , \qquad \rho_m^{c-} = -r_m^{c-} + v_m^{-} \tag{3.2}$$

the expressions for vector A and scalar ϕ have the form (A is the magnetic vector potential and ϕ is the scalar potential)

$$A^{\pm}_{m,n} = \frac{\mu}{4\pi}\left[\frac{I_n}{2A_n^{+}}\int\limits_{T_n^{-}} \rho_n^{+}(r')g_m^{\pm}(r')dS' + \frac{I_n}{2A_n^{-}}\int\limits_{T_n^{-}} \rho_n^{-}(r')g_m^{\pm}(r')dS'\right] \tag{3.3}$$

$$\phi^{\pm}_{m,n} = -\frac{1}{4\pi j\omega\epsilon}\left[\frac{I_n}{A_n^{-}}\int\limits_{T_n^{-}} g_m^{\pm}(r')dS' - \frac{I_n}{A_n^{-}}\int\limits_{T_n^{-}} g_m^{\pm}(r')dS'\right] \tag{3.4}$$

Where

$$g_m^{\pm}(r') = \frac{e^{-jk|r_m^{c-}-r'|}}{|r_m^{c-}-r'|} \tag{3.5}$$

3.2 Moments Equations And Surface Currents

The surface current density on a surface *S* of the plate or on other perfectly electrically conducting (PEC) structures is given by an expression into RWG basis functions over *M* edge elements

$$J = \sum_{m=1}^{M} I_m f_m \ , \quad f_m = \begin{cases} \left(\frac{l_m}{2A_m^{+}}\right)\rho_m^{+}(r), & r\ in\ T_m^{+} \\ \left(\frac{l_m}{2A_m^{-}}\right)\rho_m^{-}(r), & r\ in\ T_m^{-} \\ 0, & otherwise \end{cases} \tag{3.6}$$

If S is open ,we regard J as the vector sum of surface currents on opposite sides of S. The units of J are A/m. The expansion coefficients $I_m$form vector I, which is the unique solution of the impedance equation(or the moment equation)

$$Z.I = V \tag{3.7}$$

When the scattering problem is considered voltage vector is expressed by

$$V_m = I_m\left(E_m^+.\frac{\rho_m^{c-}}{2} + E_m^-.\frac{\rho_m^{c-}}{2}\right), \quad E_m^{\pm} = E^{inc}(r_m^{c\pm}), \qquad m = 1 \ldots\ldots M \tag{3.8}$$

Where E^{inc} is the electric feild of an incident electromagnetic signal; (.) denotes the dot product .The voltage excitation vector to the circuit voltage but has units of V.m.

For the plate assume that the incident signal is a plane wave directed perpendicular to the plate(normal incidence).The plane wave has only one E-component in the x-direction,$E^{inc} = [E_x\ 0\ 0]$, and this component is equal to $E_x = 1 \times \exp(-jkz)\,V/m$,where k=ω/c is the wave number .If the plate is located at z=0, then $E^{inc} = [1\ 0\ 0]V/m$.Vector [1 0 0] describes the polarization of the plane wave .

3.3 Visualization of Surface Currents

The expansion coefficients I_m are not yet the surface current. The surface current density, J_k for a given triangle k is obtained in the form

$$J_k = \sum_{m=1}^{M} I_M f_m(r)\,, \qquad R\ in\ T_k \tag{3.9}$$

A maximum of three edge elements contribute to triangle k. The y-component of the surface current in Figure3.1 is small in comparison with the x-component, so it is not shown there. It might appear at first sight that the results of Figure a and b are rather contradictory. The reason for this is that the surface current in the middle of the plate appears to be higher in Figure 3.1(a), whereas the surface current peaks are closer to two horizontal edges in figure 3.1(b). As a matter of fact such a difference is due to a singular behaviour of the current at two horizontal edges of the plate where its value tends to infinity on an ideal case.

The more boundary elements we have , the higher the currents at the boundary are. When the colour bar extends from the minimum to the maximum current magnitude, as in Figure 3.1 ,

then the current on the rest of the plate appears smaller in comparison with these high values. That is why the middle part of the plate seems "darker" in Figure3.1 (b) that in Figure 3.1(a).

To put some numbers on these data, we consider two plate cuts: at AA' and BB', as shown in Figure 3.2(a) and Figure 3.2 (b) shows the surface current distribution along these cuts normalized to the incident magnetic field.

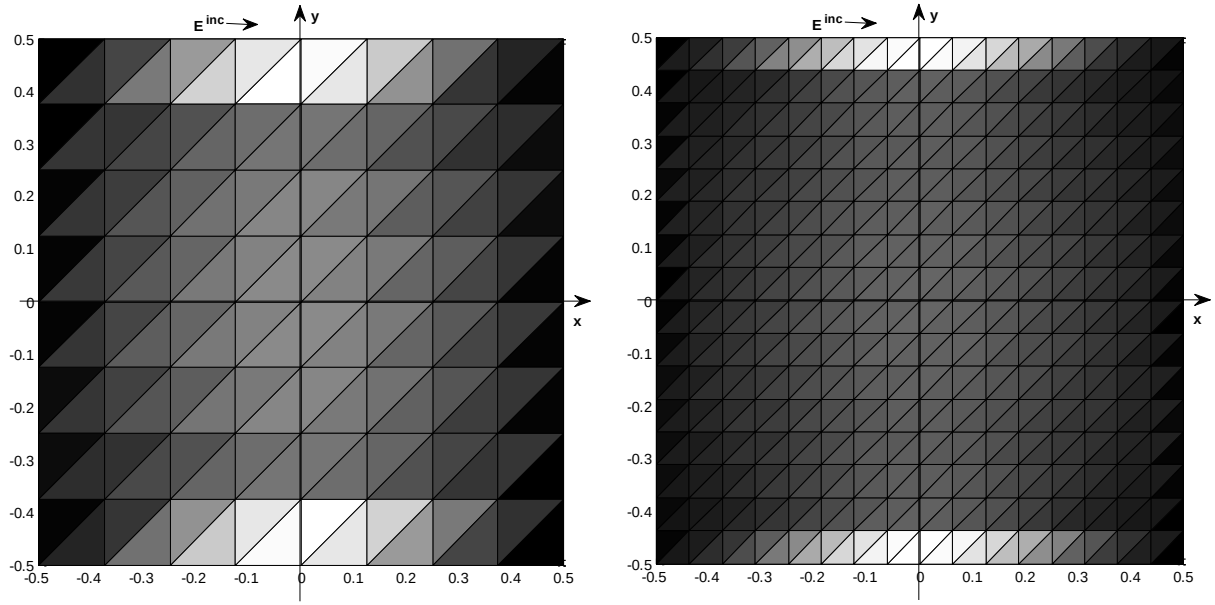

(a) (b)

Figure 3.1: The surface current distribution on, $|J_x|$, on a 1×1m plate at a frequency of 300 MHz (plate length is equal to the wavelength). The white colour corresponds to higher current magnitudes. (a) 176 edge elements; (b) 736 edge elements.

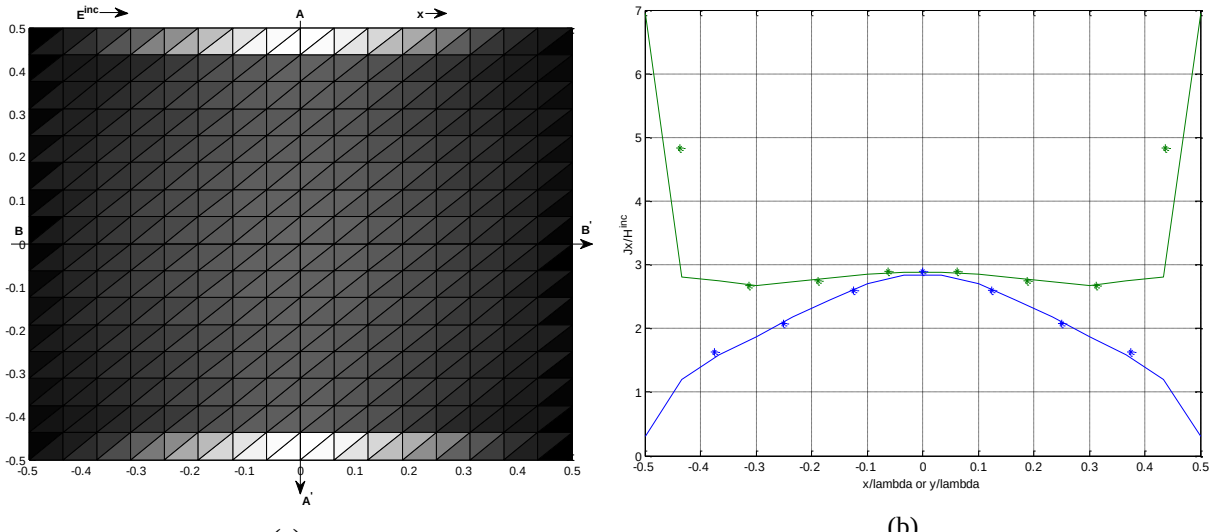

(a) (b)

Figure 3.2: Distribution of the dominant component of surface current, $|J_x|$, across the 1λ square flat plate with 736 edge elements. (a) two plate cuts; (b) co-polar current $|J_x|$ (solid line). The corresponding results of [64] are shown by stars.

3.4 Induced Electric Current of a Dipole Antenna

Although the case of the plate is worthy of note for the scattering purposes and radar cross-sectional modelling, the plate itself is hardly to be used as an antenna. A problem arises when we try to introduce the voltage gap into the plate.

The simplest practical antenna is a thin straight wire, whose direction coincides with the direction of incident electric field E^{inc}. It does not matter if we are using a cylinder wire or a thin strip equivalent thickness.

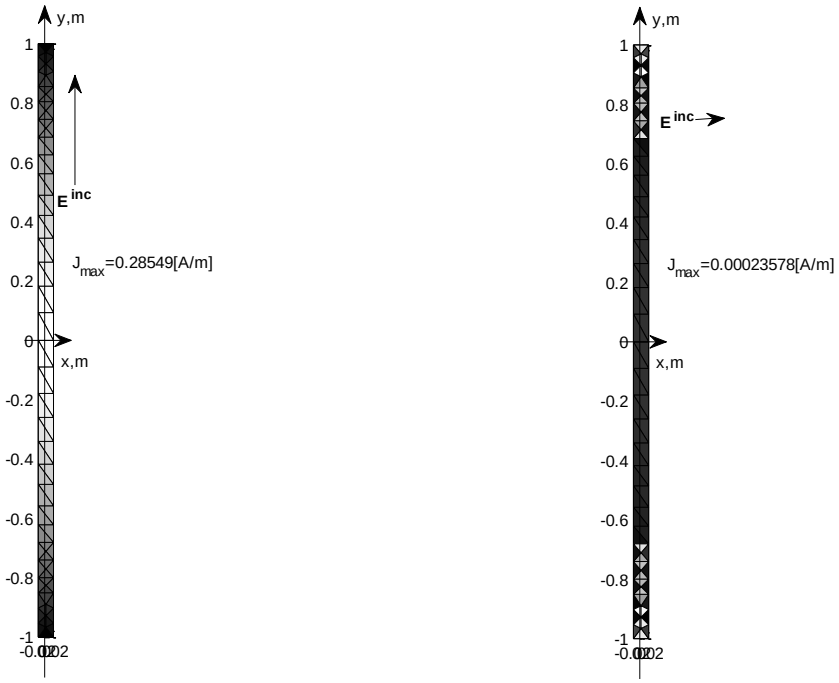

(a) (b)

Figure 3.3: Magnitude of the surface current density along the half-wavelength strip. (a) Incident electric field is directed along the strip axis; (b) incident electric field is perpendicular to the strip axis. The white colour corresponds to higher current density.

In case of Figure 3.3a, the incident electric field is having the amplitude of $1\,V/m$ and is directed along the dipole axis, the value of maximum surface current obtained is $0.2855\,A/m$ The maximum current in the middle of the dipole is thus $0.2855\,A/m \times 0.05m \approx 14mA$.

However if the incident electric field is directed perpendicular to the dipole axis, the maximum current density magnitude drops down to $2.36 \times 10^{-4} A/m$, which is more than a factor of 1000 (Figure 3.3b). This means that the dipole antenna is receiving nothing. Thus the dipole antenna is capable of receiving those signals whose E-field has a component

parallel to the dipole axis. Such antennas are known as polarized antennas or antennas with linear polarization.

3.5 Induced Electric Current of a Bowtie Antenna

In this section current distribution on a bowtie antenna is under study. The antenna length is $0.2m$ and the flare angle is 90^0. The width of the neck is $0.012m$.

If the incident signal is polarized along the y-axis, the maximum currents density appears in the area of the anticipated antenna feed (the neck area in figure 3.4a). However, if the signal is x-polarized the maximum current density appears at the edge of the antenna and is considerably small (figure 3.4b). The entire current distribution resembles that of a square plate (figure 3.1). The bowtie antenna is thus linearly polarized, similar to the dipole.

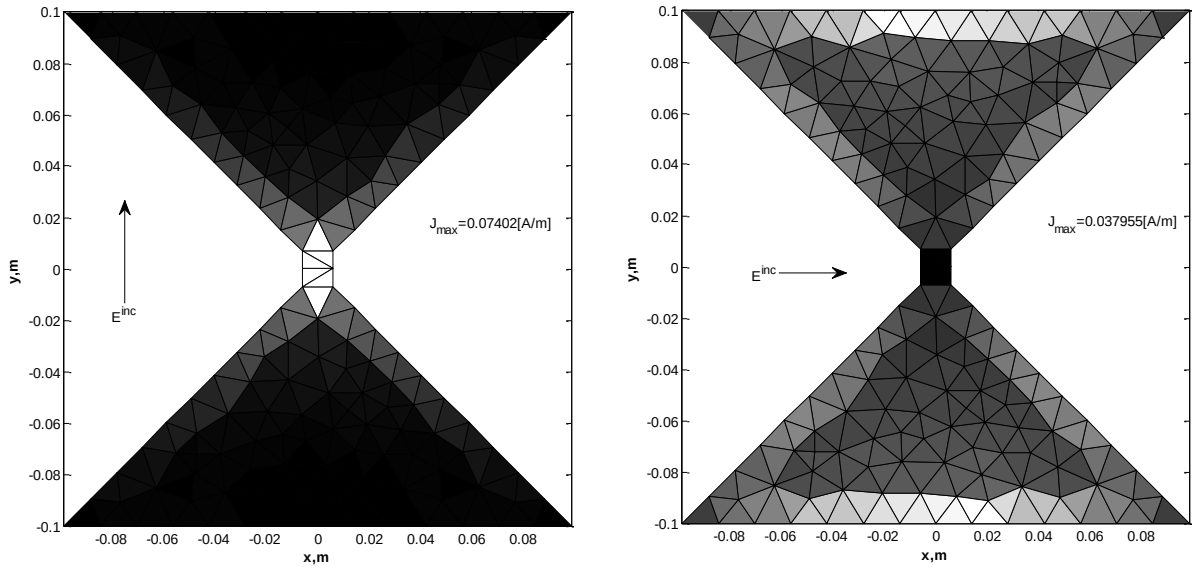

(a) (b)

Figure 3.4: Magnitude of the surface current for the bowtie antenna at 750MHz (a) The incident field is directed along the antenna axis; (b) the incident field is perpendicular to the axis. The white colour corresponds to higher current magnitudes.

For the bowtie antenna in Figure 3.4a, the maximum current in the antenna feed is $0.074 \times 0.012 \approx 0.012mA$. this value is considerable smaller than the corresponding result for the dipole ($14mA$). Th reason for the difference is that the dipole is 10 times longer than the bowtie antenna. If the dipole and the bowtie antenna will have the same lengths, comparable results must be obtained.

3.6 Induced Electric Current of a Slot Antenna

A simplest slot antennas is a slot cut in flat sheet metal surface .The slot antenna may have a very narrow central voltage gap .To simulate this gap, we introduce a junction in the middle of the gap . The length of the slot is 2m ,the width is 0.06m,the length of junction bridge is 0.06m,and the plate size is $3 \times 3m$.

Surprisingly, nothing really happens when the incident electric field is directed along the y-axis .The current in the slot junction is very close to zero (the junction is very dark), and the entire slot antenna just behaves like a solid plate .Such a situation is exactly the opposite of the dipole excitation from section 3.4. However, if the incident is wave is x-polarised ,then a large surface current flows through the gap.

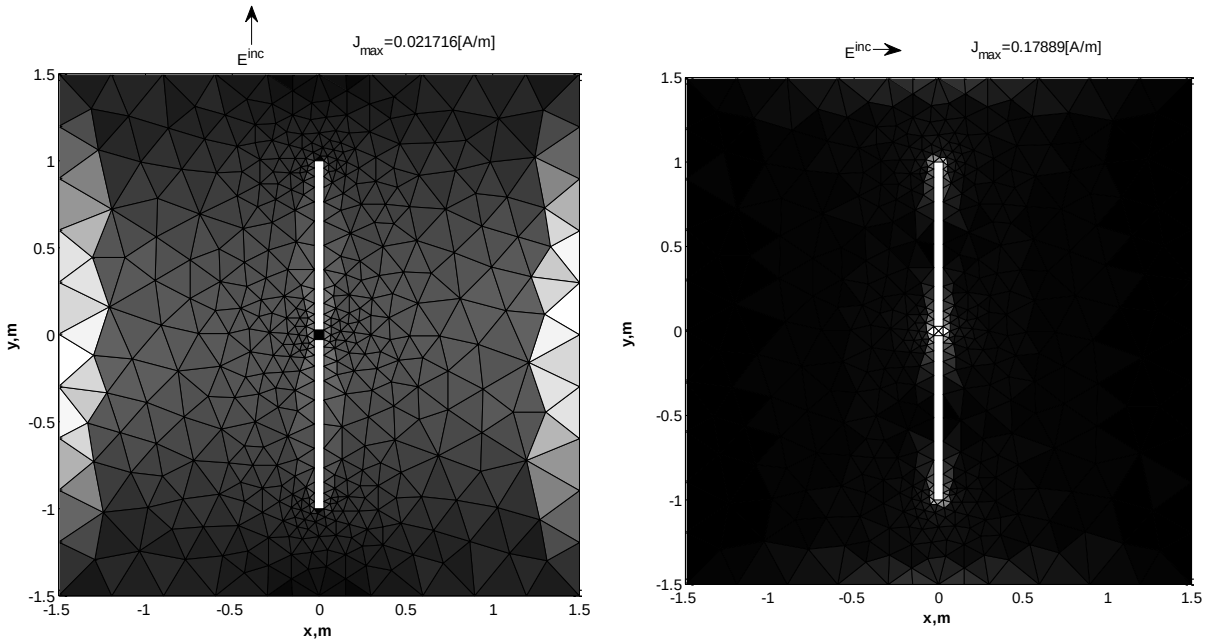

(a) (b)

Figure 3.5: Enlarged area of slot. (a) The incident field is directed along the slot axis; (b) the incident field is perpendicular to the slot.

For the slot antenna of total length $2m$ in figure 3.5b, the maximum current in the antenna feed is $0.179 \times 0.06 \approx 11\ mA$. This value is quite similar to the result for the dipole of the same length (14mA). Thus the dipole and slot antennas can be considered as "electric" and "magnetic" complementary antennas; a slot can be interchanged with the dipole of the same length, if we simultaneously interchange polarization (replace the electric field by the magnetic field).The slot and the dipole therefore constitute two linearly polarized complementary antennas with the perpendicular polarization directions. A coplanar

combination of the slot and the perpendicular dipole will thus receive a signal of nay polarization. Such a combination is frequently used in the patch antenna design.

3.7 Radiation of Surface Currents

Once surface currents are known on the antenna surface ,a radiated electromagnetic signal in free space can be found by a number of approaches .We are generally interested in the value of the electric field ,**E** and magnetic field, **H**, at any spatial point ,including both near and far field. In the near field **E** and **H** are independent and should be calculated separately.

One method is to use the electric and magnetic field integral equations with the observation point located somewhere outside the antenna surface [65-66].

Another approach, of nearly the same computational accuracy, is the so called dipole model [67]. In the dipole model the surface current distribution for each RWG edge element containing two triangles [68] is replaced by an infinitesimal dipole, having an equivalent dipole moment or strength .The radiated field of a small dipole is well known analytical expression [69-72].The total radiated field is then obtained as a sum of all these contributions of infinitesimal dipoles.

To find the equivalent dipole moment ,we refer to notations of [67] and consider a RWG element m with two inner triangles $T_m^{\pm}$adjacent to the edge of length l_m.The dipole moment ,**m**,which is the product of an effective dipole current and effective dipole length [73],is obtained by the integration of the surface current ,corresponding to the edge element m over the element surface:

$$\mathbf{m} = \int_{T_m^{+}-T_m^{-}} I_m \mathbf{f}_m(\mathbf{r}) dS = \int_{T_m^{+}-T_m^{-}} \mathbf{f}_m(\mathbf{r}) dS = l_m I_m (\mathbf{r}_m^{c-} - \mathbf{r}_m^{c+}) \tag{3.10}$$

Here $\mathbf{f}_m(\mathbf{r})$ is the RWG basis function corresponding to element m.The surface current coefficients $l_m$are known from the solution of the moment equations .The derivation of integral (3.10) is discussed in [67].The product $l_m I_m$is assocaited with the dipole current ,whereas the effective dipole length ,l is given by $|\mathbf{r}_m^{c-} - \mathbf{r}_m^{c+}|$ and is shown .

The radiated magnetic and electric fields of an infinitesimal dipole located at the origin [69] are expressed at a point r in terms of vector notations as

$$\mathbf{H}(\mathbf{r}) = \frac{jk}{4\pi}(\mathbf{m} \times \mathbf{r})Ce^{-jkr}, C = \frac{1}{r^2}\left[1 + \frac{1}{jkr}\right] \tag{3.11}$$

$$\mathbf{E}(\mathbf{r}) = \frac{\eta}{4\pi}\left((\mathbf{M} - \mathbf{m})\left[\frac{jk}{r} + C\right] + \mathbf{2MC}\right)e^{-jkr}, \boldsymbol{M} = \frac{(\mathbf{r} - \mathbf{m})\mathbf{r}}{r^2} \tag{3.12}$$

Here r=$|\mathbf{r}|; \eta = \sqrt{\mu/\varepsilon} = 377\Omega$ is the free space impedence .Eq 3.11 and 3.12 are the exact expressions ,without any far field approximations .Therefore they are valid at arbitrary distances from the dipole and not only in the far field .The practical limitation of the dipole model is thus restricted by size of the RWG elements .If the observation distance is on order of dipole length (on the order of RWG element length),then the model of the infinitesimal dipole performs poorly.

The total electric and magnetic field at appoint **r** are obtained as a sum over all edge elements .Equations 3.10 and 3.13 are programmed in the matlab.

$$\mathbf{E}(\mathbf{r}) = \sum_{m=1}^{M} \mathbf{E}_{\mathrm{m}}\left(\mathbf{r} - \frac{1}{2}(\mathbf{r}_m^{c+} + \mathbf{r}_m^{c-})\right) \qquad \mathbf{H}(\mathbf{r}) = \sum_{m=1}^{M} \mathbf{H}_m\left(\mathbf{r} - \frac{1}{2}(\mathbf{r}_m^{c+} + \mathbf{r}_m^{c-})\right) \tag{3.13}$$

3.8 Far Field

The results could be somewhat simplified in the far field ,at large radial distances r from the antenna or a scatterer .When viewed from a global perspective ,the field fronts in that zone have spherical form.However when viewed over a small range of nagles ,these fronts appearplanar ,which is one indication that they can be approximated as plane wves .E and H are prependicular to both each other and to the direction of propagation .Namely a right hand coordinate system is formed by the E and H field vectors and the direction of propagation .More precisely[69]

$$\mathbf{E}(\mathbf{r}) = \eta\mathbf{H}(\mathbf{r}) \times \frac{\mathbf{r}}{r}, \quad \mathbf{H}(\mathbf{r}) = \frac{1}{\eta}\frac{\mathbf{r}}{r} \times \mathbf{E}(\mathbf{r}) \tag{3.14}$$

We call the field given by equation (3.14) transverse electromagnetic TEM (to **r**) waves. These waves may be polarized in the direction perpendicular to the propagation direction but do not have a component in the direction of propogation.

More precise meaning of the far field (Fraunhofer region)by defining the far-field distancein the form

$$R_f = \frac{2D^2}{\lambda} \tag{3.15}$$

Where D is the maximum dimension of the antenna and λ is the wavelength .At $r > R_f$,equation 3.14 are a very good approx.

3.9 Field Regions

The space surrounding an antenna is usually subdivided into three regions : (a)reactive near field (b)radiating near field (c) far field (fraunhofer) regions shown in figure 3.6. These regions are so designated to identify the field structure in each. Although no abrupt changes in the field configurations are noted as the boundaries are crossed there are distinct differences among them .The boundaries separating these regions are not unique,although various criteria have been established and are commonly used to identify the regions.

Reactive near field region is defined as "that portion of the near field region immediately surrounding the antennas where in the reactive field predominates."For most common antennas ,the outer boundary of this region is commonly taken to exist at a distance $R < 0.62\sqrt{\frac{D^3}{\lambda}}$ from the antenna surface ,where $\lambda$is thewavelength and D is the largest dimension of the antenna .For a very short dipole radiator ,the outer boundary is commonly taken to a exist at a distance $\lambda/2\pi$ from the antenna surface .

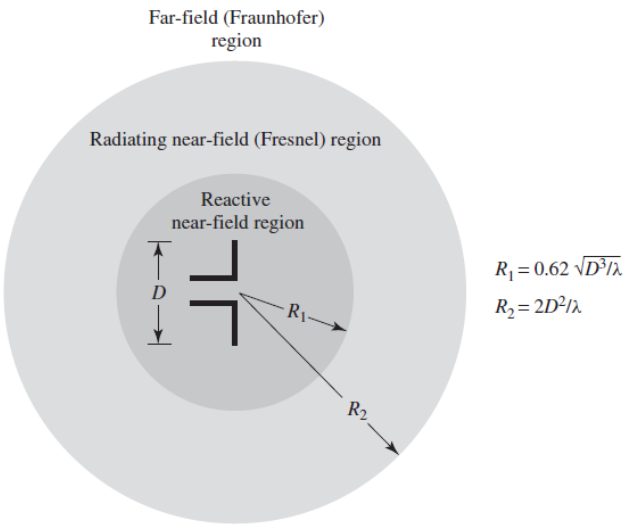

Figure 3.6: field regions of an antenna.

Radiating near field (Fresnel) region is defined as "that region of the field of an antenna between the reactive near field region and the far field region wherein radiation fields predominate and wherein the angular field distribution is dependent upon the distance from the antenna .If the antenna has a maximum dimension that is not large compared to the wavelength ,this region may not exist .For an antenna focused at infinity, the radiating near field region is sometimes referred to as the Fresnel region on the basis of analogy to optical terminology. If the antenna has a maximum overall dimension which is very small compared to the wavelength ,this field region may not exist."The inner boundary is taken to be a distance $R < 0.62\sqrt{D^3/\lambda}$and the outer boundary the distance $R < 2D^2/\lambda$ where D id the largest * dimension of the antenna .This criterion is based on a maximum phase error of $\pi/8$.In this region the field pattern is, in general a function of the radial distance And the radial field component may be appreciable.

Far field (Fraunhofer) region is defined as "that region of the field of an antenna where the angular field distribution is essentially independent of the distance from the antenna .If the antenna has a maximum overall dimension D the far field region is commonly taken to exist at distances greater than $2D^2/\lambda$ from the antenna .λ being the wavelength .The far field patterns of certain antennas ,such as multibeam reflector antennas are sensitive in phase over their certain antennas .For these antennas $2D^2/\lambda$ may be inadequate .In physical media ,if the antenna has a maximum overall dimension D which is large compared to $\pi/|\gamma|$,the far field can be taken to begin approximately at a distance equal to $|\gamma|D^2/\pi$ from the antenna ,γ being the propagation constant in the medium .For an antenna focused at infinity ,the far field region sometimes referred to as the fraunhofer region on the basis of analogy to optical terminology."In this region ,the field components are essentially transverse and the angular distribution is independent of the radial distance where the measurements are made .The inner boundary is taken to be radial distance $R = 2D^2/\lambda$ And the outer one at infinity.

To iliistrate the pattern variation as a function of radial distance ,we have included three patterns of a parabolic reflector calculated at distances of $R = \frac{2D^2}{\lambda}$, $R = 4D^2/\lambda$,and infinity. It is observed that the patterns are almost identical, except for some differences in the pattern structure around the first null and at a level below 25dB.Because infinite distances are not realizable in practice ,the most commonly used criterion for the maximum distance of far field observations is $\frac{2D^2}{\lambda}$.

3.10 Radiation Intensity

Radiation intensity in a given direction is defined as "the power radiated from an antenna per unit solid angle". The radiation intensity is afar field parameter, and it can be obtained by simply multiplying the radiation density by the square of the distance .In mathematical form it is expressed as

$$U = r^2 W_{rad} \tag{3.16}$$

Where

$U =$ radiation intensity $(W/unit\ solid\ angle)$

$W_{rad} =$ radiation density (W/m^2)

The radiation intensity is also related to the far-zone electric field of an antenna by

$$U(\theta,\varphi) = \frac{r^2}{2\eta}|E(r,\theta,\phi|^2 \simeq \frac{r^2}{2\eta}\left[|E_\theta(r,\theta,\phi|^2 + \left|E_\phi(r,\theta,\phi\right|^2\right]$$

$$\simeq \frac{1}{2\eta}\left[|E_\theta^o(\theta,\phi)|^2 + \left|E_\phi^o(\theta,\phi)\right|^2\right] \tag{3.17}$$

Where

$E(r,\theta,\phi) =$ far zone electric field intensity of the antenna $= E^o(\theta,\phi)\frac{e^{-jkr}}{r}$

$E_\theta, E_\phi =$ far zone electric field components of the antenna

$\eta =$ intrinsic impedance of the medium

Thus the power pattern is also a measure of the radiation intensity.The total power is obtained by integrating the radiation intensity,as given by 12,over the entire solid angle of 4π.thus

$$P_{rad} = \oiint_\Omega U d\Omega = \int_0^{2\pi}\int_0^{\pi} U \sin\theta\ d\theta\ d\phi \tag{3.18}$$

Where $d\Omega =$element of solid angle $=\sin\theta\ d\theta d\phi$

For an isotropic source ,U will be dependent of the angles θ ,as was the case for W_{rad}. Thus 3.18 can be written as

$$P_{rad} = \oiint_{\Omega} U_0 \, d\Omega = U_0 \oiint_{\Omega} d\Omega = 4\pi U_0 \tag{3.19}$$

Or the radiation intensity of an isotropic source as

$$U_0 = \frac{P_{rad}}{4\pi} \tag{3.20}$$

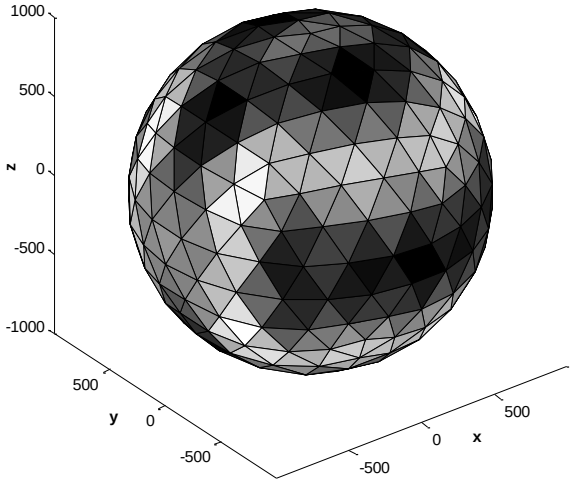

Figure 3.7: Radiation intensity distribution of the bowtie antenna at $4GHz$.

3.11 Directivity

Directivity of an antenna defined as the ratio of the radiation intensity in a given direction from the antenna to the radiation intensity averaged overall directions .The average radiation intensity is equal to the total power radiated by the antenna divided by 4π.If the direction is not specified ,the direction of the maximum radiation intensity is implied. "Stated more simply, the directivity of a nonisotropic source is equal to the ratio of its radiation intensity in a given direction over that of an isotropic source". In mathematical form using 3.20 ,it can be written as

$$D = \frac{U}{U_0} = \frac{4\pi U}{P_{rad}} \tag{3.21}$$

If the direction is not specified,it simply implies the direction of maximum radiation intensity(maximum directivity)expressed as

$$D_{max} = D_0 = \frac{U|_{max}}{U_0} = \frac{U_{max}}{U_0} = \frac{4\pi U_{max}}{P_{rad}} \tag{3.22}$$

D =directivity (dimensionless)

D_0 =maximum directivity (dimensionless)

U =radiation intensity (W/unit solid angle)

U_{max} =maximum radiation intensity (w/unit solid angle)

U_0 = radiation intensity of isotropic source (w/unit solid angle)

P_{rad} =total radiated power (W)

For an isotropic ,it is very obvious from 3.21 and 3.22 that the directivity is unity since $U, U_{max}, and\ U_0$ are all equal to each other.

For antennas with orthogonal polarization components ,we define the partial directivity of an antenna for a given polarization in a given direction as "that part of the radiation intensity corresponding to a given polarization divided by the total radiation intensity averaged overall directions ."With this definition for the partial directivity ,then in a given direction "the total directivity is the sum of the partial directivities for nay two orthogonal polarizations ."For a spheriacl coordinate system ,the total maximum directivity D_0 for the orthogonal $\theta\ and\ \varphi$ components of an antenna can be written as

$$D_0 = D_\theta + D_\phi \tag{3.23}$$

While the partial directivities $D_\theta$and D_ϕ are expressed as

$$D_\theta = \frac{4\pi U_\theta}{(P_{rad})_\theta + (P_{rad})_\phi} \tag{3.24}$$

$$D_\phi = \frac{4\pi U_\phi}{(P_{rad})_\theta + (P_{rad})_\phi} \tag{3.25}$$

where

U_θ =radiation intensity in a given direction contained in θfield component

U_ϕ =radiation intensity ina given direction contained in φfield component

$(P_{rad})_\phi$ =Radiated power in all directions contained in θ field component

$(P_{rad})_{\phi}$ =radiated power in all directions contained in φ field component

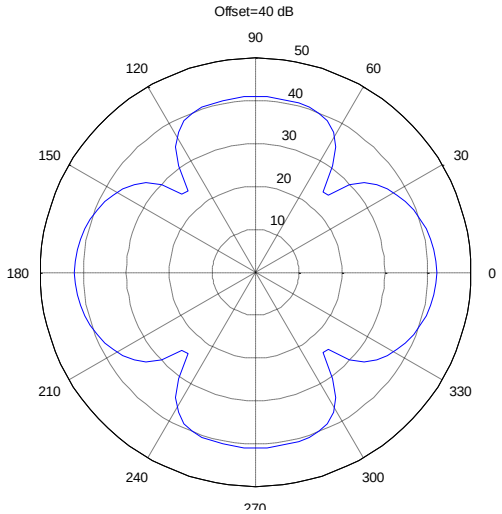

Figure 3.8: Directivity patterns of the bowtie antenna at $4GHz$ in the xz-plane.

Chapter IV: Results and Discussions

Fractals have self similar property in their geometry, which is a feature where a section of the fractal appears the same regardless of how many times the section is zoomed in upon. Self-similarity in the geometry creates effective antennas of different scales. This can lead to multiband characteristics in antennas, which is displayed when an antenna operates with a similar performance at various frequencies

The object of this chapter is to show how fractals can be used as multiband antennas. Bowtie and fractal antenna structures will be under study. The Sierpinski sieve fractal is chosen as the geometry to test this feature due to its astounding similarities in performance as an antenna at various frequencies. This type of fractal as an antenna can be compared to a bowtie dipole antenna. It can be fed in a similar fashsion as shown in figure 4.1.

This fractal antenna has also been closely studied by Carles Puente-Baliarda *et al.*[52] this type of antenna, while not being frequency independent, but having several bands of resonance, can be compared with classical frequency independent antennas such as log-periodics and spirals. The antennas are investigated in detail in [54]. It is known that frequency independence is a result of retaining the similar shape at many scales. It is interesting to point out that while this property of spiral and log-periodics holds as these antennas grow larger, the self-similarity of the fractal is contained in itself and does not require additional property for spirals and log-periodics holds as these antennas grow larger, the self-similarity of the fractal is contained in itself and does not require additional area.

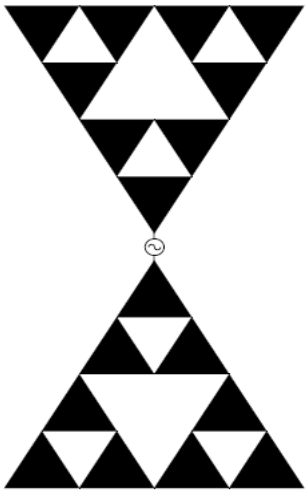

Figure 4.1: Sierpinski gasket fractal fed as a dipole.

4.1 Generation of Sierpinski Gasket Fractal Geometry

The generation of Sierpinski gasket geometry is explained using figures 4.2 and figure 4.3. Although the geometry presented here consist of equilateral triangles, the description here holds good for any triangular geometry. Explanation of its generation are in two ways:

- The multiple copy approach
- Decomposition approach

For the first, one starts with a small triangle. Two more copies of this triangle (same size) are generated and attached to the original triangle. This process can be done n number of times, n being the order of fractal iteration. In the decomposition approach, one starts with a large triangle encompassing the entire geometry. The midpoints of the sides are joined together, and a hollow space in the middle is created. This process divides the original triangle to three scaled down (half sized) versions of the larger triangle. The same division process can be done on each of the copies. After n such divisions, the geometry shown in figure 4.3 is obtained. Affine transformations, of which similarity transformations form a convenient sub-class, are important characteristics of fractal geometries. These involve scalling, rotation and translation. These transformations can be expressed in the mathematical form as:

$$W\begin{pmatrix} x \\ y \end{pmatrix} = \begin{bmatrix} r\cos\theta & -s\cos\phi \\ r\sin\theta & s\sin\phi \end{bmatrix}\begin{pmatrix} x \\ y \end{pmatrix} + \begin{pmatrix} x_0 \\ y_0 \end{pmatrix} \tag{4.1}$$

r and s are the scale factors

θ and ϕ correspond to rotation angles

x_0 and y_0 are translations involved in the transformation

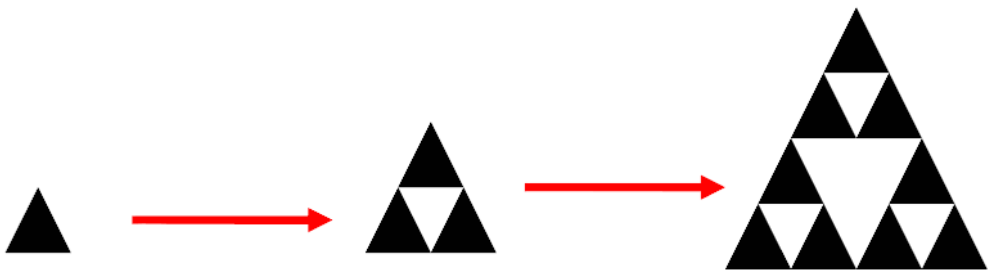

Figure 4.2: Multiple copy generation approach.

If r and s are both reductions $(r, s < 1)$ or both magnifications $(r, s > 1)$ the transformation is self-affine. If $r = s$ and $\theta = \phi$, the transformation is self-similar. First the generation of 'strictly self-similar' Sierpinski gasket is considered. Starting with an equilateral triangle of unit length side the transformations involved to get the next iterated geometry.

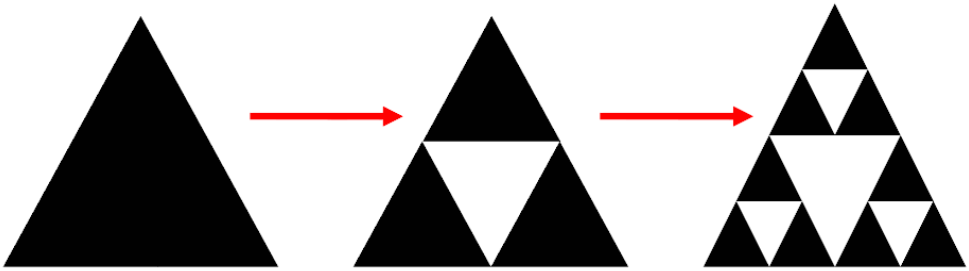

Figure 4.3: Decomposition generation approach

It is assumed that the origin of the co-ordinate system is at the bottom left corner of the triangle, and the x-axis pass through the base (bottom) side of the triangle. The transformations W_1, W_2, W_3 are indicated in figure 4.4. The second geometry is obtained with a union of these three transformations:

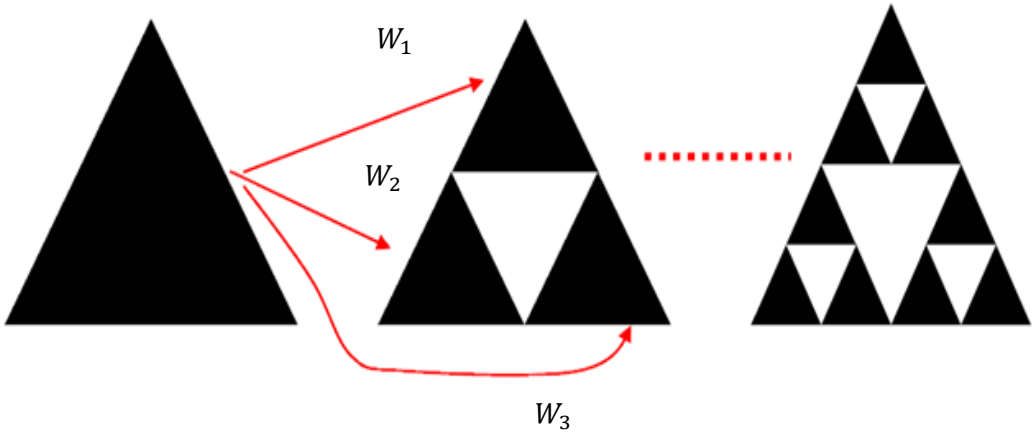

Figure 4.4: Iterated Function System (IFS) for generation of self-similar Sierpinski gasket geometry.

$$W_1\begin{pmatrix} x \\ y \end{pmatrix} = \begin{bmatrix} 0.5 & 0 \\ 0 & 0.5 \end{bmatrix}\begin{pmatrix} x \\ y \end{pmatrix} \tag{4.2}$$

$$W_2\begin{pmatrix} x \\ y \end{pmatrix} = \begin{bmatrix} 0.5 & 0 \\ 0 & 0.5 \end{bmatrix}\begin{pmatrix} x \\ y \end{pmatrix} + \begin{pmatrix} 0.5 \\ 0 \end{pmatrix} \tag{4.3}$$

$$W_3\begin{pmatrix}x\\y\end{pmatrix} = \begin{bmatrix}0.5 & 0\\ 0 & 0.5\end{bmatrix}\begin{pmatrix}x\\y\end{pmatrix} + \begin{pmatrix}0.25\\0.433\end{pmatrix} \tag{4.4}$$

$$W(A) = W_1(A) \cup W_2(A) \cup W_3(A) \tag{4.5}$$

This process of generation of the geometry is very convenient in the context of computer platforms, and is often called multiple reaction copy machine (MRCM). In mathematics, these are referred to as iterated function systems (IFS).

4.1.1 Mod –p Sierpinski Gaskets

Sierpinski gasket is a special case of a wider class of fractals that can be derived from the well known Pascal's triangle [75]. This class of fractals can be derived in the following way. Consider an equiangular triangular grid whose rows shall be labeled by $n = 1, 2, 3 \ldots\ldots\ldots$ each row contain n nodes and to each node a number is attached. This number is the coefficient of the binomial expansion of $(x + y)^{n-1}$. Now delete from this grid those nodes that are attached to numbers that are exactly divisible by p, where p is a prime number. The result is a self similar fractal that will be referred as the mod-p sierpinski gasket in figure 4.5, this process is shown for the mod-2 sierpinski gasket and the blank nodes represent those deleted from the grid.

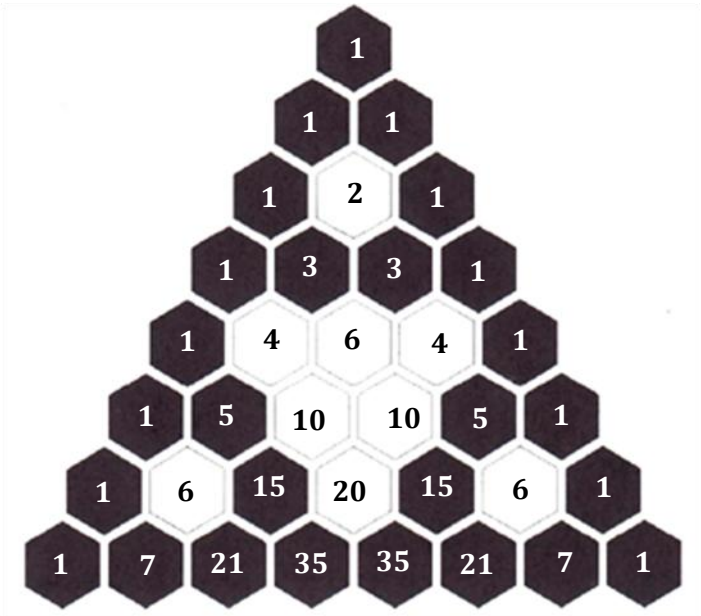

Figure 4.5: Derivation of the Sierpinski Gasket from Pascal's triangle. When those numbers divisible by *2* are deleted the mod-*2* sierpinski gasket is obtained.

To obtain the mod-3 and mod-5 sierpinski gaskets, those nodes attached to numbers divisible by 3 and 5 should be deleted from the Pascal's. In figure 4.6 three iteration mod-3 and mod-5 sierpinski gaskets are shown. In this case it is clear that the scaling of the different replicas is p. This antenna is basically used for fractal multi band antenna.

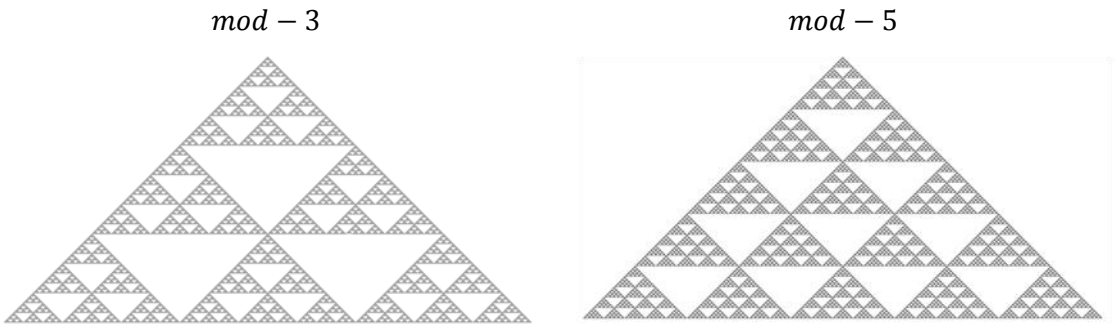

Figure 4.6 - Two Sierpinski Gaskets mod -*3* and mod-*5* sierpinski gasket.

4.1.2 Fractals as Space Filling Geometries

Euclidean geometries are limited to points, lines, sheets & volumes, Fractal include geometries that fall in between these distinctions .Therefore, a fractal can be line that approaches a sheet. These space filling properties lead to curve that are electrically very long [47], but fit into a compact physical space. This property leads to miniaturization of antenna elements. Fractals could be used to define the spacing in arrays for thinning or to define radiation pattern.

For Sierpenski triangle with each iteration the area of the holes and circumference of solid pieces changes. If the area of original triangle is 1, then first iteration removes $1/4$ of the area. Second iteration removes a further $3/16$ and third iteration $9/64$.Then total area removed after the nth iteration

$$A_n = 1/3 \sum_{i=1}^{n} (3/4)^i \tag{4.6}$$

$$A_\infty = 1$$

If circumference of original triangle is 1, then after first iteration the circumference increases by $1/2$. After second iteration it increases by $3/4$, after nth iteration.

$$C_n = 1 + 1/3 \sum_{i=1}^{n} (3/2)^i \tag{4.7}$$

$$C_\infty = \infty$$

This means gasket has no area but boundary is of infinite length. Table shows how with each iteration the area and circumference changes.

Table 4.1: Different iteration of Gasket and variation of area and circumference.

Figure	Area	Perimeter
	$A_0 = \frac{\sqrt{3}}{4}$	$P_0 = 3$
	$A_1 = \frac{3}{4} A_0$	$P_1 = 3 + 3(1/2)$ $= 3 + 3/2$
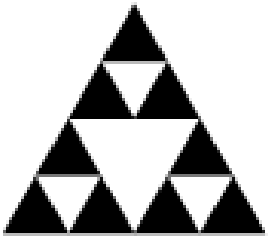	$A_2 = \left(\frac{3}{4}\right)^2 A_0$	$P2 = 3 + 3/2 + 3 * 3 * 1/4$ $= 3 + 3/2 + 9/4$
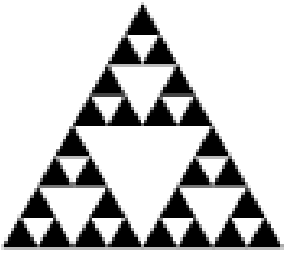	$A_3 = \left(\frac{3}{4}\right)^3 A_0$	$P3 = 3 + 3/2 + 9/4 + 9 * 3 * 1/8$ $= 3 + 3/2 + 9/4 + 27/8$
Stage n	$A_n = \left(\frac{3}{4}\right)^n A_0$	$P_n = 3 + 3/2 + \ldots + (3/2)^n$
Sierpenski Triangle	0	infinity (geometric series with $r > 1$)

4.2 Wideband Antennas: Bowtie antenna

In many applications an antenna must operate effectively over a wide range of frequencies. An antenna with wide bandwidth is referred to as a broadband antenna. The term "broadband" is a relative measure of bandwidth and varies with the circumstances. Here we provide a brief definition of bandwidth. The bandwidth is computed in one of two ways. Let f_u and f_l be the upper and lower frequencies of operation for which satisfactory performance is obtained. The center (or sometimes the design frequency) is denoted by f_c. The bandwidth as a percent of center frequency is

$$\frac{f_u - f_l}{f_c} \times 100\% \tag{4.8}$$

This definition holds for narrow band antennas, only such as the dipole or a loop. For example, a 5% bandwidth indicates that the frequency difference of acceptable operation is 5% of the center frequency of the bandwidth. For broadband antennas the bandwidth is defined as a ratio by

$$f_u : f_l \tag{4.9}$$

For example, a $10:1$ bandwidth indicates that the upper frequency is 10 times greater than the lower. The half-wave dipoles have small bandwidth from 8 to 16%. On the other hand, antennas that have travelling waves on them rather than standing waves (as in resonant antennas) operate over a significantly wider frequency range. If the impedance and the principal radiation pattern of an antenna do not change significantly over an octave ($f_u/f_l = 2$) or more, the antenna will be classified as a broadband antenna. For ultra-wideband antennas capable of transmitting voltage pulses, the bandwidth of $f_u/f_l \geq 10$ is usually required.

The subject of broadband antennas is well covered in the literature. Most conventional broadband antennas include the helical antenna, the biconical/bowtie antenna, the spiral antenna, the horn antenna, and the log-periodic antenna.

The so called ultra-wideband (UWB) antennas should not only keep nearly the same impedance and radiation pattern but also have a small phase variation of the transmitted signal over the bandwidth. Otherwise, the pulse form would be distorted because of dispersion of different harmonics. Because of their dispersive characteristics conventional

wideband antennas, such as log-periodic arrays, spiral antennas, and rigid horn type antennas perform poorly as high-fidelity antennas for UWB impulse waveforms.

Examples of ultra-wideband communication antennas include loaded dipoles, (loaded) bowties, conical antennas, and vee configurations. Bowtie antenna is considered here which will be further converted to a fractal antenna.

A bowtie antenna is made from a bitriangular sheet of metal with the feed at its vertex. It is used extensively in many applications such as ground penetrating radars and mobile stations. A bowtie antenna can be printed on a substrate where each arm is placed either on the upper or lower surface of the substrate. The feeding of such structure is done by designing appropriate striplines that are connected to a coaxial feed which is placed on one of the edges of the substrate. The bowtie antenna (336 triangles, $\alpha = 90^{o}$ flare angle, $0.2m$ total height) used for simulation is shown in figure 4.7 the bowtie plane is xy-plane. The frequency band of 25 MHz to $5GHz$ is chosen for the simulation of bowtie antenna.

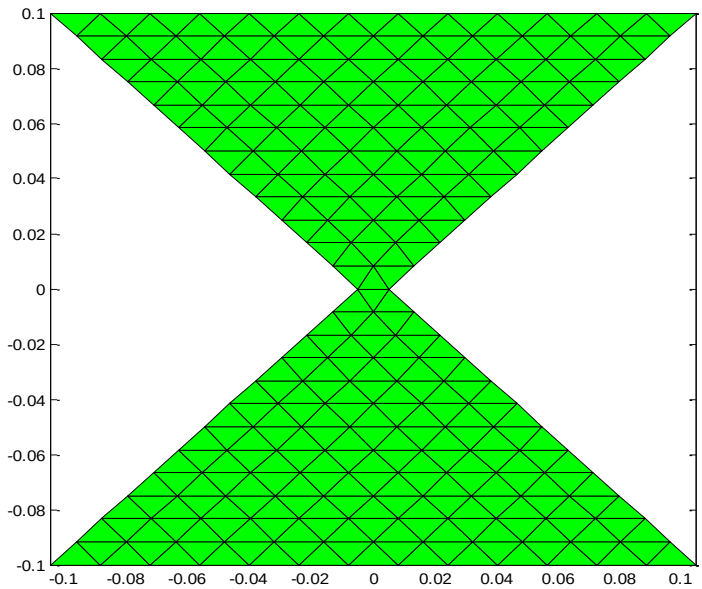

Figure 4.7: Simulated Bow-tie antenna with flare angle 90^{o}.

4.2.1 Results

Figure 4.8 and figure 4.9 shows the impedance values of the bowtie antenna, the graph shows very smooth impedance characteristics. Especially inviting is the behaviour of the reactance which has nearly constant negative value (capacitive reactance) in the band 1.5 to $5GHz$. The impedance behaviour of the bowtie is considerably affected by the value of the flare angle, α.

Only one power resonance can be indentified for the present bowtie with $\alpha = 90^{o}$. This resonance occurs when the antenna length/wavelength ratio is slightly smaller than $1:3$. The first resonance is very strongly developed and a high output power of about $15mW$ is observed at the resonance. The bowtie gain varies from approximately 2 to $5dB$. When the frequency increases, the output power exhibits moderate oscillations and generally increases as well. For the bowtie antenna the current is distributed over a larger surface and eventually dissipates into the radiated field before it reaches the antenna's end. Therefore reflections from the antenna's end are significantly reduced, which makes the bowtie antenna an essentially nonresonant structure, attractive for both broadband and UWB applications.

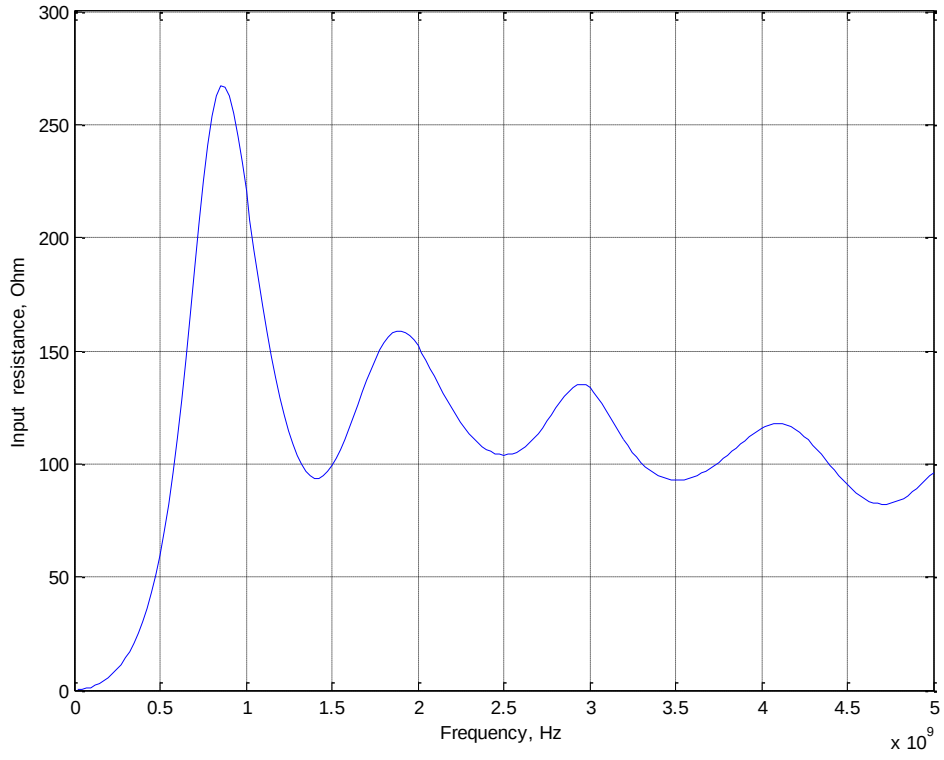

Figure 4.8: Bowtie input resistance as a function of frequency (ratio of total length/wavelength).

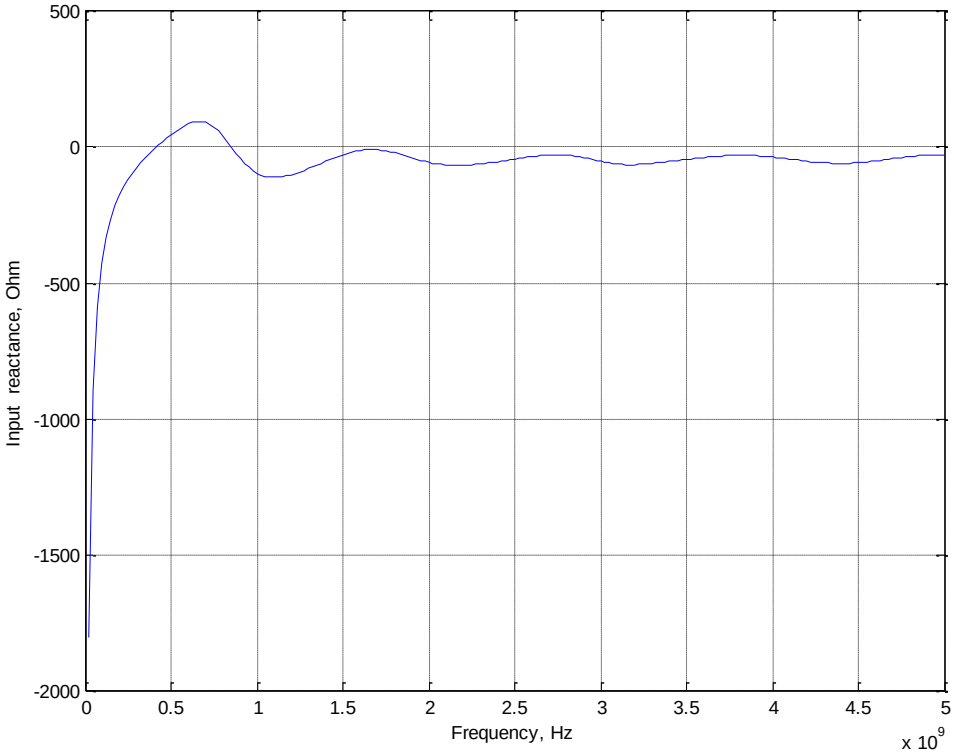

Figure 4.9: Bowtie input reactance as a function of frequency (ratio of total length/wavelength).

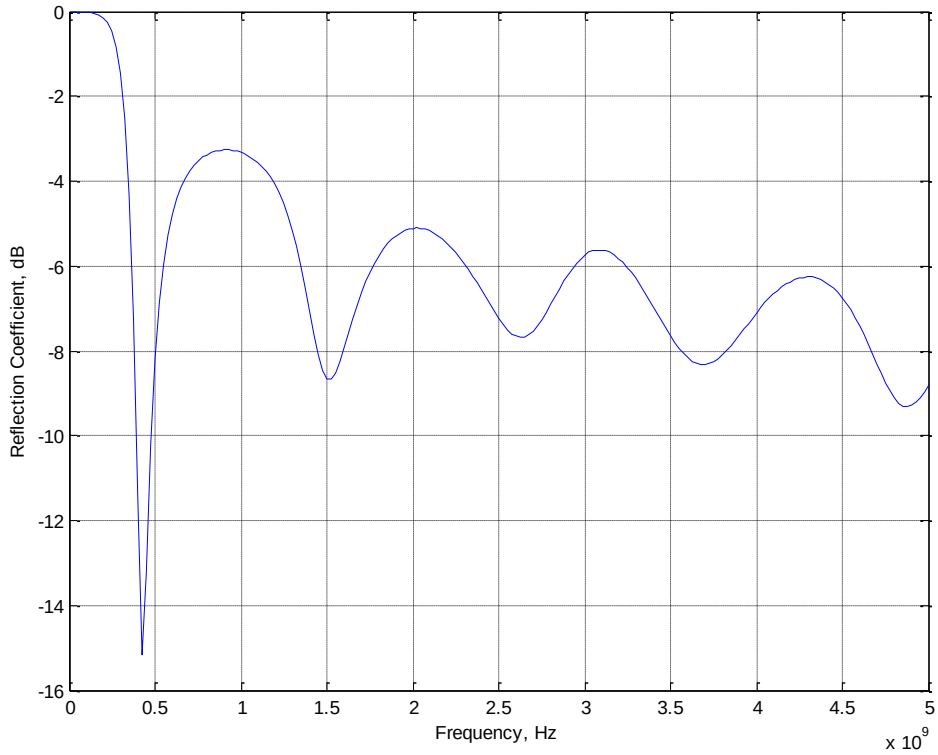

Figure 4.10: Bowtie input reflection coefficient as a function of frequency (ratio of total length/wavelength).

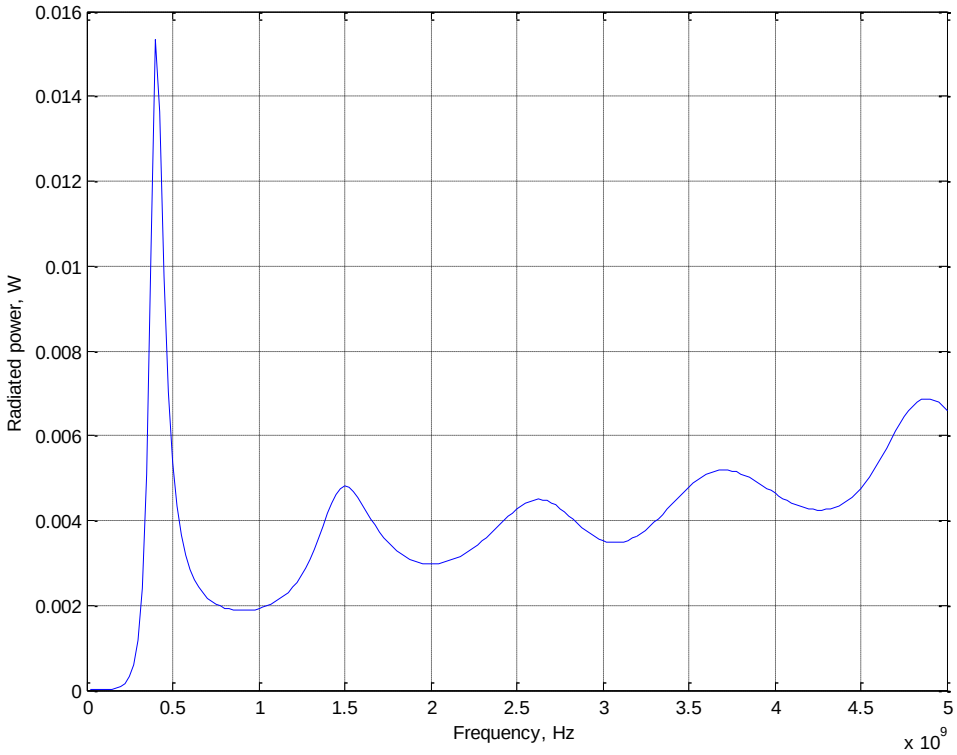

Figure 4.11: Bowtie radiated power as a function of frequency (ratio of total length/wavelength).

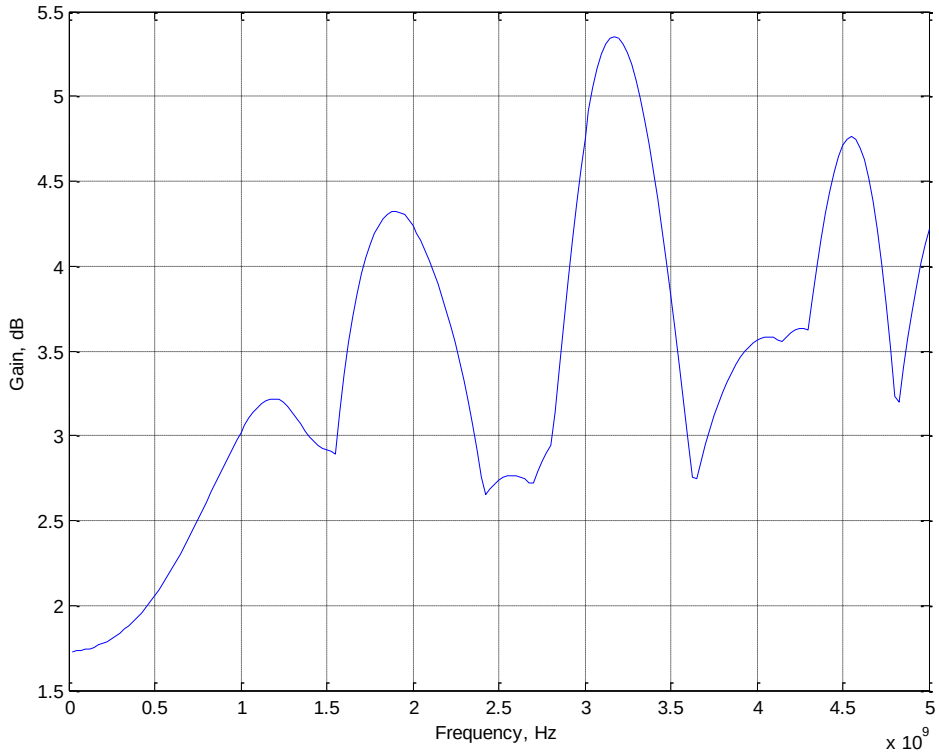

Figure 4.12: Bowtie gain as a function of frequency (ratio of total length/wavelength).

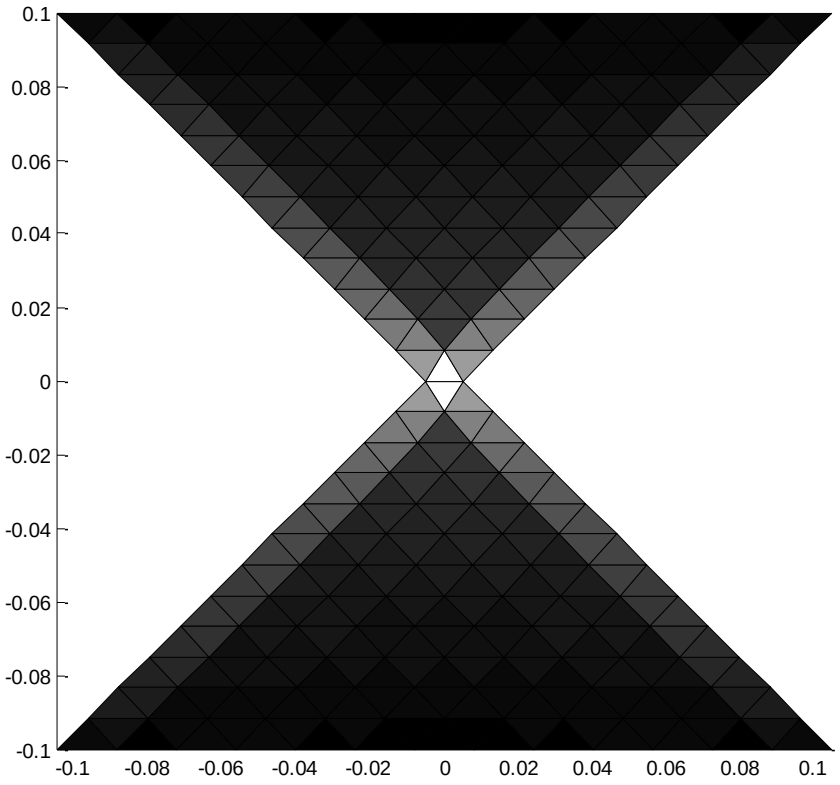

Figure 4.13: Magnitude of the surface current for the bowtie antenna at $500MHz$, the incident field is directed along the antenna axis.

The detail study of the radiation intensity distribution for the bowtie antenna and the corresponding directivity patterns is done at various frequencies. Figure 4.14 indicates that despite the better impedance behaviour, the present bowtie antenna might have a diverse radiation intensity distribution through the band of 1 to $4GHz$. The color bar in figure 4.14 extends from the maximum to minimum intensity magnitude. Therefore relative variations of the intensity may be not as high as they appear in figure 4.14. An additional test is necessary to quantitatively describe the intensity distribution.

For this purpose directivity patters in dB are obtained. The xz-plane is chosen for comparison. Figure 4.15 shows four directivity patterns corresponding to 1,2,3 and $4GHz$. The x-axis corresponds to reference angle zero.

It is seen in figure 4.15 that the results at 1 and $2GHz$ indicate a nearly omnidirectional (strictly speaking, bidirectional) radiation pattern, with relatively small directivity variations. Interestingly the direction of maximum radiation changes from z-direction in figure 4.15 at $1GHz$ to x-direction in figure. The radiation patterns at lower frequency are also omnidirectional and are quite similar to that shown in figure. However, the results at 3 and

$4GHz$ are hardly acceptable. This circumstances, combined with the impedance's behaviour, allows us to identify the bandwidth of the present antenna type as approximately 0.5 to $2GHz$.

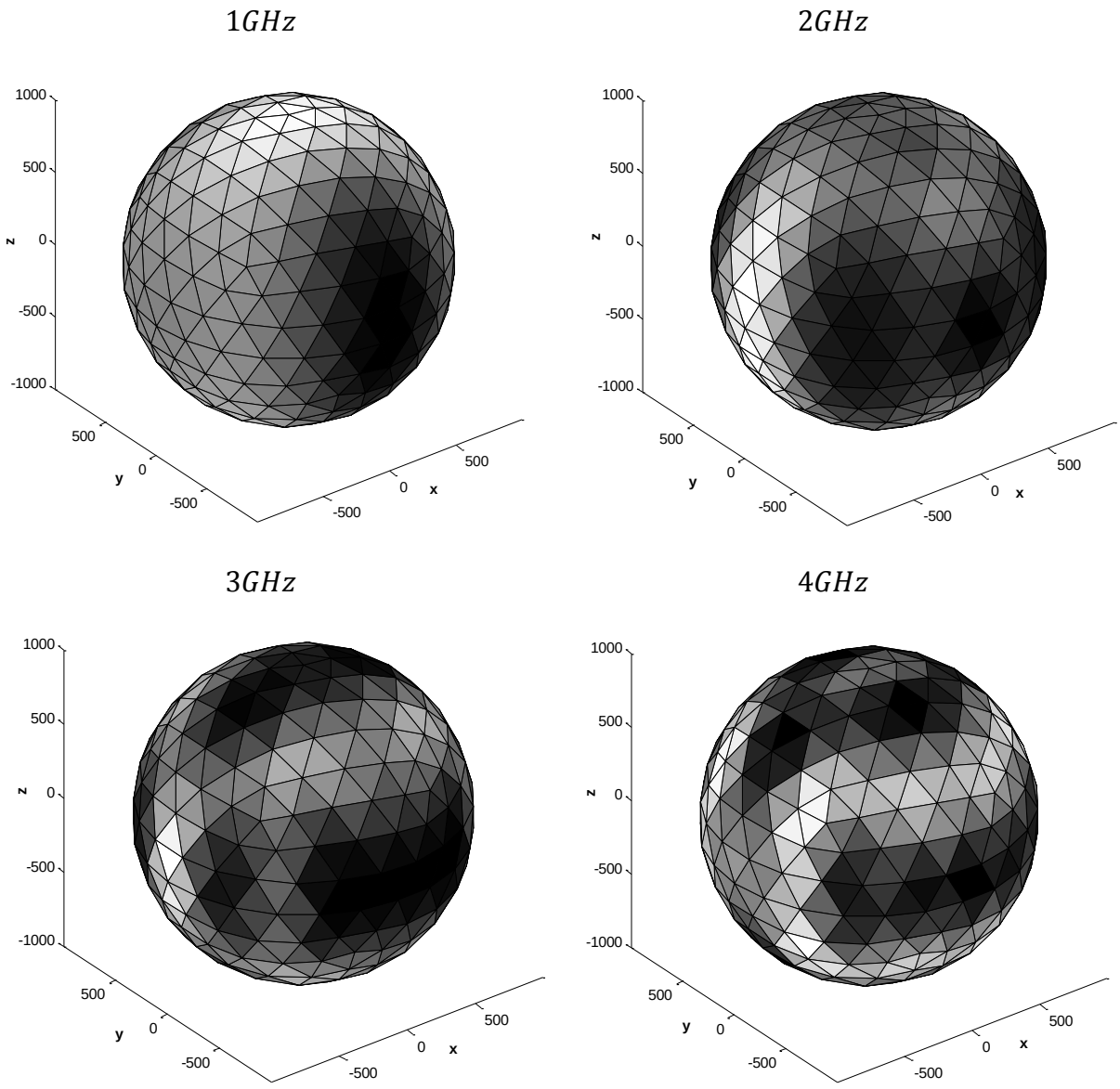

Figure 4.14: Radiation intensity distribution of the bowtie antenna at 1,2,3 and $4GHz$.

Further work may be needed to increase the bandwidth. Some of the methods include resistive loading, dielectric coating, use of cavity-backed bowtie, and the use of a volume absorber. One other possible method is further optimization of the shape of the metal sheet bowtie antenna.

The bowtie geometry studied here is straightforwardly expanded to one of the simplest fractal antennas: the so-called Sierpinski fractal antenna or Sierpinski gasket. Very basically, the Sierpinski fractal is none other than a bowtie with a specially arranged hole structure. Fractal antennas are not broadband in the conventional sense but rather "multiband". These antennas are able to keep nearly the same performance at several (up to five) relatively narrow bands. In the next section detail analysis of Sierpinski fractal antenna is done with its comparison with bowtie antenna.

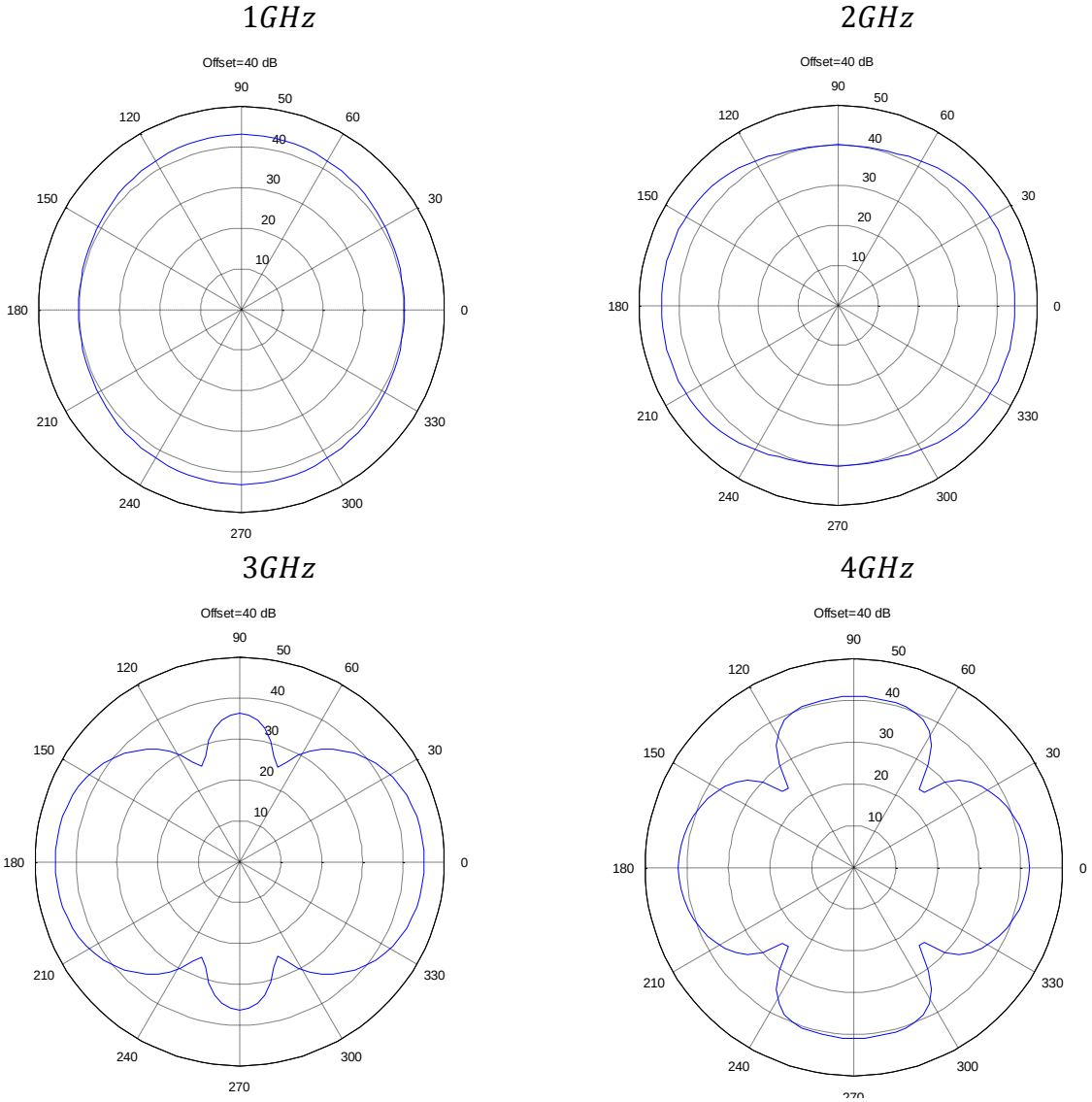

Figure 4.15: Radiation patterns of the bowtie antenna at 1,2,3 and 4GHz in the xz-plane.

4.3 Multiband Antennas: The Sierpinski Fractal

Using a bow-tie as a generator, a crescent number of triangles are removed in the half of height of the anterior space to create a Sierpinski antenna. This defines the growth of fractal. To each growth realized, a new resonant frequency is obtained. The scale factor of a location of the new triangle (half of height) defines the rate of a new resonant frequency (approximately). Figure 4.16 shows some stages obtained in a bow-tie antenna.

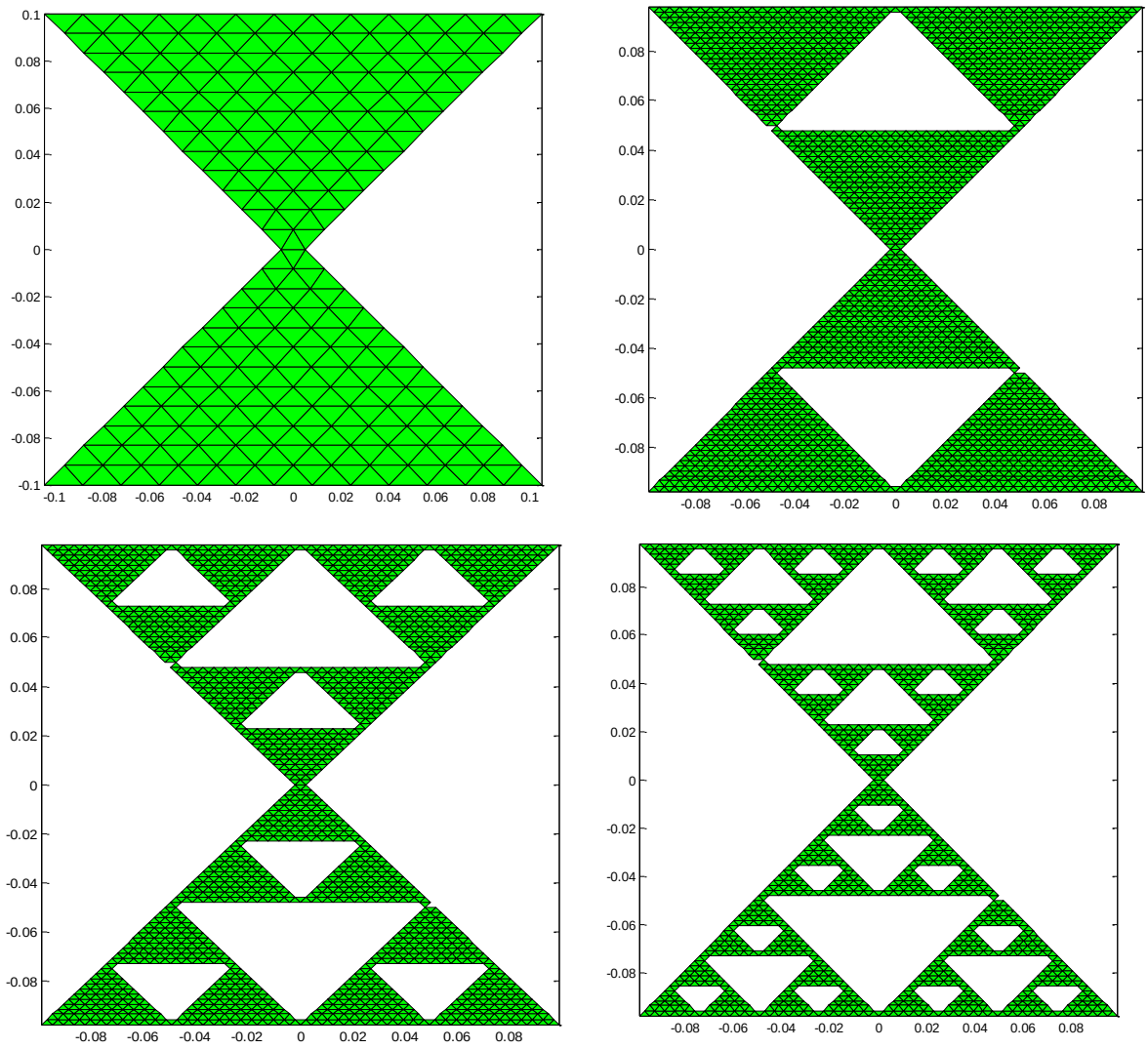

Figure 4.16: Geometry of the bow-tie fractal antenna with different stages of growth.

To the first stage, one triangle is removed of the antenna. To the second stage, one triangle is removed in each triangle created in the anterior stage, and so on.

4.3.1 Design Method

The good way to design a fractal antenna involves, basically, the definition of six items: -

- size of the seed antenna
- Number of bands wanted;
- Stage of growth of the fractal;
- Stage of growth of the dipoles in the method of the moments;
- Feeding point;
- Angle of the antenna.

The seed antenna will generate the next stages of fractal antenna. The dimensions of the seed antenna define the first frequency in the Sierpinski antenna. The number of bands wanted defines the growth of the fractal. The growth stage is the same of the number of frequencies minus one. Observe in the Figure 4.16 that when the number of stages begins to grow, the format of the generated triangles becomes round. Such effect provokes simulation mistakes with the method of the moments. Then, when the number of stages grows, it is necessary to increase the dipoles number in the method of the moments. Varying the angle of the antenna, the reason among the obtained frequencies varies. Like this, it is possible to accomplish a fine adjustment in the wanted frequencies.

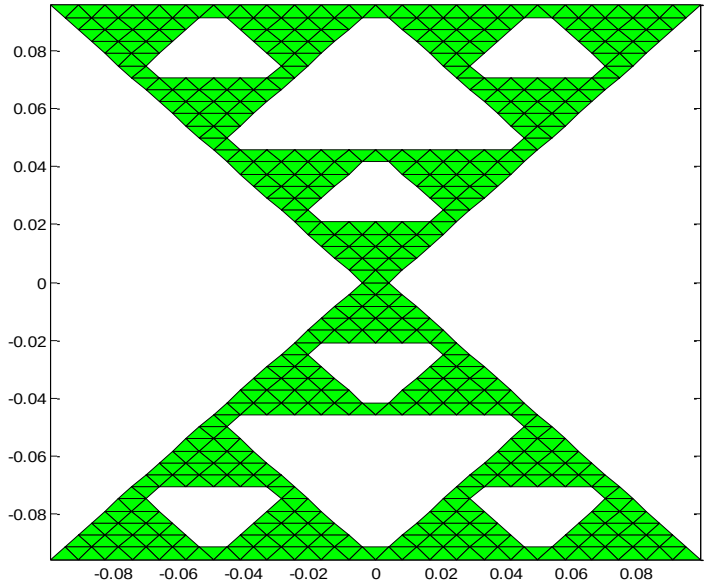

Figure 4.17: Simulated Bow-tie and Sierpinski Fractal antenna with stage of growth $S = 2$ and flare angle 90^{o}

4.3.2 Results

Figure 4.18 and Figure 4.19 compare the input impedance of the fractal antenna with input impedance of bow-tie antenna. The impedance behaviour of the fractal antenna indicates a

typical resonant structure. The input resistance has large peaks, whereas the input reactance has multiple nulls.

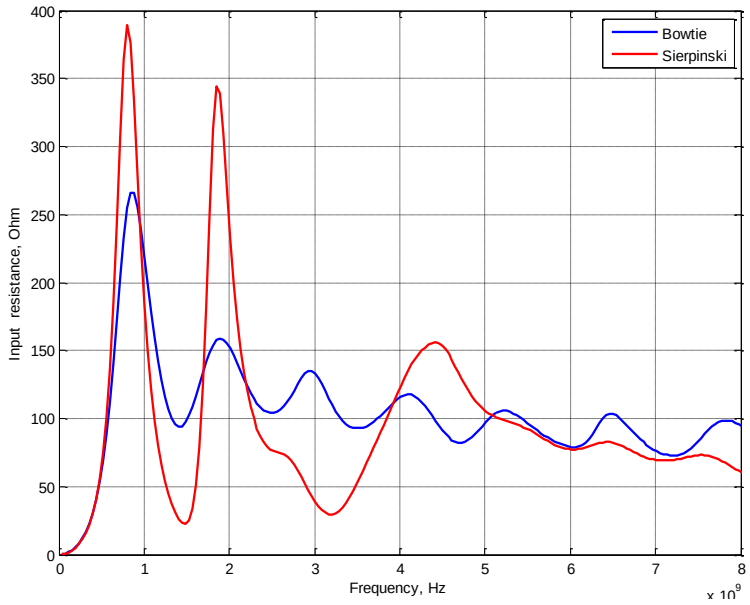

Figure 4.18: Fractal antenna input resistance as a function of frequency (ratio of total length/wavelength). Resistance of equivalent bow-tie.

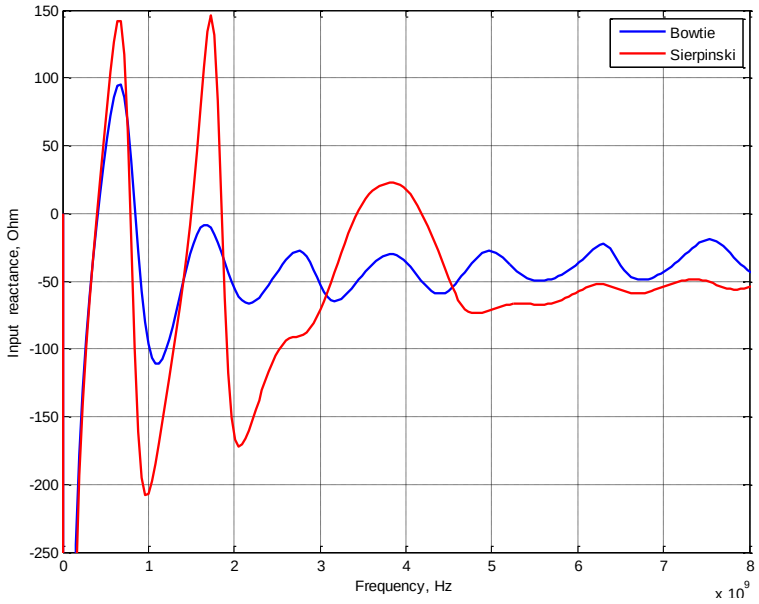

Figure 4.19: Fractal antenna input reactance as a function of frequency (ratio of total length/wavelength). Reactance of equivalent bow-tie.

In the analysis of impedances, the multi-band behaviour of the fractal is not yet specified. We are interested in the resonances that are characterized by the zero input reactance and

maximum power radiated by the antenna. Furthermore if the input resistance at these resonances will be well matched to a 50Ω load, the multi-band behaviour will be established.

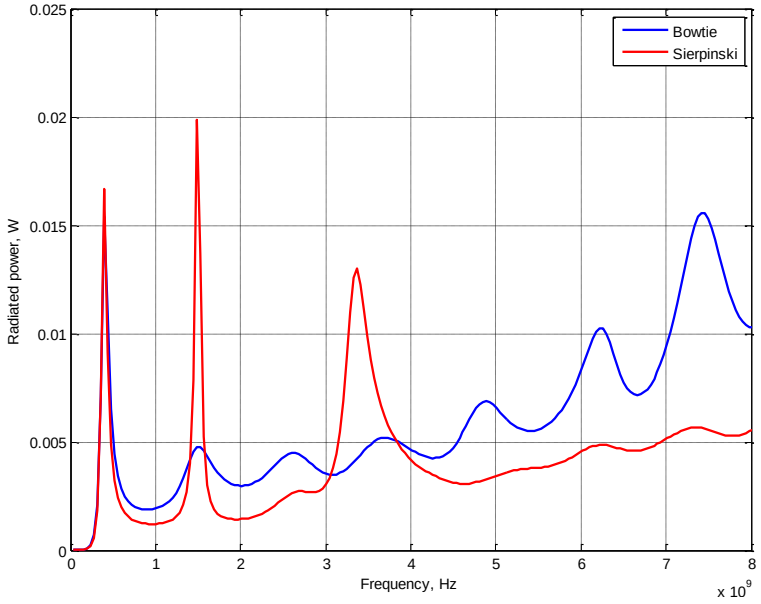

Figure 4.20: Radiated power of the fractal and bow-tie antennas.

The radiated power of the fractal antenna and of equivalent bow-tie is shown in Figure 4.20. At low frequencies (below $0.5\,GHz$) both power dependencies are nearly the same. It is observed that the fractal antenna has three resonances. The number of resonances is thus the number of fractal stages ($S = 2$) plus one. The first resonance is that of the pure bow-tie and corresponds to $f_1 = 0.4\,GHz$. This resonance occurs whether or not the fractal structure is present. The second resonance $f_2 = 1.48GHz$ corresponds to first fractal iteration, and the third resonance at $f_3 = 3.367GHz$ corresponds to the second fractal iteration. The frequency ratios

$$\frac{f_2}{f_1} = 3.7, \frac{f_3}{f_2} = 2.27, \ldots$$

Asymptotically tend to 2 when the number of fractal stages increases as predicted by theory. The resonant bands are thus log-periodically spaced, by a factor of 2, which is exactly the scale factor that relates triangle size at each stage of growth.

To investigate the resonances more properly, the input reflection coefficient, Γ, of the transmitting antenna is checked, which is given by the equation

$$\Gamma = \frac{Z_A - 50\Omega}{Z_A + 50\Omega} \tag{4.10}$$

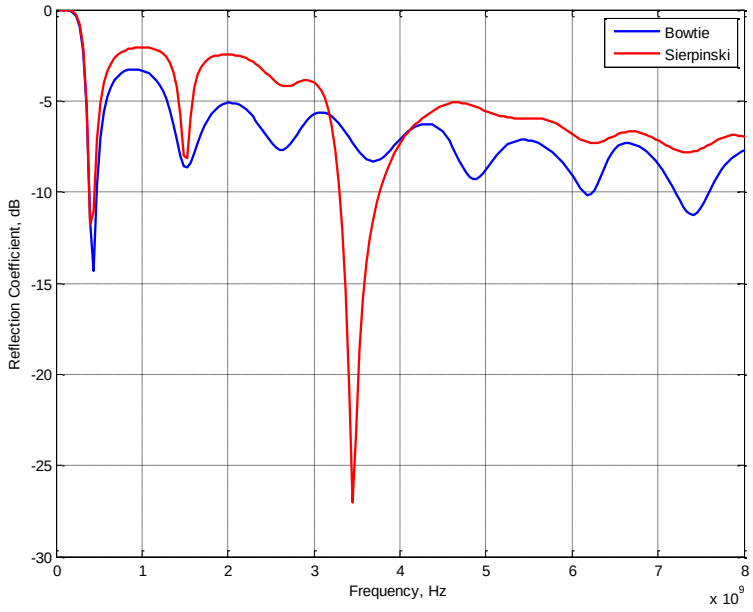

Figure 4.21: Input reflection coefficient of the fractal and bow-tie antennas

Fig.4.21 shows the magnitude of the reflection coefficient to logarithmic scale versus frequency. It is seen that the power resonances are directly associated with the minima of the reflection coefficient, which enables us to design a well-matched antenna at these frequencies.

The corresponding resonance bands are the multi-bands of the fractal antenna. The relative bandwidth at each band typically reaches 7 to 20%. Fig.4.23 shows the surface current distribution on the fractal antenna surface at $f_2 = 1.48GHz$ (second resonance). The self-similarity of the current distribution can be observed. Figure.4.23 and Figure.4.24 gives radiation patterns at second and third resonant frequencies, respectively. Compared to the bow-tie radiation patterns, the fractal antenna produces a directional beam of higher gain at the resonant frequencies.

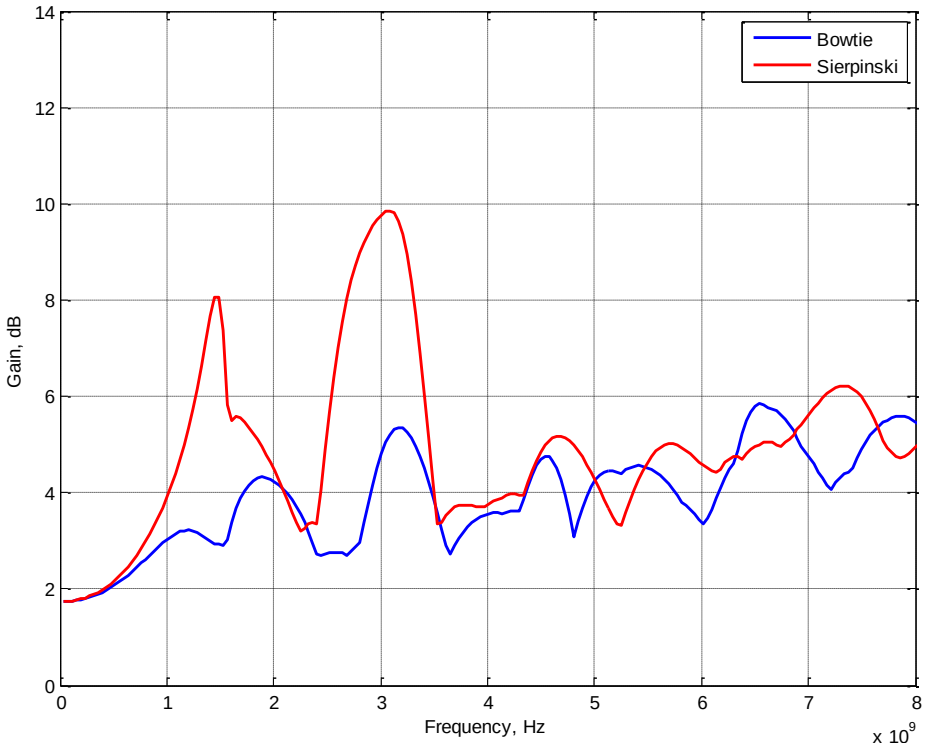

Figure 4.22: Gain of the fractal and bow-tie antennas.

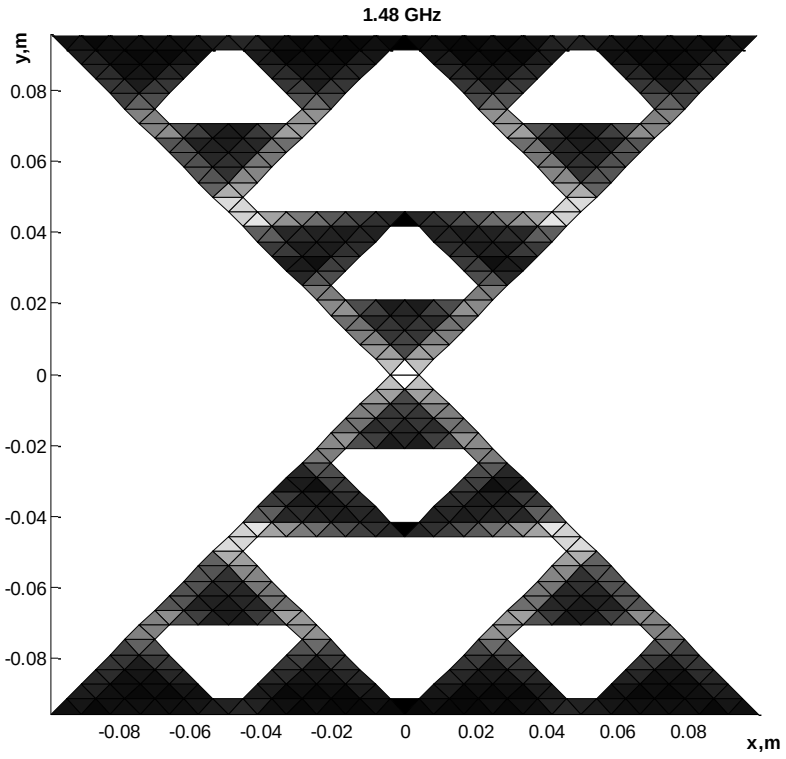

Figure 4.23: Fractal antenna surface current distribution at second resonance.

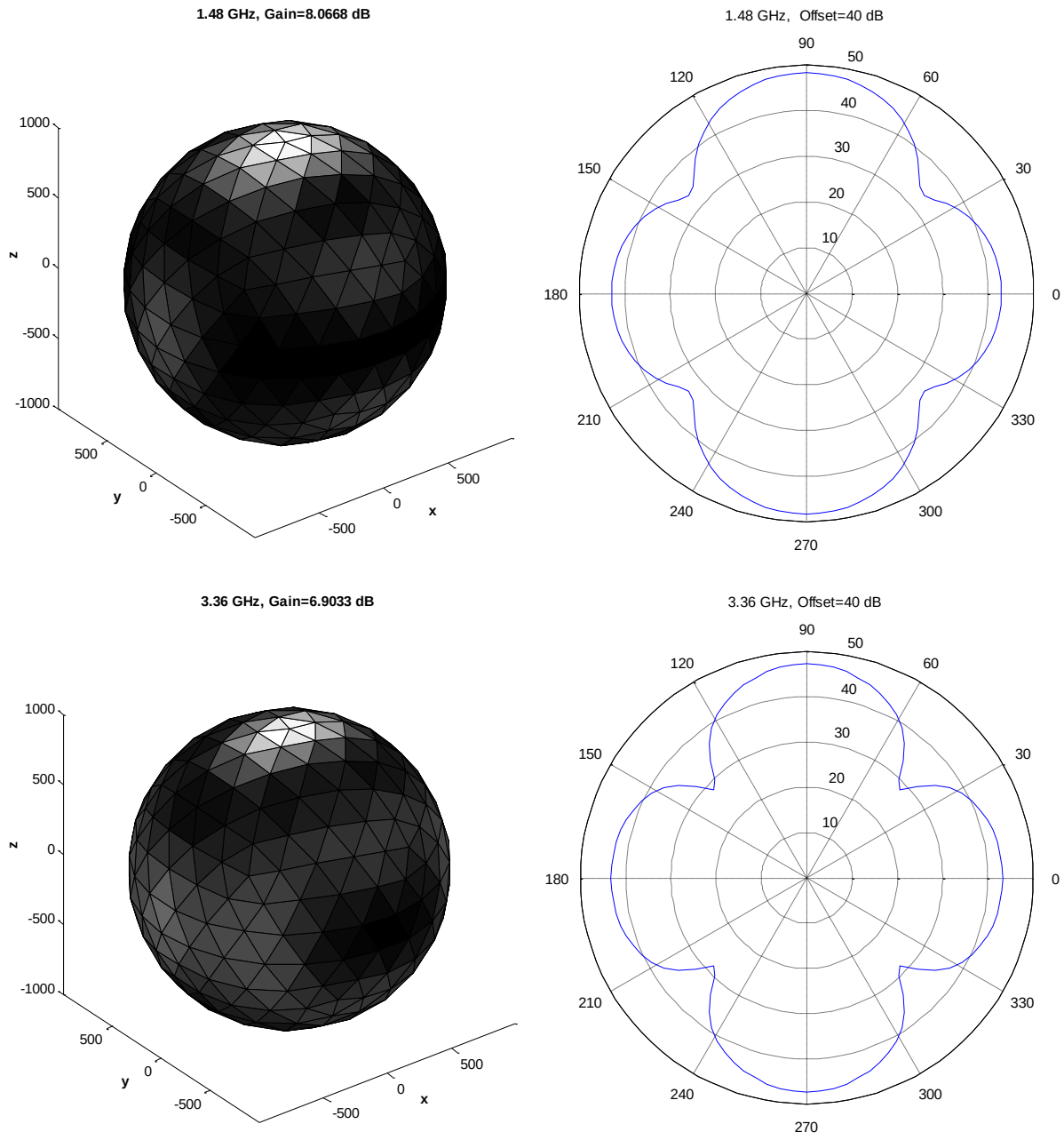

Figure 4.24: Radiation pattern for second and third resonance of the fractal antenna.

4.3.3 Discussion

Applying Sierpinski fractal shapes on a bow-tie antenna will cause the total frequency band of the antenna to be repeated in a log-period basis with a spacing factor, which is related to the mode of the fractalizing scheme. Mode-2 fractal shape is investigated in this paper to show how these fractions affect the operating band of the main antenna.

Since the primary structure of the antenna is a multiband one we can set the repeated resonances between those operating bands by using different fractal shapes, flare angles, and

proper dimensions of the main structure. In this way, fractal shapes give us an extra freedom in spacing the operating frequencies in desired bands and bandwidths; moreover, they provide multiband and wideband features simultaneously. These antennas can be used in any communication system that is supposed to operate in different frequency bands and requires a relatively high bandwidth and a constant radiation pattern in all operating frequencies.

4.4 Fractal Arrays

4.4.1 Characterization of Optimized Antenna Arrays

An optimized antenna would have no side lobes. The benefit of having only one beam is apparent when we consider airports. If the antenna array with radiation patters shown in Figure 4.25 were used in an airport, the side lobes would easily cause air traffic control to confuse a large airplane at the height of the side lobes with a small plane at the peak of the main beam. Another characteristic of an optimized beam involves a thin single main beam. Figure 4.26 shows the catastrophe that could happen if a thick main beam were to confuse two airplanes as one large plane.

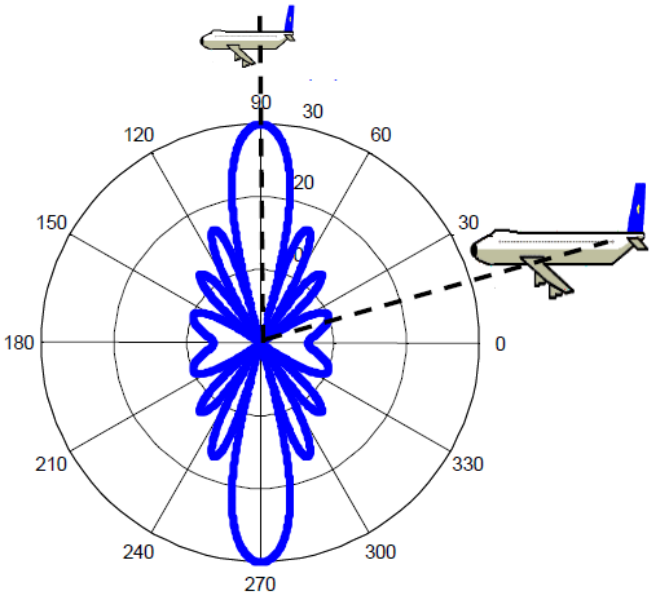

Figure 4.25: Radiation pattern with high side lobes

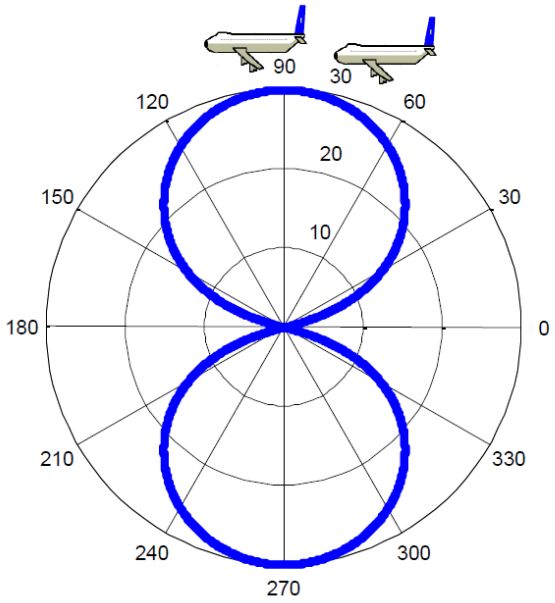

Figure 4.26: Radiation patters with thick main beam.

4.4.2 Planar Arrays

Two-dimensional antenna arrays allow for more flexibility and variety in placements of array elements. Two main ways in which elements have been placed on planar arrays are to place them on a grid or to randomly scattering them about a certain area. Although both still cause side lobes to exist, both arrangements have their advantages. We used MATLAB® to calculate the constructive and destructive interference in terms of the array factor (AF), that characterizes the radiated field. Array Factor (AF) for planar arrays is given as

$$AF = \sum_{n=0}^{N-1} \sum_{m=0}^{M-1} e^{-i2\partial \times M\left(\frac{d}{\lambda}\right)\cos\theta \sin\varphi} e^{-i2\partial \times N\left(\frac{d}{\lambda}\right)\cos\theta\cos\varphi} \tag{4.11}$$

To simplify the operation let $f_x = \frac{x}{\lambda r}$ and $f_y = \frac{y}{\lambda r}$ so that AF becomes:

$$AF = \sum_{n=0}^{N-1} e^{-i2\pi(f_x x + f_y y)} \tag{4.12}$$

4.4.3 Periodic Arrays

Planar arrays whose elements are organized in a grid have tendencies to produce main beams and side lobes of the same height. In Figure 4.27 324 elements have been placed on a rectangular grid of 1.5×2 square units. These dimensions are chosen for scaling purposes, as

our fractal array (discussed later) uses this size window. Figure 4.28 shows the Radiated field in a 3D where dark blue is the lowest point and red is the highest point.

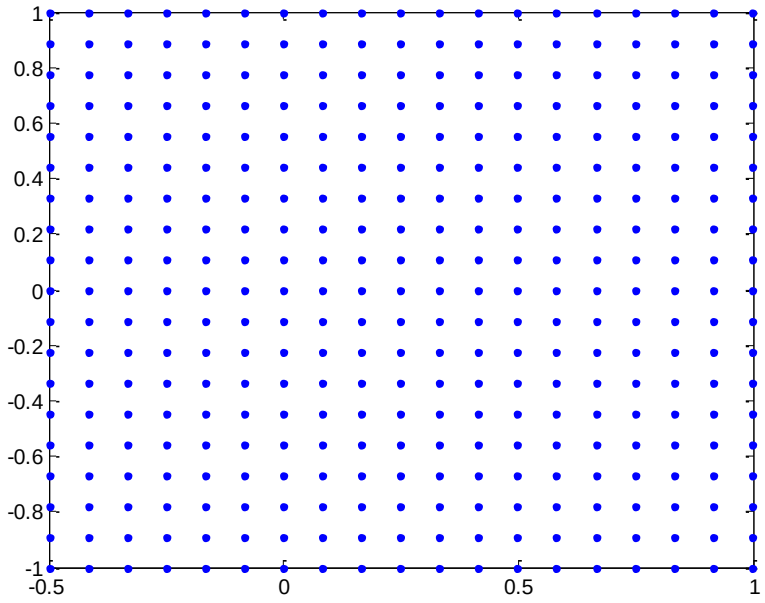

Figure 4.27: 324 elements with equal x & y distances apart.

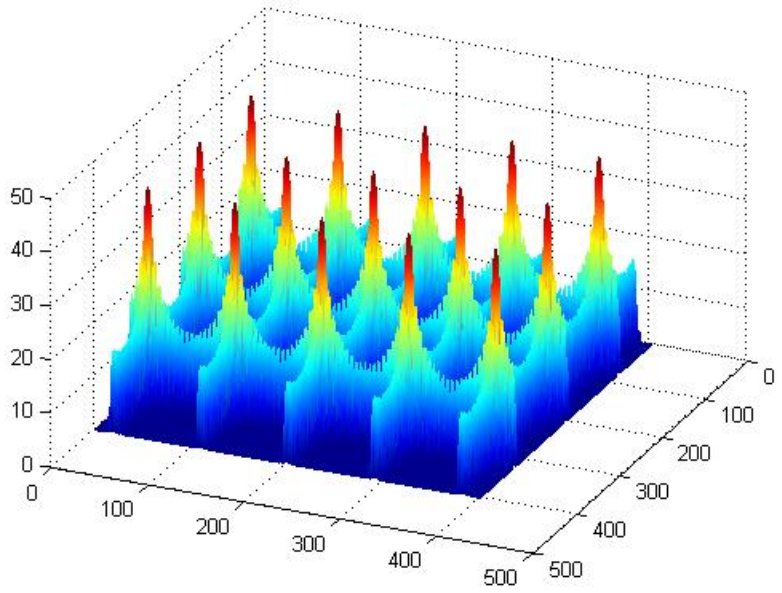

Figure 4.28: Radiated field of 324 elements with equal x & y distances apart.

4.4.4 Random Arrays

Random planar arrays have radiation characteristics that may be more desirable. We plotted 324 elements on the same rectangular area of 1.5×2 square units. Figure 4.30 shows how

side lobes are generally lower than the ones seen in the first set of ordered points. There is also an 180^0 symmetry, which is more apparent about the main beam.

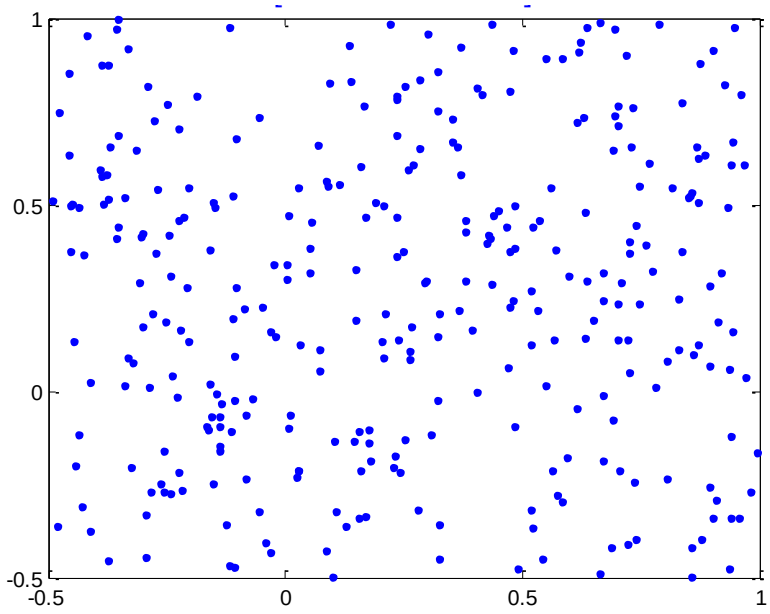

Figure 4.29: 324 elements randomly placed.

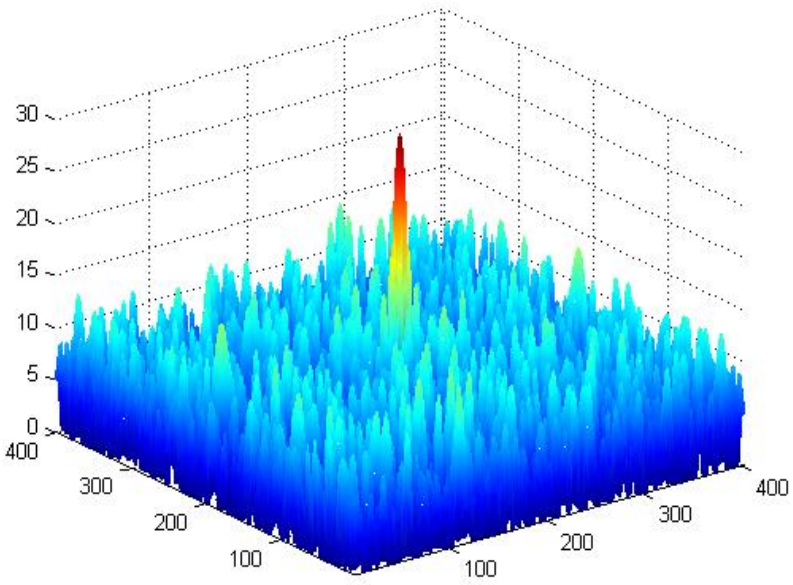

Figure 4.30: Radiated field of 324 elements randomly placed.

4.4.5 Fractal Arrays

As the goal of our work is to characterize an optimized antenna array, we propose that the radiation properties of both the ordered fractals and the random fractals have redeeming qualities. Yet, there continues to be a gap between the ordered and the disordered. Fractals

attempt to bridge that gap where they are constructed in an organized pattern, yet they also attain the qualities of random points depending on their construction and orientation of points. To first generate the fractals, we used an Iterated Function System(IFS) in the Matlab script that used probability to randomly place points within initial matrix boundaries. These initial matrix boundaries are specific to the Sierpinski gasket. For the sake of comparison and scaling, we also input the gasket to comprise only 324 points. Figure 4.31 and Figure 4.32 324 elements random point generated Sierpinski gasket shows the organization of the points and the characteristic radiation properties of this particular organization.

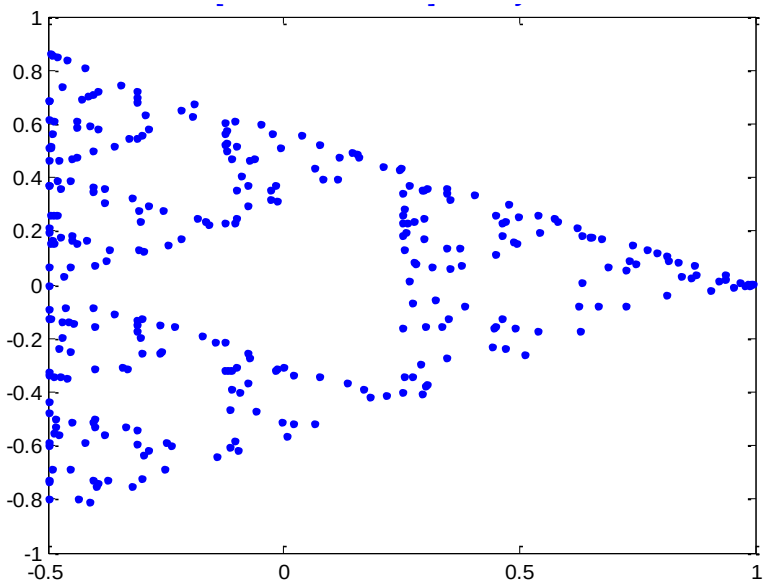

Figure 4.31: 324 elements random point generated Sierpinski gasket

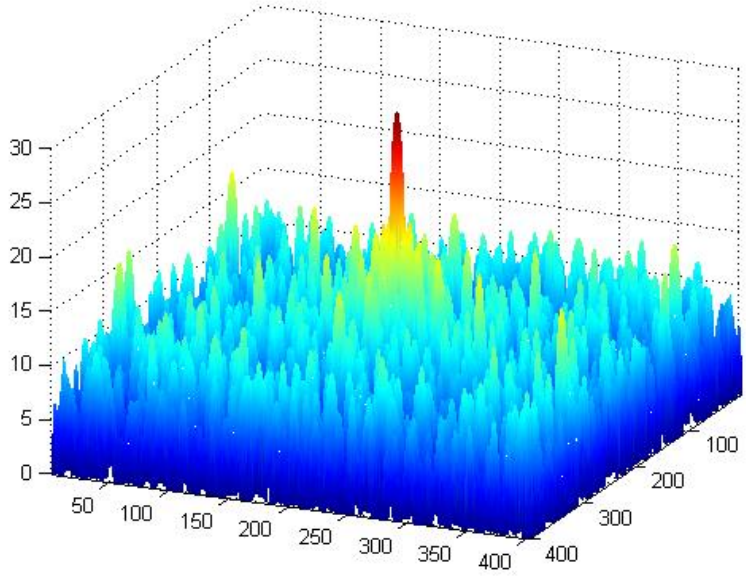

Figure 4.32: corresponding radiated field.

Array theory explains the lines that can be seen extending from the middle point. For every "line" formed by the antenna elements, the radiation will have higher side lobes on a line perpendicular to the respective lines formed. We observed this property earlier when we plotted the array factor for the points that were in a grid. Because the elements formed lines in both the x and y axes, there were lines of higher side lobes that overlapped, producing the grid-like organization of side lobes with equal heights. This is also why the random arrays are so effective in lowering the side lobes. Because the random placing of the elements on the array does not allow for "lines" to be formed, no perpendicular side lobe line is formed.

4.4.6 Discussion

The qualities of an optimized antenna array deals mainly with the quality of the main beam, and the side lobe levels. As seen in the periodic array, the main beam was good in that there was no interference from smaller side lobes coming from the side. This main beam degradation can be seen in the random array where the main beam no longer maintains its point-like appearance on our graphs. The main beam characteristics of the periodic array were imitated by the fractal array.

Side lobe levels for periodic elements are higher yet farther apart because of large amounts of elements. The random array achieves lower side lobes with significantly less elements. Like the random array, the fractal had lower side lobes at lower stages of growth. Figure 4.33, 4.34 and 4.35 compares the side lobe levels of the periodic array, random arrays and fractal array.

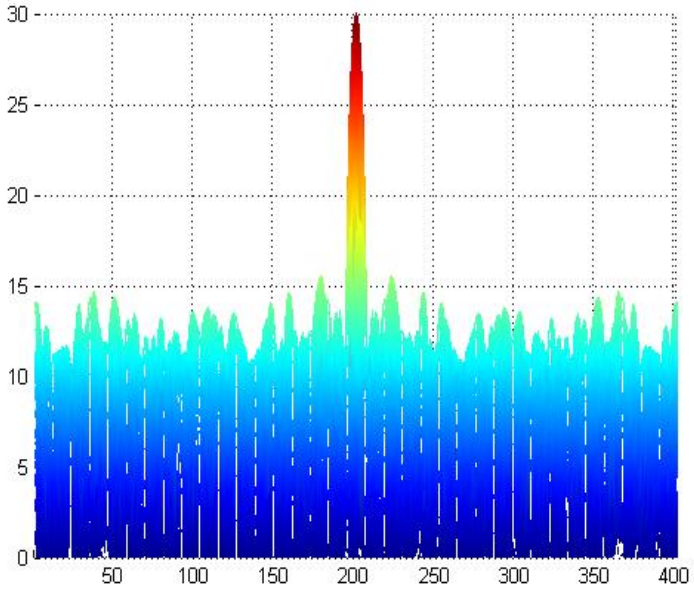

Figure 4.33: Side view of radiated field random array

It can be observed that the random array performed better than the fractal array. According to previous works, there is an intersection point where the number of elements in a fractal array and random array cause for the one to be more effective as the other. As the array holds more elements, the random arrays perform better. Yet before this intersection point we have described, certain fractal arrays perform much better. Aside from the side lobe levels, the fractal did have overall a better main beam, regardless of the number of points. A drawback for random arrays with many elements at that, as the number of elements increases, main beam degradation is quite significant. The main beam completely abandons its point-like form.

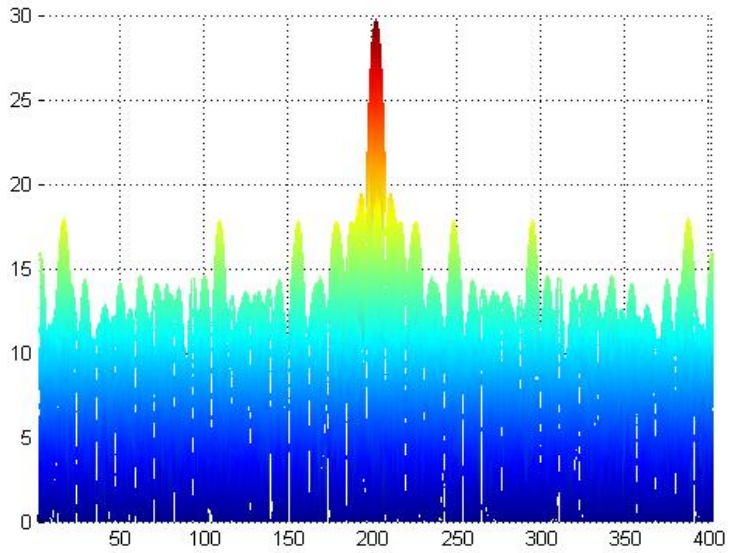

Figure 4.34: Side view of radiated field fractal array,

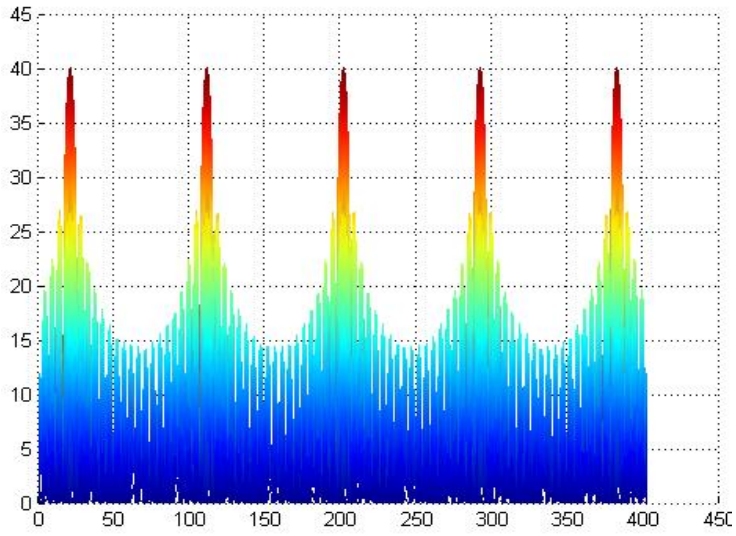

Figure 4.35: Side view of radiated field periodic array.

Chapter V: Conclusion

The bowtie antenna (336 triangles, $\alpha = 90^{o}$ flare angle, $0.2m$ total height) and the frequency band of $25\ MHz$ to $5GHz$ is chosen for its simulation. This antenna has shown very smooth impedance characteristics, especially inviting is the behaviour of the reactance which has nearly constant negative value (capacitive reactance) in the band 1.5 to $5GHz$. The impedance behavior of the bowtie is considerably affected by the value of the flare angle, α. Only one power resonance can be indentified for the present bowtie with $\alpha = 90^{o}$. This resonance occurs when the antenna length/wavelength ratio is slightly smaller than $1:3$. The first resonance is very strongly developed and a high output power of about $15mW$ is observed at the resonance. The bowtie gain varies from approximately 2 to $5dB$. When the frequency increases, the output power exhibits moderate oscillations and generally increases as well. For the bowtie antenna the current is distributed over a larger surface and eventually dissipates into the radiated field before it reaches the antenna's end. Therefore reflections from the antenna's end are significantly reduced, which makes the bowtie antenna an essentially nonresonant structure, attractive for both broadband and UWB applications.

Using a bow-tie as a generator, a crescent number of triangles are removed in the half of height of the anterior space to create a Sierpinski antenna. At low frequencies (below $0.5\ GHz$) power dependencies of fractal antenna and equivalent bowtie antenna are nearly the same. It is observed that the fractal antenna has three resonances. The number of resonances is thus the number of fractal stages $(S = 2)$ plus one. The first resonance is that of the pure bow-tie and corresponds to $f_1 = 0.4\ GHz$. This resonance occurs whether or not the fractal structure is present. The second resonance $f_2 = 1.48GHz$ corresponds to first fractal iteration, and the third resonance at $f_3 = 3.367GHz$ corresponds to the second fractal iteration. The frequency ratios asymptotically tend to 2 when the number of fractal stages increases. The resonant bands are thus log-periodically spaced, by a factor of 2, which is exactly the scale factor that relates triangle size at each stage of growth. It is seen that the power resonances are directly associated with the minima of the reflection coefficient, which enables us to design a well-matched antenna at these frequencies. The corresponding resonance bands are the multi-bands of the fractal antenna. The relative bandwidth at each band typically reaches 7 to 20%. Fig. Compared to the bow-tie radiation patterns, the fractal antenna produces a directional beam of higher gain at the resonant frequencies.

The qualities of an optimized antenna array deals mainly with the quality of the main beam, and the side lobe levels. As seen in the periodic array, the main beam was good in that there was no interference from smaller side lobes coming from the side. This main beam degradation can be seen in the random array where the main beam no longer maintains its point-like appearance on our graphs. The main beam characteristics of the periodic array were imitated by the fractal array.

Side lobe levels for periodic elements are higher yet farther apart because of large amounts of elements. The random array achieves lower side lobes with significantly less elements. Like the random array, the fractal had lower side lobes at lower stages of growth. It has been observed that the random array performed better than the fractal array. According to previous works, there is an intersection point where the number of elements in a fractal array and random array cause for the one to be more effective as the other. As the array holds more elements, the random arrays perform better. Yet before this intersection point described, certain fractal arrays perform much better. Aside from the side lobe levels, the fractal did have overall a better main beam, regardless of the number of points. A drawback for random arrays with many elements is that, as the number of elements increases, main beam degradation is quite significant. The main beam completely abandons its point-like form.

Since the primary structure of the antenna is a multiband one we can set the repeated resonances between those operating bands by using different fractal shapes, flare angles, and proper dimensions of the main structure. In this way, fractal shapes give us an extra freedom in spacing the operating frequencies in desired bands and bandwidths; moreover, they provide multiband and wideband features simultaneously. These antennas can be used in any communication system that is supposed to operate in different frequency bands and requires a relatively high bandwidth and a constant radiation pattern in all operating frequencies.

REFERENCES

[1] M. Zennaro and C. Fonda, *Radio Laboratory Handbook*, vol. 1, ICTP, Trieste, Italy, February 2004.

[2] D.H. Werner and S. Ganguly, "An Overview of Fractal Antenna Engineering Research", *IEEE Antennas and Propagation Magazine*, vol. 45, no.1, pp. 38-57, 2003

[3] T. Taga and K. Tsunekawa, "Performance Analysis of a Built-In Planar Inverted F Antenna for 800 Mhz Band Portable Radio Units," *IEEE Journal on Selected Areas in Communications*, vol. 5, pp. 921–929, June 1987.

[4] R. Yamaguchi, "Effect of Dimension of Conducting Box on Radiation Pattern of a Monopole Antenna for Portable Telephone," *IEEE Antennas and Propagation Society International Symposium Digest*, pp. 669–672, 1992.

[5] McLean, J. S., "A Re-Examination of the Fundamental Limits on the Radiation Q of Electrically Small Antennas," *IEEE Transactions on Antennas and Propagation*, vol. 44, pp. 672–676, May 1996.

[6] H. Morishita, Y. Kim, and K. Fujimoto, "Design Concept of Antennas for Small Mobile Terminals and the Future Perspective," *IEEE Antennas and Propagation Magazine*, vol. 44, no. 5, pp. 30–43, October 2002.

[7] K. L. Wong, *Planar Antennas for Wireless Communications*, Wiley-Interscience, John Wiley & Sons, 2003.

[8] Y. Rahmat-Samii, and J.P. Gianvittorio, "Fractal Antennas: A Novel Antenna Miniaturization Technique and Applications," *IEEE Antennas and Propagation*, vol. 44, no. 1, pp. 20–36, February 2002.

[9] K.J. Falconer, *Fractal Geometry: Mathematical Foundations and Applications*, John Wiley & Sons, Chinchester, New York, 1990.

[10] Z. Ying, "Some Important Innovations in the Terminal Industry in the Last Decade," Proceedings of the 1st European Conference on Antennas and Propagation (EuCAP2006), ESA SP-626, October 2006, paper no. 244664.

[11] K.J. Vinoy, "Resonant Frequency of Hilbert Curve Fractal Antennas," *Proceedings of IEEE Antennas and Propagation Society Int. Symposium*, vol. 3, pp. 648–651 July 2001.

[12] K. Sato, "Characteristics of a Planar Inverted-F Antenna on a Rectangular Conducting Body*," Electronics and Communications in Japan*, vol. 72, no. 10, pp. 43–51, 1989.

[13] D. Manteuffel, “Design Considerations for Integrated Mobile Phone Antennas,” *Proceedings of the 11th International Conference on Antennas and Propagation*, vol. 1, pp. 252–256, April 2001.

[14] P. Vainikainen, “Performance Analysis of Small Antennas Mounted on Mobile Handsets,” *Proceedings of the COST 259 Final Workshop–Mobile and Human Body Interaction*, pp. 8, 2000.

[15] P. Vainikainen, “Resonator-Based Analysis of the Combination of Mobile Handset Antenna and Chassis,” *IEEE Transactions on Antennas and Propagation*, vol. 50, no. 10, pp. 1433–1444, October 2002.

[16] K.R. Boyle and L.P. Ligthart, “Radiating and Balanced Mode Analysis of PIFA Antennas,” *IEEE Transactions on Antennas and Propagation*, vol. 54, no. 1, pp. 231–237, January 2006.

[17] Y. Kim, and D.L. Jaggard, “The Fractal Random Array,” *Proceeding of IEEE*, vol. 74, no. 9, pp. 1278–1280, 1986.

[18] A. Lakhtakia, V.K. Varadan, and V.V. Varadan, “Time-Harmonic and Time-Dependent Radiation by Bifractal Dipole Arrays,” *International Journal of Electronics*, vol. 63, no. 6, pp. 819–82, 1987.

[19] N. Cohen, “Fractal Antennas: Part 2”, *Communications Quarterly, summer*, pp. 53-66, 1996.

[20] L.J. Chu, “Physical limitations of omni-directional antennas”, *Journal of Appl. Physics*, vol.19, pp. 1163-1175, 1948.

[21] Y. Lee, J. Yeo, R. Mittra, S. Ganguly, and J. Tenbarge, “Fractal and Multiband Communication Antennas”, *IEEE Conference on Wireless Communication Technology*, pp. 273-274, 2003.

[22] Z. Baharav, “Fractal Arrays Based on Iterated Function Systems (IFS),” *IEEE Int. Symp. On Antennas and Propagation Digest, Florida*, vol. 4, pp. 2686-2689, 1999.

[23] N. Cohen, “Fractal Antennas: Part I”, *Communications Quarterly, summer*, pp. 7- 22, 1995

[24] M. Sindoy, G. Ablat, and C. Sourdois, “Multiband and wideband properties of printed fractal branched antennas”, *Electronics Letters*, vol. 35, pp. 181-182, 1999.

[25] C. Puente, J. Romeu, R. Pous, X. Garcia, and F. Benitez, “Fractal Multiband antenna based on the Sierpinski gasket”, *IEE Electronic Letters*, vol.32, pp. 1- 2,1996.

[26] N. Cohen, “Fractal Antennas: Part 2”, *Communications Quarterly, summer*, pp. 53-66, 1996.

[27] B.B. Mandelbrot, “The Fractal Geometry of Nature”, W. H. Freeman, New York, 1983.

[28] D.H. Wemer and P.L. Wemer, “Frequency independent features of self-similar fractal antennas”, Radio Science, vol. 31, no. 6, pp. 1331-1343, 1996.

[29] C. Puente-Baliarda, J. Romeu, R. Pous, and A. Cardama, “On the behaviour of the sierpinski multiband fractal antenna,” *IEEE Transactions on Antennas and Propagation*, vol. 46, pp. 517-524, April 1998.

[30] C. Puente, J. Romeu, R. Bartoleme, and R. Pous, “Perturbation of the sierpinksi antenna to allocate operating bands,” *Electronics Letters*, vol. 32, pp. 2186-2188, November 1996.

[31] C. Puente, M. Navarro, J. Romeu, and R. Pous, “Variations on the fractal sierpinski antenna flare angle,” *In IEEE Antennas and Propagation Society*, vol. 4, June 1998.

[32] R. Breden and R.J. Langley, “Printed fractal antennas,” *In IEE National Conference on Antennas and Propagation*, pp.1-4, April 1999.

[33] J.M. Gonzalez, M. Navarro, C. Puente, J. Romeu, and A. Aguasca, “Active zone self similarity of fractals-sierpinski antenna verified using infra-red thermograms,” *Electronics Letters*, vol. 35, pp. 1393-1394, August 1999.

[34] C. Borja, C. Puente, and A. Medina, “Iterative network model to predict the behaviour of a sierpinski fractal network,” *Electronics Letters*, vol. 34, pp. 1443-1445, July 1998.

[35] L. Xu and M.Y.W. Chia, “Multiband characteristics of two fractal antennas” *Microwave and Optical Technology Letters*, vol. 23, pp. 242-245, November 1999.

[36] J.F. Callejon, A.R. Bretones, and R.G. Martin, “On the application of parametric models to the transient analysis of resonant and multiband antennas,” *IEEE Transactions on Antennas and Propagation*, vol. 46, no. 3, pp. 312-17, March 1998.

[37] G.J. Walker and J.R. James, “Fractal volume antennas,” *Electronics Letters*, vol. 34, pp. 1536-1537, August 1998.

[38] C.T.P. Song, P.S. Hall, H. Ghafouri-Shiraz, and D. Wake, “Fractal stacked monopole with very wide bandwidth,” *Electronics Letters*, vol. 35, no. 12, pp. 945-946, June 1999.

[39] J. Romeu and Y. Rahmat-Samii, “Dual band fss with fractal elements,” *Electronics Letters*, vol. 35, no. 9, pp. 702-703, April 1999.

[40] R. Ghatak, D.R. Poddar, and R.K. Mishra, "Design of Sierpinski gasket fractal microstrip antenna using real coded genetic algorithm", *IET Microwaves, Antennas & Propagation*, vol.3, no.7, pp 1133-1140, 2009.

[41] K.C. Hwang, "Dual-wideband monopole antenna using a modified half-Sierpinski fractal gasket", *Electronic Letters*, vol.45, no.10, pp 487-489, 2009.

[42] R.K. Mishra, R. Ghatak, and D. Podder, "Design Formula for Sierpinski Gasket Pre-Fractal Planar-Monopole Antennas", *Antennas and Propagation Magazine*, vol. 50, no. 3, pp 104-107, 2008.

[43] Q. Xinbo, H. Zhaoxiang, S. Wei, L. Yunzhi, and Q. Zuping, "Multiband Analysis of Sierpinski Gasket Antenna with An Iterative Method", *International Conference on Wireless Communications & Signal Processing*, pp 1-4, 2009.

[44] M. Waqas, Z. Ahmed, and M. Ihsan Bin, "Multiband Sierpinski Fractal Antenna", *IEEE 13th International Multitopic Conference*, pp 1-6,2009.

[45] J. Gemio, J.P. Granados, and J.S. Castany, "Dual-Band Antenna With Fractal-Based Ground Plane for WLAN Applications," *Antennas and Wireless Propagation Letters*, vol. 8, pp. 748-751, 2009.

[46] Z. Kai, C. Chen, G.Chenjiang, and X. Jiadong, "On the Behavior of Conformal Sierpinski Fractal Microstrip Antenna," *International Conference on Microwave and Millimeter Wave Technology*, vol. 3, pp 1073-1076, 2008

[47] C. Puente, J. Romeo, R. Pous, J. Ramis, and A. Hijazo, "Small but long Koch fractal monopole," *Electronics Letters*, vol. 34, no. 1, pp. 9-10, January 1998.

[48] R.G. Hohlfed and N. Cohen, "Self Similarity and the geometric requirements for frequency independence in antennas," *Fractals*, vol. 7, no. 1, pp. 79-84, March 1999.

[49] C. Puente, J. Claret, F. Sagues, J.Romeu, M.Q. Lopez–Salvans ,and R. Pous, "Multiband properties of a fractal tree antenna generated by electrochemical deposition," *Electronics Letters*, vol. 32, no. 25, pp. 2298-2299, December 1996.

[50] M. Sindou, G. Ablart, and C.Sourdois, "Multiband and wideband properties of printed fractal branched antennas," *Electronics Letters*, vol. 35, no. 3, pp. 181-182, February 1999.

[51] D.H. Werner, A.R. Bretones, and B.R. Long, "Radiation characteristics of thing wire ternary fractal trees." *Electronics Letters*, vol. 35, no. 8, pp. 609-610, April 1999

[52] C. Puente-Baliarda and R. Pous, "Fractal design of multiband and low side-lobe arrays," *IEEE Transactions on Antennas and Propagation*, vol. 44, no. 5, pp. 730-739, May 1996.

[53] D.H.Werner and R.L.Haupt, “Fractal constructions of linear and planar arrays,” *In IEEE Antennas and Propagation Society*, vol. 3, July 1997.

[54] D.H. Werner, R.L. Haupt, and P.L. Werner. “Fractal antenna engineering:The theory and design of fractal antenna arrays,” *IEEE Antennas and Propagation Magazine*, vol. 41, no. 5, pp. 37-59, October 1999.

[55] D.L. Jaggard and A.D. Jaggard, “Cantor ring arrays,” *Microwave and Optical Technology Letters*, vol. 19, no. 2, pp. 121-125, October 1998.

[56] D.L. Jaggard and A.D. Jaggard, “Cantor ring arrays,” *In IEEE Antennas and Propagation Society*, vol. 2,pp. 862-5, 1998.

[57] X. Liang , W. Zhensen, and W. Wenbing, “Synthesis of fractal patterns from concentric-ring arrays,” *Electronics Letters*, vol. 32, no. 21, pp. 1940-1941, October 1996.

[58] L. Xu, Z.S. Wu, and W.B. Wang, “Fractal linear arrays,” *Chinese Physics Letters*, vol. 15, no. 2, pp. 140-142, 1998.

[59] T. Aubreton, P. Vaudon, and B. Jecko, “Theoretical analysis of a fractal surface radiation,” *Annales desTelecommunications*, vol. 52, no. 7, pp. 427-434, July-Aug 1997.

[60] D.H. Werner, K.C. Anushko, and P.L. Werner, “The generation of sum and difference patterns using fractal subarrays,” *Microwave and Optical Technology Letters*, vol. 22, no.1, pp. 54-57, July 1999.

[61] W. Kuhirun,” A Simple Procedure for Evaluating the Impedance Matrix of the Peano-Gosper Fractal Array”, *Asia-Pacific Microwave Conference*, pp 1-4, 2008.

[62] K.H. Sayidmarie and E.U.T Al-Shabkhoon, “Investigation of the Focusing Properties of Some Fractal Arrays”, *International Conference on Advances in Computational Tools for Engineering Applications*, pp 203-207, 2009.

[63] J. Kaur and A. Kansal, “Sierpinski Gasket Fractal Array Antenna”, International journal of computer science and Communication, vol. 1, no. 2, 2010.

[64] M.F. Caterda, J.G. Cuevas, and L. Nuno, “A scheme to analyze conducting plates of resonant size using the conjugate gradient method and the fast Fourier transform,” IEEE Transactions Antenna and Propagation, vol. 36, no. 12, pp. 1744-1752, 1988.

[65] A.J. Poggio and E.K. Miller, *Integral equation solutions of three dimensional scattering problems*, In R.Mittra, ed., Computer Techniques for Electromagnetics, 2nd ed. Pergamon Press, Oxford, pp. 159-274, 1973.

[66] A.F. Peterson, S.L. Ray, and R. Mittra, *Computational Methods for Electromagnetics*, IEEE Press, Piscataway, NJ, 1998.

[67] S.M. Rao, D.R. Wilton, and A.W.Glisson, "Electromagnetic scattering by surfaces of arbitrary shape" *IEEE Transaction Antennas and Propagation*, vol. 30, no. 3, pp. 409-418, 1982.

[68] C.J. Leat, N.V. Shuley, and G.F. Stickley, "Triangular-patch modelling of bowtie antennas: Validation against Brown and Woodward" *IEE Proc. Microwave Antennna Propagation*, vol. 145, no. 6, pp. 465-470, 1998.

[69] C.A. Balanis ,*Antenna Theory:Analysis and Design*,2nd ed.Wiley ,New York,1997.

[70] J.D. Kraus, *Antenna*, Mc Graw Hill, New York,1950.

[71] K.R. Demarest, *Engineering Electromagntics*, Prentice Hall, Upper Saddle River, NJ. 1998.

[72] A. Ishimary, *Electromagnetic Wave Propagation,Radiation,and Scattering*, Prentice Hall, Upper Saddle River,NJ.1991.

[73] J.D.Kraus, *Electromagnetics*, 4th ed., Mc Graw Hill, New York,1992.

[74] D.M. Pozar, *Microwave and RF Design of Wireless Sytems*. Wiley, New York, 2001

[75] J. Romeu and J. Soler, "Generalized Sierpinski Fractal Multiband Antenna," *IEEE Transactions on Antennas and Propogation*, vol. 49, no. 8, pp. 1237-1239, 2001.